AN INVESTIGATION OF THE OUT-OF-PLANE DEFLECTION BEHAVIOR OF THIN SHEETS WITH CUT-OUTS IN A TENSILE FIELD

A THESIS

Presented to

The Faculty of the Division of Graduate

Studies and Research

by

George Frank Zielsdorff

In Partial Fulfillment

of the Requirements for the Degree

Doctor of Philosophy

in the School of Aerospace Engineering

Georgia Institute of Technology

April 1971

AN INVESTIGATION OF THE OUT-OF-PLANE DEFLECTION

BEHAVIOR OF THIN SHEETS WITH CUT-OUTS IN A TENSILE FIELD

Approved:

_____

Chairman

_____

_____

Date approved by Chairman: 5-3-71

In presenting the dissertation as a partial fulfillment of the requirements for an advanced degree from the Georgia Institute of Technology, I agree that the Library of the Institute shall make it available for inspection and circulation in accordance with its regulations governing materials of this type. I agree that permission to copy from, or to publish from, this dissertation may be granted by the professor under whose direction it was written, or, in his absence, by the Dean of the Graduate Division when such copying or publication is solely for scholarly purposes and does not involve potential financial gain. It is understood that any copying from, or publication of, this dissertation which involves potential financial gain will not be allowed without written permission.

_____

_____

7/25/68

ACKNOWLEDGMENTS

I would like to express my grateful appreciation to my thesis advisor, Dr. Robert L. Carlson. It was through his suggestion that this work was initiated and through his many hours of personal consultation it has been brought to its successful conclusion.

My deepest appreciation also goes to the members of my reading committee, and most especially to Drs. Robert L. Carlson and C. V. Smith for their scrutiny, constructive criticism and suggestions which proved so helpful in producing the final form of the manuscript.

This work has been supported by the U. S. Army Research Office-Durham under contract No. DAHC 04 68C 0004. I would also like to acknowledge the support of the U. S. Air Force under whose sponsorship I have been enrolled in school since June 1966.

My special thanks go to Ruth Shaw for her untiring dedication to the typing of both the rough draft and the final manuscript. The final form and appearance of this manuscript are unending tributes to her skill and patience.

To my wife, Barbara, there are no words to express my feelings. Her love and encouragement beyond all else are responsible for the completion of this work. With love I dedicate this work to her.

TABLE OF CONTENTS

LIST OF TABLES

LIST OF FIGURES

NOMENCLATURE

A	square of magnitude of complex variable, ξ
A_i	quantity defined by Equation (51) Chapter II
$A(I)$	coefficients of a power series
$\lvert\vec{AC}\rvert$	magnitude of vector from the center of the circular end of the slot to the inverse of the mapped point with respect to the circular arc
$\lvert\vec{AP}\rvert$	magnitude of vector from the center of the circular end of the slot to the mapped point
a	characteristic length
a_i	amplitude of dislocation in u for the i^{th} boundary
B_i	quantity defined by Equation (51) Chapter II
$B(I)$	coefficients of a power series expansion of the mapping function
$BB(I)$	coefficients of a power series
b_i	amplitude of dislocation in v for the i^{th} boundary
b_n	coefficients of a power series
C	curve representing a hole boundary
C'	curve in the z-plane which corresponds to the unit circle in the ζ-plane

CN(I)	coefficients of a power series
CP(I)	coefficients of a power series
CQ(I)	coefficients of a power series
CR(I)	coefficients of a power series
CS(I)	coefficients of a power series
CT(I)	coefficients of a power series
c_i	amplitude of rotational dislocation for the i^{th} boundary
D	flexural stiffness, $Et^3/12(1 - \mu^2)$
E	Young's modulus
e_x	midsurface normal strain in x direction
e_y	midsurface normal strain in y direction
$\tilde{e}_x$	normal strain in x direction at any point
$\tilde{e}_y$	normal strain in y direction at any point
F	Airy's stress function
$\tilde{F}$	a defined parameter
G	shear modulus
H	slot half length

h	plate thickness
I	integer
i	complex constant $\sqrt{-1}$
K	parameter of critical stress formula
ℓ	direction cosine; $\cos(x, \nu)$
M_x	bending moment distribution associated with σ_x
M_y	bending moment distribution associated with σ_y
M_{xy}	twisting moment distribution associated with τ_{xy}
m	direction cosine, $\cos(y, \nu)$
$m(\zeta)$	mapping function
N	integer representing maximum number of terms in the mapping function
N_x	stress resultant in x direction
N_y	stress resultant in y direction
N_{xy}	shear stress resultant
$\bar{N}_{x\nu}$	applied resultant traction; x direction
$\bar{N}_{y\nu}$	applied resultant traction; y direction
n	integer number of internal boundaries
P	continuous function of x and y

P_{cr}	critical load
P_0	Lundquist zero load
P_1	continuous function of x and y
P_2	continuous function of x and y
$p_1(x,y)$	stress distribution function
$p_2(x,y)$	stress distribution function
$p_3(x,y)$	stress distribution function
Q	continuous function of x and y
Q_1	continuous function of x and y
Q_2	continuous function of x and y
Q_x	transverse shear distribution on x-face
Q_y	transverse shear distribution on y-face
R	slot end radius
r	local radius of curvature
S	constant; $(3 - 4\mu)$ for plane strain; $(3 - \mu)/(1 + \mu)$ for generalized plane stress
s	tangential boundary coordinate
T	temperature difference distribution function

t	plate thickness
U	difference of principal stresses
u	midsurface displacement function in x direction
$u(\theta)$	Melentiev coordinate on hole boundary in Z-plane
V	sum of principal stresses
v	midsurface displacement function in y direction
$v(\theta)$	Melentiev coordinate on hole boundary in Z-plane
W	deflection function due to applied load
$\tilde{W}$	plate width
W_i	eigenfunctions
$W_o(Z)$	complex variable stress function
$W(\zeta)$	complex variable stress function
w_o	initial deviation from flatness function
$w(Z)$	complete variable stress function
$w(\zeta)$	complex variable stress function
w	displacement function in z direction
x	coordinate direction

x_c	x coordinate of boundary curve in Z-plane
x_i	x coordinate of starting point of integration on i^{th} boundary
x_r	x coordinate of starting point of integration on Γ
y	coordinate direction
y_c	y coordinate of boundary curve in Z-plane
y_i	y coordinate of starting point of integration on i^{th} boundary
y_r	y coordinate of starting point of integration on Γ
Z	complex variable
Z_c	boundary curve in Z-plane
z	coordinate direction
α	coefficient of thermal expansion
α_i	constant of integration
β	ratio of plate thickness to slot length (t/2H)
β_i	constant of integration
Γ	any closed curve in a plate
Γ_i	internal closed boundary

γ	ratio of slot length to plate width ($2H/\widetilde{W}$)
γ_i	constant of integration
γ_{xy}	midsurface shearing strain
$\widetilde{\gamma}_{xy}$	shearing strain at any point
$\Delta\varepsilon$	twice the bending strain; i.e., the difference between the surface strains
$\Delta\varepsilon_0$	$\Delta\varepsilon$ corresponding to P_0
δ	measure of discrepancy between C and C′
$\delta u(I)$	correction to $u(\theta)$ coordinate
$\delta x(I)$	correction to x coordinate
$\delta y(I)$	correction to y coordinate
ζ	complex variable
η	modulus of complex variable ζ
θ	argument of complex variable ζ
λ	load intensity factor
λ_i	eigenvalues
μ	Poisson's ratio
ν	*normal boundary direction*

ξ	complex variable
ρ	ratio of slot height to slot length (2R/2H)
σ	applied tension at infinity
σ_{AVG}	the average stress in a section far above the slot; i.e., load/(total area)
σ_{cr}	critical applied tensile traction
$\bar{\sigma}_{cr}$	a nondimensional critical stress parameter
σ_{MAX}	maximum stress occurring at end of slot
σ_{NET}	average stress at section through center of slot; i.e., load/(net area at section through slot)
σ_p	principal stress
σ_q	principal stress
σ_t	tangential boundary stress
σ_x	midsurface normal stress in x direction
σ_y	midsurface normal stress in y direction
σ_z	midsurface normal stress in z direction
$\tilde{\sigma}_x$	normal stress in x direction at any point
$\tilde{\sigma}_y$	normal stress in y direction at any point

σ_1	principal stress
σ_2	principal stress
τ_{xy}	midsurface shearing stress
$\tilde{\tau}_{xy}$	shearing stress at any point
Φ	body force potential function
φ	angle between tangent to the boundary and the x-axis
Ψ	angle between applied tension and x-axis
ω_z	infinitesimal rotation
$O(\ )$	order symbol
$\frac{\partial}{\partial x} = (\ )_{,x}$	partial differentiation
$\frac{d}{dx}$	total differentiation

ABSTRACT

A thin plate containing a centrally located hole can experience a local buckling in the vicinity of the hole when subjected to a uniaxial tension. From a stability viewpoint this problem involves a nonuniform prebuckle stress state. The solution of the problem of interest necessarily includes consideration of moderately large deflections of multiply connected plates. The Karman plate formulation is extended to include multiply connected plates. The difference between the simply and multiply connected formulations is the presence of a set of auxiliary conditions which must be satisfied on each internal boundary. Restrictions that are applicable to the modeling of this class of problems are presented and discussed.

The coupled, nonlinear Karman equations may be linearized under some circumstances and it is shown by an examination of the properties of the resulting uncoupled equations that a Southwell type load-displacement relation can be obtained. The limit of applicability of this extended Southwell technique is shown to depend on the extent to which middle surface stretching due to bending influences the load-deflection response.

A complex variable solution for the prebuckling stress distribution in the vicinity of a hole in an infinite sheet is developed and presented. Results of a photoelastic stress analysis for the stress distribution in finite width plates subjected to uniaxial tension are presented and

compared with the complex variable solution for the same hole geometries in infinite sheets. The effect of finite plate width on the region of compression is discussed.

The extended Southwell method is used as a basis for an experimental study of the local buckling behavior of tensioned sheets with slots. The parameters of interest are the plate thickness to slot length ratio, the slot height to slot length ratio, and the slot length to plate width ratio. A comparison of trends observed in the stress analyses shows that plate width effect is not a factor over the ranges of parameters investigated. The data are analyzed on the basis of these observations and an empirical relation is obtained for the tensile stress which produces local buckling. This relation is shown to apply to the data obtained for this dissertation and also to the results presented by other investigators. Limits of applicability of the empirically derived relation are discussed.

CHAPTER I

INTRODUCTION

Cut-Outs in Aircraft Structures

There are many features of modern structures which continually present new and challenging problems to the designer and engineer. The opening, although it has been a part of man's structures throughout civilized history, is still considered a major engineering problem in structures today.

The importance of the opening or cut-out in structures extends beyond the obvious function as a point of ingress and egress for people and material. The design of modern structures, whether they be bridges, skyscrapers, ships, or airplanes, must be based not only on static criteria, but also on weight and dynamic considerations. The cut-out is one of the basic means which the designer can use to alter these characteristics. One can, for example, alter the dynamic characteristics of a structural element while still maintaining a constant weight by introducing a reinforced cut-out into a simple element. The cut-out can also be used to optimize the weight to strength characteristics of a structural element. This use of the cut-out was explored in an extensive series of tests conducted by the U. S. National Bureau of Standards [1].* These tests were designed to determine the optimum use

* Numbers in brackets refer to references.

of cut-outs in the cover plates of built-up beams.

As one might suspect, the use of cut-outs involves more than just technical considerations. The technology developed by man has become complex, and often psychological factors may be involved in design decisions. For example, confinement in closed quarters with no view of the exterior surroundings is unbearable for many people. Recognizing and accepting this, aircraft designers continue to place windows in the passenger sections of fuselages even though they add significantly to the overall weight and stress concentration problems. The problems associated with passengers' fears fears and the methods of relieving them have been described by R. A. McFarland [2,3]. Whether or not the passenger would accept travel in windowless supersonic planes was recently, in fact, the subject of much debate. The difference in opinion regarding the feasibility of windows in supersonic transports can be shown by excerpts from two papers presented in 1960 at the Fifth European Congress of Aviation Medicine, London, England. C. S. R. Marshall [4] writes:

> High aircraft skin temperatures and the necessity for insulations and pressurization makes the use of transparencies a major engineer-problem. For this reason ... the passenger cabin will be windowless.

On the other hand, P. G. Masefield [5] writes:

> On the window question I may say here both as an ex-airline operator and as a long time air traveler, that anyone who suggest(s) that a supersonic airline should be built without passenger cabin windows will have to think again.

The above statements indicate that the problems caused by cut-outs are neither trivial nor can they be ignored.

The development of the types of structures used in aircraft has been outlined by Nicholas J. Hoff in two excellent papers [6,7]. The first of these appeared in 1946 and the second in 1967. The basic type of aircraft structure used today had been established by the time Hoff wrote the first of these historical accounts. During the period between the writing of these two papers, the structure was refined and much work was done in the fields of both theoretical and experimental stress analysis.

Hoff points out that the basic operational requirements, such as speed, altitude, maneuverability, etc., that are placed on aerospace vehicles strongly influence the details of the structural design of the vehicle. For instance, a major breakthrough in structural design was the remarkable discovery of Wagner [8] that sheets could serve as satisfactory structural elements even after buckling. It became necessary, however, to eliminate sheet buckling on exposed panels if the performance specifications included speeds near the speed of sound. At these speeds the drag created by buckled sheets is intolerable. In space-flight, on the other hand, where atmospheres are not encountered, the use of buckled sheets as structural elements can again be applied to great advantage.

As the modern aircraft structure evolved to a stressed skin, monocoque or semi-monocoque construction, the problems associated with the presence of cut-outs became evident. In these types of structures the skin carried all or some of the in-plane loads as well as pressure type loads. Failures caused by the development of fatigue cracks in the skin became more and more frequent, and it was observed that often

these cracks propagated from a cut-out or other form of discontinuity.

As new methods of construction were developed, new materials were introduced into aircraft structures. Wood, which initially was the chief aircraft material, was not suited for large scale production of the stressed skin aircraft. Obvious needs were thus created for high strength yet relatively light metal components. Some of the problems encountered during this period of transition are discussed by H. J. Pollard [9]. Of special interest in this latter article are the figures which show sheet specimens with central, reinforced holes that had buckled under the application of externally applied shearing forces.

The aircraft designer usually tries to determine an optimum design. The presence of cut-outs makes this an impossibility in actual practice. F. R. Shanley [10] expresses these views concerning the cut-out:

> One well-known source of non-optimum weight is the 'cut-out'. Any discontinuity in the structure tends to require additional reinforcing material. Removable doors or cover plates generally increase the weight beyond the optimum value.

The design of cut-outs in the early days of stressed skin type structures could hardly be called optimum. It is interesting that the basic concept of reinforcing to eliminate the effect of the cut-out is present in even the modern concept of "neutral holes" to be discussed later. The design practice in 1935 as given by J. E. Younger [11] was:

> The bracking and reinforcement about the windows and doors must be such that the distortion of the ring about the opening will not be greater than the distortion of a similarly placed ring on the sheet metal if the opening did not exist.

A few years later E. E. Sechler and L. G. Dunn [12] made these comments:

> Methods are not available for calculating the exact influence of such cut-outs on the stress distribution. The usual procedure is to make an analysis based on the elementary beam theory with suitable allowances for the material at or near the cut-outs, which is not fully effective.

The continued need for further evaluation of the effects of the stress distribution around cut-outs caused many reports to be written on the subject. G. Henson [13] reported test results conducted on large (100.6" outside diameter) circular cylinders loaded in compression in 1952. These tests were designed to show the effect of a cut-out on skin buckling. Hoff, et al. [14-21] had previously looked at this problem in smaller cylinders under several loading conditions. These studies, though interesting, were not sufficiently comprehensive and the same problem is still being studied today (see, for example, the report by F. Brogan and B. Almroth [22]).

Certain design problems arise in aircraft with large cut-outs which are necessary for under-carriages, bomb-bays, or the wing fold joints in naval aircraft. These problems concern the diffusion of stresses into the panels surrounding the cut-out from the stiffened structure in the neighborhood of the cut-out [23]. The methods of analysis available ("Finite Stringer" or "Stringer Sheet") in the early 1950's led to conflicting descriptions of the stress distributions in panels adjacent to such cut-outs. L. W. Brown [24] undertook an experimental investigation which proved to be very revealing in that neither theoretical method gave results which agreed well with what

actually was observed in the neighborhood of a corner. Of special interest to the research described in this dissertation are the large compressive stresses which Brown noticed along the edge of the panel. These were, in fact, observed to be large enough to cause local buckling along the panel edge when the edge stiffener was removed. This behavior is described by Brown and a discussion of the effect of the end fixity of this stiffener is given in one of the conclusions of that paper. Figure 1 indicates the panel tested and the type of loading applied.

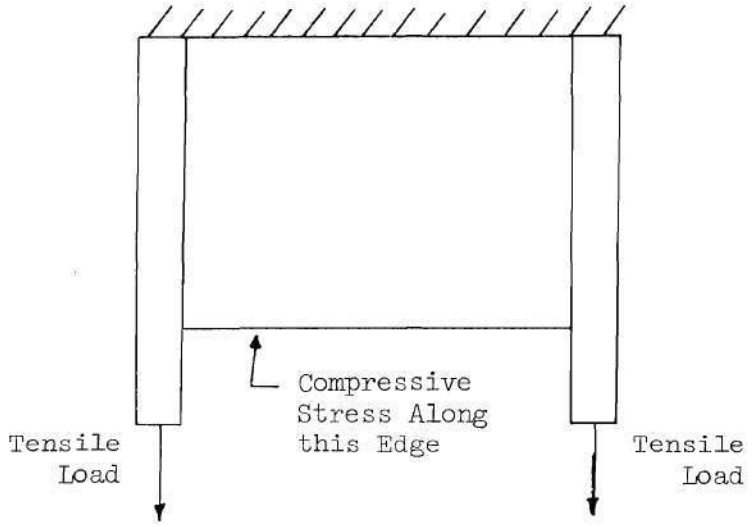

Figure 1. L. W. Brown's Test Panel

Stresses Around Cut-Outs

The stresses in plates with cut-outs cannot be predicted by a simple strength of materials type of analysis. The distribution of the stresses is usually a rapidly varying function of position in the neighnorhood of the cut-out. The effect of a cut-out on the stress

distribution is local in nature if the size of the cut-out is small in relation to the plate dimensions. Most of the attention of investigators has been focused on the stress concentration created by the cut-out. In these studies the objective has been to develop a solution for the stress field in the neighborhood of the cut-out and then to evaluate the hoop-stress along the cut-out boundary.

The first such solution was obtained by G. Kirsch [25] in 1898 for a circular hole in an infinite plate under uniaxial tension. The solution has become a standard example in most books on the theory of elasticity. It is based upon the superposition of two stress fields in order to satisfy the boundary conditions on the edge of the hole. The solution for a circular hole in a tensile field in a finite width strip was obtained in 1929 by R. C. J. Howland [26].

In 1937 H. Neuber [27] wrote a book in which he presented a unified treatment of stress concentration problems. His nomographs are still used today by many engineers and designers who must consider stress concentrations. An extremely good review of stress concentrations was given by H. Neuber and H. G. Hahn [28] in the March 1966 issue of the Applied Mechanics Review.

In 1909 the Russian mathematician, G. V. Kolosov [29] applied the method of complex variables to the theory of elasticity. He used this method to solve the problem of the stress distribution in an infinite plate with an elliptic hole under uniaxial tension. The Russian mathematician and elastician, N. I. Muskhelishvili [30] introduced the use of conformal mapping, and developed procedures which made it possible to solve a great number of problems in an elegant and efficient manner.

The primary problem in the use of this method is the selection of a suitable mapping function. For many practical problems it is difficult and sometimes impossible to obtain exact mapping functions. In such cases a truncated series can, however, often be utilized.

As an extension of the previous work, J. R. M. Radok [31] has proposed a complex variable method that uses variational procedures instead of conformal mapping to represent the hole boundary. L. S. D. Morley [32] also has developed a variational procedure and has been able to include reinforcement effects. The disadvantage of these methods, however, is that convergence is not guaranteed unless a proper set of curvilinear coordinates is chosen (see Chen Lin Si [33]). Choosing these coordinates usually represents as difficult a task as the original one of finding a conformal mapping function. A perturbation technique has been used by E. F. Low and Wen F. Cheng [34] and suitable results were obtained for the hoop stresses around some simple hole contours. For the problem of more complex shapes, however, the convergence of the latter method can be very slow, and it is difficult to determine when enough terms have been used.

Howland succeeded in deriving a fairly good solution for the stress distribution in a finite width plate with a circular hole by an interation process. The same procedure has been proposed by G. N. Savin [35] for use in the complex variable theory for other than circular hole. The application of this procedure, however, is extremely tedious and convergence is slower and slower as the size of the hole increases. For this reason most available solutions are for infinitely wide plates. In practice it has been found that these solutions give

acceptable results if the maximum dimension of the hole is less than one-fourth the plate width [36].

There are quite a few papers in the literature dealing with the experimental determination of stresses in a sheet with a hole. Again, however, most of these are confined to a determination of hoop stresses. The papers in this area of primary interest are photoelastic studies of sheets with various kinds of holes [37, 38, 39, 40, 41].

In addition to discussions of stresses in plates with holes, many papers have appeared in which the effects of reinforcement have been included. Of particular interest is the concept proposed by E. H. Mansfield [42] for designing a hole reinforcement which produces a so-called "neutral" hole. That is, the stress distribution is essentially unchanged by the presence of the hole. This would be ideal if there were no other factors to consider. For example, while in theory the "neutral" hole can be defined for any particular type of loading, the hole is no longer "neutral" if the external loading conditions change. Also the theoretical distribution of stiffness required to create a "neutral" hole is not always obtainable in reality. Several authors, including Mansfield [43], have recently used this idea with some modifications to help in the optimum design of cut-outs in aircraft structures.

The effect of curvature on the stress distribution around cut-outs in curved panels and shells has not yet been fully resolved. Several authors [44, 45, 46] have expressed the opinion that curvature effects are small if the hole dimensions are small in comparison to the radius of curvature of the panel. D. S. Houghton and A. Rothwell [46]

included this conclusion in a paper in 1961 and they appeared to agree with previous investigators. Further studies by Houghton and Rothwell [47] have shown, however, that the curvature effect can be very significant under certain conditions of loading (i.e., shear, biaxial load, or internal pressure).

Local Buckling in a Tensioned Sheet

As has already been observed, the objective of most analyses is the determination of hoop stresses or simply the maximum stress. Many investigators, in fact, consider it superfluous to obtain the entire stress distribution. This disregard for the total stress distribution was discussed by R. E. Peterson in the William M. Murray Lecture, 1960 [48]. Peterson remarked that in order "... to understand the strength behavior of members under service conditions, one must consider the stress distribution as well as the maximum stress." He cited as two reasons for this, (1) the effective utilization of surface hardening, and (2) the analysis of the behavior of notched members.

Peterson's remarks were made ten years ago and yet to date little progress has been made in regards to number (2) above for the case of internal notches. Many studies that have been undertaken begin, in fact, by ignoring or restraining some of the possible modes of behavior.

An example of the type of behavior alluded to is the buckling in the region of compressive stresses around a hole in a sheet loaded in tension. Although it is entirely reasonable to anyone studying the stress distribution in such sheets that buckling might occur, the difficulty of predicting the buckling load has, to a large extent,

encouraged workers to circumvent the problem by various means.

Some of the difficulties which are encountered in an analysis of the problem are:

(1) a nonuniform prebuckle stress state,

(2) an undefined boundary of the buckled region.

The only mathematical treatments of this problem have been the work of G. P. Cherepanov [49, 50] and that of D. A. Pellett, et al. [51]. Cherepanov's solution was for a membrane, that is, a plate with zero flexural regidity. Cherepanov's comment concerning a finite flexural rigidity was that "... the problem of buckling for a plate with a finite flexural regidity at this time presents apparently insurmountable difficulties of a mathematical and even more fundamental nature." By limiting his analysis to a membrane, Cherepanov was able to derive a solution that described the boundary of the buckled region. The buckled region is this case was related to the property which states that a membrane cannot support a compressive stress. The only result which he obtained in closed form was for a long slot or crack.

Pellett, et al., presented an energy type solution for an infinite plate with a circular hole. By assuming a suitable deflection function and using the membrane stress values of Kirch [25], an eigenvalue problem was formulated and solved by use of a digital computer.

The problem of buckling of plates with holes and loaded in uniaxial tension has been well documented in experimental investigations. Most noteworthy of these studies are those which appear in the literature on crack analysis [41, 52, 54, 54, 55]. The extent of influence

of buckling on fatigue and crack propagation rates, though considered, has not been clearly established. It has been observed, however, that there is a significant effect on the static strength of cracked sheets which are not restrained from buckling [41].

Results of other experimental studies have also been presented by J. F. Danis [56] on a circular hole and by W. L. Bingham [57] on a rectangular hole with rounded corners. Pellett indicated that Danis' results were unreliable and had been biased by his test technique. Bingham's tests were performed mainly as an application of an experimental device which he had developed. Bingham examined only three hole configurations and the results, being limited in scope, could not be used as a basis for developing any firm, general conclusions.

Objectives

The preceding section of this chapter has described a local buckling phenomenon that can take place in tensioned sheets with holes. The primary objective of the study described in this dissertation was to investigate this phenomenon for a particular class of openings and to develop a method for predicting the stress at which buckling occurs.

Before discussing the plan for achieving the primary objective, however, it is desirable to describe clearly certain important features of the problem. The problem of multiply connected plates undergoing moderately large transverse deflections has not received attention in the literature. Therefore, it is appropriate to specify carefully a complete set of governing equations for this class of problems. Also, in the execution of experimental work the specification of modeling

requirements for these problems must be considered.

To develop an understanding of the problem of local buckling adjacent to a cut-out, it is necessary to determine the stress distribution throughout the plate. For very wide sheets the stress distributions around holes can be examined by the application of the method of complex variables. The effect that plate width has on the stress distributions can be examined experimentally by the method of two dimensional photoelasticity. The objective of performing the stress analyses is to determine how the stress distribution changes as the geometric parameters of the problem are varied. Observations based on these results can be used as a basis for the interpretation of the tensile buckling behavior.

After having established how the stress distribution changes with the geometric parameters of the problem, particular emphasis will be directed toward an examination of the general relations for the class of problems of interest. This examination will particularly emphasize those properties of the governing equations and their solutions which are especially relevant to buckling problems. This involves a consideration of the complete coupled stress-deflection features of the buckling problem and includes the nonlinear effects introduced by stretching due to bending.

The theoretical background for the problem will then have been properly established. A parametric study designed to determine buckling loads over a systematically varied range of the geometric parameters of the problem will then be presented. Application of the theoretical

study of the properties of the governing equations to the experimental program will be demonstrated and the resulting data will be presented and analyzed.

By relating the trends observed in the stress distribution problem with those established in the determination of buckling loads, the parameters of primary interest will be clearly identified. The buckling load data will then be analyzed to develop a buckling equation which properly describes the effect of each of the important parameters. The validity of the relationship developed will be evaluated both by the use of data generated in the present study and that obtained by other investigators.

CHAPTER II

MULTIPLY CONNECTED THIN PLATES

The governing differential equations for a thin plate experiencing moderately large deflections were first formulated by T. von Karman in 1910. These equations, which commonly bear his name (the Karman equations), are expressions of the transverse equilibrium and of the in-plane compatibility of the plate. This theory includes rotations about in-plane axes in the kinematic relations and in the equilibrium equations. For a plane stress formulation of the problem the Kirchhoff assumption is adopted and σ_z, the transverse normal stress, is neglected as being small compared to the in-plane stresses.

The kinematic relations for the midsurface strains are

$$\left.\begin{aligned} e_x &= u_{,x} + \frac{1}{2}\left(w_{,x}\right)^2 \quad , \\ e_y &= v_{,y} + \frac{1}{2}\left(w_{,y}\right)^2 \quad , \\ \text{and} \qquad \gamma_{xy} &= v_{,x} + u_{,y} + w_{,x}w_{,y} \quad . \end{aligned}\right\} \qquad (1)$$

In Equations (1) u, v, and w are the midsurface displacement functions in the x,y, and z directions respectively. The strains at any point are related to midsurface strains by

$$\left.\begin{aligned} \tilde{e}_x &= e_x - zw_{,xx} \quad , \\ \tilde{e}_y &= e_y - zw_{,yy} \quad , \\ \text{and} \quad \tilde{\gamma}_{xy} &= \gamma_{xy} - 2zw_{,xy} \quad . \end{aligned}\right\} \tag{2}$$

The constitutive relations are

$$\left.\begin{aligned} \tilde{e}_x &= \frac{1}{E}\left(\tilde{\sigma}_x - \mu\tilde{\sigma}_y\right) + \alpha T \quad , \\ \tilde{e}_y &= \frac{1}{E}\left(\tilde{\sigma}_y - \mu\tilde{\sigma}_x\right) + \alpha T \quad , \\ \text{and} \quad \tilde{\gamma}_{xy} &= \frac{2(1+\mu)}{E}\tilde{\tau}_{xy} \quad . \end{aligned}\right\} \tag{3}$$

The Airy stress function, F, is defined by the relations

$$\left.\begin{aligned} \sigma_x &= F_{,yy} + \Phi \quad , \\ \sigma_y &= F_{,xx} + \Phi \quad , \\ \text{and} \quad \tau_{xy} &= -F_{,xy} \quad . \end{aligned}\right\} \tag{4}$$

For the purposes of this derivation, the plate will be assumed to be loaded only by in-plane edge tractions and body forces; that is, the transverse pressure as well as that component of the body force in the transverse direction are zero. The equilibrium equations for the plates are

$$
\left.
\begin{aligned}
& N_{x,x} + N_{xy,y} - h\Phi_{,x} = 0 \\
& N_{xy,x} + N_{y,y} - h\Phi_{,y} = 0 \\
& M_{y,y} + M_{xy,x} - Q_y = 0 \\
& M_{x,x} + M_{xy,y} - Q_x = 0 \\
\text{and} \quad & (N_x w_{,x} + N_{xy} w_{,y} + Q_x)_{,x} \\
& + (N_{xy} w_{,x} + N_y w_{,y} + Q_y)_{,y} = 0
\end{aligned}
\right\} \quad (5)
$$

The transverse shears can be eliminated from the last of Equations (5) to yield

$$
\left.
\begin{aligned}
& N_{x,x} + N_{xy,y} - h\Phi_{,x} = 0 \\
& N_{xy,x} + N_{y,y} - h\Phi_{,y} = 0 \\
\text{and} \quad & M_{x,xx} + 2 M_{xy,xy} + M_{y,yy} + (N_x w_{,x} + N_{xy} w_{,y})_{,x} \\
& + (N_{xy} w_{,x} + N_y w_{,y})_{,y} = 0 \quad .
\end{aligned}
\right\} \quad (5a)
$$

The bending moments are related to the curvatures by

$$
\left.
\begin{aligned}
& M_x = - D(w_{,xx} + \mu w_{,yy}) \\
& M_y = - D(w_{,yy} + \mu w_{,xx}) \\
\text{and} \quad & M_{xy} = - D(1 - \mu)\, w_{,xy} \quad .
\end{aligned}
\right\} \quad (6)
$$

The stress and moment resultants used in Equations (5, 5a, and 6) are defined as

$$N_x = \int_{-h/2}^{h/2} \tilde{\sigma}_x dz \quad , \quad M_x = \int_{-h/2}^{h/2} z\tilde{\sigma}_x dz \quad ,$$

$$N_y = \int_{-h/2}^{h/2} \tilde{\sigma}_y dz \quad , \quad M_y = \int_{-h/2}^{h/2} z\tilde{\sigma}_y dz \quad ,$$

$$N_{xy} = \int_{-h/2}^{h/2} \tilde{\tau}_{xy} dz \quad , \quad \text{and} \quad M_{xy} = \int_{-h/2}^{h/2} z\tilde{\tau}_{xy} dz \quad .$$

In order to present the boundary conditions in a general form, consider that the boundary is curvilinear and has an outward normal in the ν direction and a tangential direction designated by s . This is illustrated in Figure 2 below.

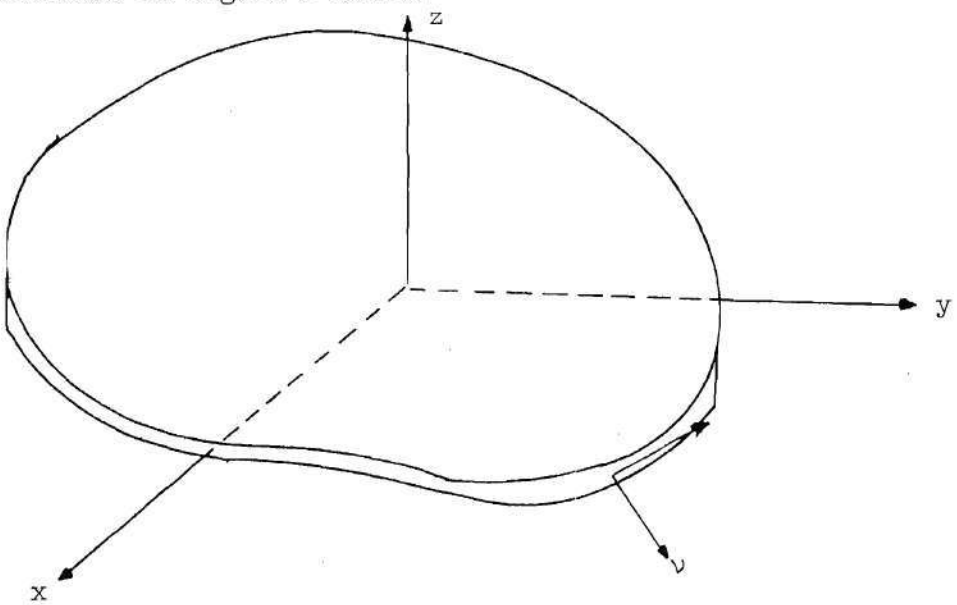

Figure 2. Plate Coordinates

Let ℓ and m be the direction cosines of ν such that

$$\left.\begin{aligned} \ell &= \cos(x,\nu) \quad , \\ \text{and} \qquad m &= \cos(y,\nu) \quad . \end{aligned}\right\} \tag{7}$$

The following definitions are made for convenience in discussing boundary conditions:

$$\left.\begin{aligned} N_{x\nu} &= N_x\ell + N_{xy}m \quad , \quad N_{y\nu} = N_{xy}\ell + N_y m \quad , \\ M_{x\nu} &= M_x\ell + M_{xy}m \quad , \quad M_{y\nu} = M_{xy} + M_y m \quad , \\ M_\nu &= M_{x\nu}\ell + M_{y\nu}m \quad \text{and} \quad M_{\nu s} = -M_{x\nu}m + M_{y\nu}\ell \quad . \end{aligned}\right\} \tag{8}$$

The local radius of curvature of the boundary curve will be designated as r where

$$\frac{1}{r} = \frac{d\varphi}{ds} \quad ,$$

and φ is the angle between the tangent to the boundary and the x-axis. The quantities r and φ are illustrated in Figure 3.

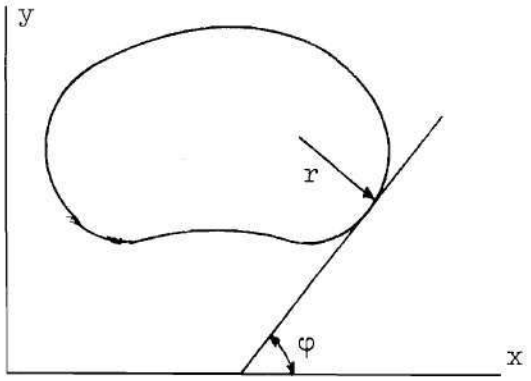

Figure 3. Local Radius of Curvature

The boundary conditions on the function w may be either*

a) the transverse displacement is prevented,

$$w = 0 \quad , \tag{9a}$$

or b) the effective shear in the transverse direction is zero,

$$-D \left\{ \frac{\partial}{\partial \nu} \left(\nabla^2 w \right) + \left(1 - \mu \right) \frac{\partial}{\partial s} \left[\frac{\partial}{\partial \nu} \left(\frac{\partial w}{\partial s} \right) \right] \right\} + \left(\bar{N}_{x\nu} \frac{\partial w}{\partial x} + \bar{N}_{y\nu} \frac{\partial w}{\partial y} \right) = 0 \quad , \tag{9b}$$

and either c) the rotation about the in-plane tangent vector is prevented,

$$\frac{\partial w}{\partial \nu} = 0 \quad , \tag{9c}$$

or d) the moment about the in-plane tangent vector is zero, i.e., $M_\nu = 0$,

$$- D \left[\frac{\partial^2 w}{\partial \nu^2} + \mu \left(\frac{\partial^2 w}{\partial s^2} + \frac{1}{r} \frac{\partial w}{\partial \nu} \right) \right] = 0 \quad . \tag{9d}$$

Along with the above boundary conditions, in-plane boundary conditions must also be provided. Since it is appropriate to include these conditions in conjunction with the derivation of the compatibility relations, a discussion of them will be introduced later.

There are two possible formulations of the plate problem. These are either a displacement or a stress formulation. In a displacement

---

* In the problems of interest the boundary conditions on w are homogeneous. This restriction is not necessary in the development which follows.

formulation the governing differential Equations (5a) together with the appropriate boundary conditions from Equations (9) and the in-plane boundary conditions are all expressed in terms of the mid-surface displacements u, v, and w. This system of equations is complete for either simply or multiply connected plates. To complete the solution of a problem, the strains are obtained from the kinematic relations (1) and (2), and the stresses from the constitutive relations (3).

For some problems, the displacement formulation may be too difficult or inconvenient to use. It may then be more appropriate to solve for the in-plane stresses rather than for the displacements. One way of solving for the stresses is to introduce Airy's stress function, as defined in Equations (4), into the equilibrium Equation (5a). This results in the first two equilibrium equations being satisfied exactly. After making use of Equations (6) the third equilibrium equation becomes

$$D\nabla^4 w = hF_{,yy}w_{,xx} + hF_{,xx}w_{,yy} - 2hF_{,xy}w_{,xy} \qquad (10)$$

$$+ h(\Phi w_{,x})_{,x} + h(\Phi w_{,y})_{,y}$$

It is noted that both F and w appear in the last equation; thus, additional information is required to obtain a solution. The additional information comes from the equation which requires that the associated stress field be one which will result in a compatible state of deformation. This equation is obtained by eliminating u and v from Equations (1). As will be seen, satisfaction of the resulting equation,

though necessary and sufficient for compatibility in a simply connected plate, is only necessary in a multiply connected plate.

Derivation of Compatibility Requirements

This development will parallel that of Mindlin and Salvadori [58], who examined the compatibility requirements for plates with linear kinematic relations. Let Γ be any closed curve in a plate (the plate may be simply or multiply connected) and examine the following line integrals around this curve:

$$\int_\Gamma du \quad \text{and} \quad \int_\Gamma dv \quad . \tag{11}$$

The first of these integrals is expanded in the form

$$\int_\Gamma du = \int_\Gamma \left(u_{,x} dx + u_{,y} dy \right) \quad . \tag{12}$$

Defining the infinitesimal rotation as

$$\omega_z = \frac{1}{2} \left(v_{,x} - u_{,y} \right) \quad , \tag{13}$$

and by noting from the last of Equations (1) that

$$v_{,x} = \gamma_{xy} - u_{,y} - w_{,x} w_{,y} \quad , \tag{14}$$

it is possible to solve for $u_{,y}$ in the form

$$u,_y = \frac{1}{2}\gamma_{xy} - \frac{1}{2}w,_x w,_y - \omega_z \quad . \tag{15}$$

Thus, substitution of (15) into (12) yields

$$\int_\Gamma du = \int_\Gamma \left[u,_x dx + \left(\frac{1}{2}\gamma_{xy} - \frac{1}{2}w,_x w,_y - \omega_x\right)dy\right] \quad . \tag{16}$$

Substituting from the first of Equations (1) for $u,_x$ yields

$$\int_\Gamma du = \int_\Gamma \left[e_x dx + \frac{1}{2}\gamma_{xy}dy\right] - \frac{1}{2}\int_\Gamma \left[\left(w,_x\right)^2 dx + w,_x w,_y dy\right] \tag{17}$$

$$- \int_\Gamma \omega_z dy \quad .$$

The last integral of Equation (17) can be written as

$$\int_\Gamma \omega_z dy = y_r \int_\Gamma d\omega_z - \int_\Gamma y d\omega_z \quad , \tag{18}$$

where y_r is the y coordinate of the starting point of integration on Γ. The differential $d\omega_z$ may be expanded as

$$\int_\Gamma d\omega_z = \int_\Gamma \left(\frac{\partial \omega_z}{\partial x}\,dx + \frac{\partial \omega_z}{\partial y}\,dy\right) \quad . \tag{19}$$

Using the definition of ω_z,

$$\int_\Gamma \frac{\partial \omega_z}{\partial x}\, dx = \int_\Gamma \frac{1}{2}\left(v_{,x} - u_{,y}\right)_{,x}\, dx \quad . \tag{20}$$

Substituting for $v_{,x}$ from Equation (14) then gives

$$\int_\Gamma \frac{\partial \omega_z}{\partial x}\, dx = \int_\Gamma \left[\frac{1}{2}\gamma_{xy,x} - u_{,yx} - \frac{1}{2}\left(w_{,x}w_{,y}\right)_{,x}\right]dx \quad . \tag{21}$$

Requiring that the second derivatives of the displacements be continuous permits the order of differentiation in Equation (21) to be interchanged. It is then possible to substitute for $u_{,x}$ from the first of Equations (1). Thus

$$\int_\Gamma \frac{\partial \omega_z}{\partial x}\, dx = \int_\Gamma \left\{\frac{1}{2}\gamma_{xy,x} - e_{x,y} + \frac{1}{2}\left[\left(w_{,x}\right)^2_{,y} - \left(w_{,x}w_{,y}\right)_{,x}\right]\right\} dx \quad . \tag{22}$$

A similar procedure yields

$$\int_\Gamma \frac{\partial \omega_z}{\partial y}\, dy = \int_\Gamma \left\{e_{y,x} - \frac{1}{2}\gamma_{xy,y} - \frac{1}{2}\left[\left(w_{,y}\right)^2_{,x} - \left(w_{,x}w_{,y}\right)_{,y}\right]\right\} dy \quad . \tag{23}$$

Substitution of (22) and (23) into (19) results in

$$\int_\Gamma d\omega_z = \int_\Gamma \left[\left(\frac{1}{2}\gamma_{xy,x} - e_{x,y}\right)dx + \left(e_{y,x} - \frac{1}{2}\gamma_{xy,y}\right)dy\right] \tag{24}$$

$$+ \frac{1}{2}\int_\Gamma \left\{\left[\left(w_{,x}\right)^2_{,y} - \left(w_{,x}w_{,y}\right)_{,x}\right]dx - \left[\left(w_{,y}\right)^2_{,x} - \left(w_{,x}w_{,y}\right)_{,y}\right]dy\right\} \quad .$$

The multiplication of $d\omega_z$ by y could be carried through the exact same procedure to obtain

$$\int_\Gamma y d\omega_z = \int_\Gamma y \left[\left(\frac{1}{2} \gamma_{xy,x} - e_{x,y}\right)dx + \left(e_{y,x} - \frac{1}{2} \gamma_{xy,y}\right)dy\right] \tag{25}$$

$$+ \frac{1}{2} \int_\Gamma y \left\{\left[\left(w_{,x}\right)_{,y}^2 - \left(w_{,x}w_{,y}\right)_{,x}\right]dx - \left[\left(w_{,y}\right)_{,x}^2 - \left(w_{,x}w_{,y}\right)_{,y}\right]dy \right\} .$$

Finally, it is possible to write from Equations (17), (18), (24) and (25) that

$$\int_\Gamma du = \int_\Gamma \left[e_x dx + \frac{1}{2} \gamma_{xy} dy\right] - \frac{1}{2} \int_\Gamma \left[\left(w_{,x}\right)^2 dx + w_{,x}w_{,y}dy\right] \tag{26}$$

$$+ \int_\Gamma \left(y - y_r\right) \left[\frac{1}{2} \gamma_{xy,x} - e_{x,y}\right)dx + \left(e_{y,x} - \frac{1}{2} \gamma_{xy,y}\right)dy\right]$$

$$+ \frac{1}{2} \int \left(y - y_r\right) \left\{\left[\left(w_{,x}\right)_{,y}^2 - \left(w_{,x}w_{,y}\right)_{,x}\right]dx - \left[\left(w_{,y}\right)_{,x}^2 - \left(w_{,x}w_{,y}\right)_{,y}\right]dy\right\} .$$

Before proceeding any further an important feature of Green's Theorem should be pointed out. Green's Theorem as normally presented is valid only in simply connected regions but can be extended so as to be useful for multiply connected regions by artificially cutting the region. Using this artifice, Green's Theorem can be stated as

$$\int_{\Gamma}\left(Pdx + Qdy\right) = \int\int_{R}\left(\frac{\partial Q}{\partial x} - \frac{\partial P}{\partial y}\right)dxdy - \sum_{i}\int_{\Gamma_i}\left(Pdx + Qdy\right) \quad , \qquad (27)$$

where the summation on i is taken over all internal boundaries that may be enclosed in Γ and R is the solid region enclosed in Γ. It should be noted that all the line integrals should be taken in the positive sense; i.e., with the external normal always to the right as the tangential coordinate is traversed in an increasing sense.

In applying Equation (27) to Equation (26) let

$$P = P_1 + P_2$$

and

$$Q = Q_1 + Q_2$$

where

$$\left.\begin{aligned} P_1 &= e_x + \left(y - y_r\right)\left(\tfrac{1}{2}\gamma_{xy,x} - e_{x,y}\right) \quad , \\ Q_1 &= \tfrac{1}{2}\gamma_{xy} + \left(y - y_r\right)\left(e_{y,x} - \tfrac{1}{2}\gamma_{xy,y}\right) \quad , \\ P_2 &= -\tfrac{1}{2}\left\{\left(w_{,x}\right)^2 - \left(y - y_r\right)\left[\left(w_{,x}\right)^2_{,y} - \left(w_{,x}w_{,y}\right)_{,x}\right]\right\} \quad , \\ Q_2 &= -\tfrac{1}{2}\left\{\left(w_{,x}w_{,y}\right) + \left(y - y_r\right)\left[\left(w_{,y}\right)^2_{,x} - \left(w_{,x}w_{,y}\right)_{,y}\right]\right\} \quad . \end{aligned}\right\} \qquad (28)$$

Then Equation (27) becomes

$$\int_{\Gamma} du = \int_{\Gamma} Pdx + Qdy = \int\int_{R}\left(\frac{\partial Q_1}{\partial x} - \frac{\partial P_1}{\partial y}\right)dxdy \qquad (29)$$

$$+ \int\int_{R}\left(\frac{\partial Q_2}{\partial x} - \frac{\partial P_2}{\partial y}\right)dxdy - \sum_i \int_{\Gamma_i} du \quad .$$

By differentiation of Equations (28), it can be shown that

$$\left(Q_{1,x} - P_{1,y}\right) = \left(y - y_r\right)\left(e_{y,xx} + e_{x,yy} - \gamma_{xy,xy}\right) \quad , \qquad (30)$$

and

$$\left(Q_{2,x} - P_{2,y}\right) = -\left(y - y_r\right)\left[\left(w_{,xy}\right)^2 - w_{,xx}w_{,yy}\right] \quad . \qquad (31)$$

Substituting Equations (30) and (31) into (29) gives

$$\int_{\Gamma} du = \int\int_{R}\left(y - y_r\right)\left[\left(e_{y,xx} - e_{x,yy} - \gamma_{xy,xy}\right)\right. \qquad (32)$$

$$\left. - \left(w_{,xy}\right)^2 + w_{,xx}w_{,yy}\right]dxdy - \sum_i \int_{\Gamma_i} du \quad .$$

If the second integral of (11) is evaluated, the result is

$$\int_{\Gamma} dv = \int\int_{R} \left(x_r - x\right)\left[\left(e_{x,yy} + e_{y,xx} - \gamma_{xy,xy}\right)\right. \tag{33}$$

$$\left. - \left(w,_{xy}\right)^2 + w,_{xx}w,_{yy}\right]dxdy - \sum_i \int_{\Gamma_i} dv \quad .$$

If the plate is simply connected, a necessary and sufficient condition for a single valued displacement field would be that

$$e_{x,yy} + e_{y,xx} - \gamma_{xy,xy} = \left(w,_{xy}\right)^2 - w,_{xx}w,_{yy} \quad . \tag{34}$$

As expected, Equation (34) is the same result as would have been obtained by eliminating u and v from Equation (1). However, the benefit of the derivation obtained herein is that the sufficiency of Equation (34) has been proven.

If the plate is multiply connected, it is still necessary that Equation (34) be satisfied within the plate. This condition is no longer sufficient to insure compatible deformations, however. It is now also necessary that each of the line integrals

$$\int_{\Gamma_i} du \quad \text{and} \quad \int_{\Gamma_i} dv$$

vanishes. The condition that they vanish separately comes about since the original curve Γ could be chosen to arbitrarily include any of the internal boundaries, in any combination. In a multiply connected plate, it is possible that a displacement known as a dislocation may be present.

Thus, the displacements need not be single valued from a physical argument. Calling the amplitude of the dislocation in u for the i^{th} boundary a_i, then

$$a_i = \int_{\Gamma_i} du \qquad (i = 1, 2, \ldots n) \quad .$$

In a manner exactly analogous to the derivation for $\int_\Gamma du$, it may be seen from Equation (26) that

$$a_i = \int_{\Gamma_i} du = \int_{\Gamma_i} \left[e_x + \left(y - y_i\right)\left(\frac{1}{2}\gamma_{xy,x} - e_{x,y}\right)\right] dx \tag{35}$$

$$+ \int_{\Gamma_i} \left[\frac{1}{2}\gamma_{xy} + \left(y - y_i\right)\left(e_{y,x} - \frac{1}{2}\gamma_{xy,y}\right)\right] dy$$

$$- \frac{1}{2}\int_{\Gamma_i} \left\{\left(w_{,x}\right)^2 - \left(y - y_i\right)\left[\left(w_{,x}\right)^2_{,y} - \left(w_{,x}w_{,y}\right)_{,x}\right]\right\} dx$$

$$- \frac{1}{2}\int_{\Gamma_i} \left\{w_{,x}w_{,y} + \left(y - y_i\right)\left[\left(w_{,y}\right)^2_{,x} - \left(w_{,x}w_{,y}\right)_{,y}\right]\right\} dy$$

where y_i is the starting point of integration on the i^{th} boundary. If, in addition, a rotational dislocation, c_i is defined such that

$$c_i = \int_{\Gamma_i} d\omega_z \quad ,$$

then it follows from Equation (24) that

$$c_i = \int_{\Gamma_i} d\omega_z = \int_{\Gamma_i} \left[\left(\frac{1}{2}\gamma_{xy,x} - e_{x,y}\right)dx + \left(e_{y,x} - \frac{1}{2}\gamma_{xy,y}\right)dy\right] \tag{36}$$

$$+ \frac{1}{2}\int_{\Gamma_i} \left\{\left[\left(w_{,x}\right)^2_{,y} - \left(w_{,x}w_{,y}\right)_{,x}\right]dx - \left[\left(w_{,y}\right)^2_{,x} - \left(w_{,x}w_{,y}\right)_{,y}\right]dy\right\} \quad .$$

It is observed that Equation (35) can be rewritten as

$$a_i + y_i c_i = \int_{\Gamma_i} \left[e_x + y\left(\frac{1}{2}\gamma_{xy,x} - e_{x,y}\right)\right]dx \tag{37}$$

$$+ \int_{\Gamma_i} \left[\frac{1}{2}\gamma_{xy} + y\left(e_{y,x} - \frac{1}{2}\gamma_{xy,y}\right)\right]dy$$

$$- \frac{1}{2}\int_{\Gamma_i} \left\{\left(w_{,x}\right)^2 - y\left[\left(w_{,x}\right)^2_{,y} - \left(w_{,x}w_{,y}\right)_{,x}\right]\right\}dx$$

$$- \frac{1}{2}\int_{\Gamma_i} \left\{w_{,x}w_{,y} + y\left[\left(w_{,y}\right)^2_{,x} - \left(w_{,x}w_{,y}\right)_{,y}\right]\right\} dy \quad .$$

Similarly, if a dislocation in the displacement v of magnitude b_i

is allowed, then

$$b_i = \int_{\Gamma_i} dv = \int_{\Gamma_i} \left(\frac{\partial v}{\partial x}\, dx + \frac{\partial v}{\partial y}\, dy \right) \quad .$$

With a similar derivation as with a_i it can be shown that

$$b_i - x_i c_i = \int_{\Gamma_i} \left[\frac{1}{2}\gamma_{xy} + x\left(e_{x,y} - \frac{1}{2}\gamma_{xy,x} \right) \right] dx \tag{38}$$

$$+ \int_{\Gamma_i} \left[e_y + x\left(\frac{1}{2}\gamma_{xy,y} - e_{y,x} \right) \right] dy$$

$$- \frac{1}{2} \int_{\Gamma_i} \left\{ w_{,x} w_{,y} + x \left[\left(w_{,x} \right)_{,y}^{2} - \left(w_{,x} w_{,y} \right)_{,x} \right] \right\} dx$$

$$- \frac{1}{2} \int_{\Gamma_i} \left\{ \left(w_{,y} \right)^2 - x \left[\left(w_{,y} \right)_{,x}^{2} - \left(w_{,x} w_{,y} \right)_{,y} \right] \right\} dy \quad .$$

If the terms on the right hand side of Equation (37) which are not multiplied by y, and those of on the right hand side of Equation (38) which are not multiplied by x are integrated by parts, then

$$\int_{\Gamma_i} \left\{ \left[e_x - \frac{1}{2}\left(w_{,x} \right)^2 \right] dx + \left[\frac{1}{2}\gamma_{xy} - \frac{1}{2} w_{,x} w_{,y} \right] dy \right\} \tag{39}$$

$$= x\left[e_x - \frac{1}{2}\left(w_{,x} \right)^2 \right] \Big|_0^0 + y \left[\frac{1}{2}\gamma_{xy} - \frac{1}{2} w_{,x} w_{,y} \right] \Big|_0^0$$

$$- \int_{\Gamma_i} \left[x \left(e_{x,x} - w_{,x} w_{,xx} \right) dx + y \left(\frac{1}{2} \gamma_{xy,y} - \frac{1}{2} w_{,x} w_{,yy} - \frac{1}{2} w_{,y} w_{,xy} \right) dy \right]$$

$$- \int_{\Gamma_i} \left[x \left(e_{x,y} - w_{,x} w_{,xy} \right) dy + y \left(\frac{1}{2} \gamma_{xy,x} - \frac{1}{2} w_{,x} w_{,xy} - \frac{1}{2} w_{,xx} w_{,y} \right) dx \right] ,$$

and

$$\int_{\Gamma_i} \left\{ \left[\frac{1}{2} \gamma_{xy} - \frac{1}{2} w_{,x} w_{,y} \right] dx + \left[e_y - \frac{1}{2} \left(w_{,y} \right)^2 \right] dy \right\} \tag{40}$$

$$= x \left[\frac{1}{2} \gamma_{xy} - \frac{1}{2} w_{,x} w_{,y} \right] \Big|_0^0 + y \left[e_y - \frac{1}{2} \left(w_{,y} \right)^2 \right] \Big|_0^0$$

$$- \int_{\Gamma_i} \left[x \left(\frac{1}{2} \gamma_{xy,x} - \frac{1}{2} w_{,x} w_{,xy} - \frac{1}{2} w_{,xx} w_{,y} \right) dx + y \left(e_{y,y} - w_{,y} w_{,yy} \right) dy \right]$$

$$- \int_{\Gamma_i} \left[x \left(\frac{1}{2} \gamma_{xy,y} - \frac{1}{2} w_{,x} w_{,yy} - \frac{1}{2} w_{,xy} w_{,y} \right) dy + y \left(e_{y,x} - w_{,y} w_{,xy} \right) dx \right]$$

The strains and the displacements in w are considered to be continuous and smooth around each contour. The terms outside the integrals in Equations (39) and (40) may then be discarded, and Equation (37) becomes

$$a_i + y_i c_i = - \int_{\Gamma_i} \left[\left(y e_{x,y} + x e_{x,x} \right) dx - y \left(e_{y,x} - \gamma_{xy,y} \right) dy \right. \tag{41}$$

$$- \int_{\Gamma_i} xe_{x,y}dy + \int_{\Gamma_i} \left[yw,_x w,_{xy} + xw,_x w,_{xx} \right) dx + \left(yw,_x w,_{yy} + xw,_x w,_{xy} \right) dy \Big] \quad .$$

Equation (38) becomes

$$b_i - x_i c_i = \int_{\Gamma_i} \left[x \left(e_{x,y} - \gamma_{xy,x} \right) dx - \left(xe_{y,x} + ye_{y,y} \right) dy \right] \tag{42}$$

$$- \int_{\Gamma_i} ye_{y,x}dx + \int_{\Gamma_i} \Big[\left(yw,_y w,_{xy} + xw,_y w,_{xx} \right) dx$$

$$+ \left(xw,_y w,_{xy} + yw,_y w,_{yy} \right) dy \Big] \quad .$$

Thus, in addition to the condition stated in Equation (34), Equations (36), (41), and (42) are auxiliary conditions which must be satisfied on each internal boundary of the plate. All of these equations must be satisfied to insure single valued displacements. It should, of course, be noted that the possibility of non-zero dislocations on a cut boundary has been included in the development.

Stress Formulation of Plate Problem

A stress formulation of the problem can be obtained by requiring that the governing equations (i.e., the equilibrium equation and the compatibility equation) as well as the boundary conditions and the auxiliary conditions on each boundary all be expressed in terms of the stress function, F. Equation (10) has already expressed the

equilibrium equation in the proper form for the stress formulation. The compatibility equation is obtained in terms of F by substituting for the strains in terms of stresses and then replacing the stresses by appropriate derivatives of F. The equation thus obtained is

$$\nabla^4 F = - E \alpha \nabla^2 T - (1 - \mu)\nabla^2 \Phi + E\left[\left(w,_{xy}\right)^2 - w,_{xx} w,_{yy}\right] \quad . \quad (43)$$

The in-plane boundary conditions for stress problems are

$$\bar{N}_{x\nu} = N_x \ell + N_{xy} m \quad \text{and} \quad \bar{N}_{y\nu} = N_{xy} \ell + N_y m \quad . \quad (44)$$

where $\bar{N}_{x\nu}$ and $\bar{N}_{y\nu}$ are the components of the resultant stress vector in the x and y directions respectively. The direction cosines ℓ and m can be expressed as

$$\ell = \frac{dy}{ds} \quad \text{and} \quad m = - \frac{dx}{ds} \quad , \quad (45)$$

where s is the tangential coordinate. It should also be realized that

$$\ell = \frac{dx}{d\nu} = \frac{dy}{ds} \quad \text{and} \quad m = \frac{dy}{d\nu} = - \frac{dx}{ds} \quad , \quad (46)$$

where ν is the normal coordinate of the boundary. The boundary conditions can be expressed in terms of the stress function, F, as

$$\bar{N}_{x\nu} = h\left(F,_{yy} + \Phi \right) \frac{dy}{ds} + h\left(F,_{xy} \right) \frac{dx}{ds} = h \frac{\partial}{\partial s} \left(F,_{y} \right) + h\Phi\ell \quad . \tag{47}$$

and

$$\bar{N}_{y\nu} = - h \left(F,_{xy} \right) \frac{dy}{ds} - h\left(F,_{xx} + \Phi \right) \frac{dx}{ds} = - h \frac{\partial}{\partial s} \left(F,_{x} \right) + h\Phi m \quad . \tag{48}$$

A coordinate system reference point may be chosen on each boundary such that $s = 0$ at this point. Then integration of Equations (47) and (48) from $s = 0$ to any arbitrary point results in

$$F,_{y} \Big|_{\Gamma_i} = \frac{1}{h} \int_0^s \bar{N}_{x\nu} \, ds - \int_0^s \Phi\ell \, ds + \beta_i \tag{49}$$

and

$$F,_{x} \Big|_{\Gamma_i} = \frac{1}{h} \int_0^s \bar{N}_{y\nu} \, ds + \int_0^s \Phi m \, ds + \alpha_i \quad , \tag{50}$$

where α_i and β_i are constants which in general are different for each boundary $\Gamma_i (i = 0, 1, 2, \ldots, n)$. The boundary Γ_0 will be taken as the external boundary while n designates the number of internal boundaries. If the boundary tractions and the boundary force potential are known, the integrals of Equations (49) and (50) can be evaluated.

Noticing that

$$F,_s = \frac{\partial F}{\partial x}\,\frac{dx}{ds} + \frac{\partial F}{\partial y}\,\frac{dy}{ds} \quad ,$$

it is possible to evaluate F at any point on a boundary by integration. Thus,

$$F\Big|_{\Gamma_i} = \int_0^s F,_s \, ds + \gamma_i \quad .$$

Let the integrals of Equations (49) and (50) now be defined as

$$\left.\begin{aligned} A_i &= -\frac{1}{h}\int_0^s \bar{N}_{y\nu}\, ds + \int_0^s \Phi m\, ds \quad . \\ \text{and} \qquad B_i &= \frac{1}{h}\int_0^s \bar{N}_{x\nu}\, ds - \int_0^s \Phi \ell\, ds \quad . \end{aligned}\right\} \qquad (51)$$

Then

$$F,_s\Big|_{\Gamma_i} = \left(A_i + \alpha_i\right)\frac{dx}{ds} + \left(B_i + \beta_i\right)\frac{dy}{ds} \quad , \qquad (52)$$

and thus

$$F\Big|_{\Gamma_i} = \int_0^s \left(B_i\ell - A_i m\right)ds + \alpha_i x + \beta_i y + \gamma_i \quad . \qquad (53)$$

It may be noted that

$$F,_{\nu} = F,_{x} \frac{dx}{d\nu} + F,_{y} \frac{dy}{d\nu} \quad ,$$

so that

$$F,_{\nu} \Big|_{\Gamma_i} = A_i \ell + B_i m + \alpha_i \ell + \beta_i m \quad . \tag{54}$$

Equations (53) and (54) thus represent the boundary conditions of F which must be satisfied when edge tractions are specified on the boundaries. These relations apply whether the plate is simply or multiply connected. If it is simply connected the boundary conditions could be taken as

$$\left.\begin{aligned} F \Big|_{\Gamma_0} &= \int_0^s \left(B_0 \ell - A_0 m\right) ds \\ \text{and} \\ F,_{\nu} \Big|_{\Gamma_0} &= A_0 \ell + B_0 m \end{aligned}\right\} \tag{55}$$

The constants α_0, β_0, and γ_0 could be set equal to zero or, for that matter, to any arbitrary constant since their presence does not affect in any way the values of the stresses. In an (n + 1) connected slice, however, three additional conditions are required on each boundary in order to determine the 3n constants α_i, β_i, and γ_i (i = 1, 2, ..., n).

These conditions are the 3n auxiliary conditions derived to insure compatibility. The auxiliary conditions are obtained in terms of F by use of the constitutive relations and the definition of the stress function. These equations become

$$\int_{\Gamma_i} \frac{\partial(\nabla^2 F)}{\partial \nu}\, ds = Ec_i - (1-\mu)\int_{\Gamma_i} \frac{\partial \Phi}{\partial \nu}\, ds - E\alpha \int_{\Gamma_i} \frac{\partial T}{\partial \nu}\, ds \qquad (56)$$

$$+ \frac{E}{2}\int_{\Gamma_i} \left[m\left(w_{,x} w_{,xy} - w_{,y} w_{,xx} \right) - \ell \left(w_{,x} w_{,yy} - w_{,y} w_{,xy} \right) \right] ds \quad ,$$

and

$$\int_{\Gamma_i} \left[y\, \frac{(\partial(\nabla^2 F)}{\partial \nu} - x\, \frac{\partial(\nabla^2 F)}{\partial s} \right] ds = E\left(a_i + y_i\, c_i \right) \qquad (57)$$

$$- \left(1-\mu\right)\int_{\Gamma_i} \left(y\, \frac{\partial \Phi}{\partial \nu} - x\, \frac{\partial \Phi}{\partial s} \right) ds - E\alpha \int_{\Gamma_i} \left(y\, \frac{\partial T}{\partial \nu} - x\, \frac{\partial T}{\partial s} \right) ds$$

$$- \frac{(1+\mu)}{h}\int_{\Gamma_i} \left(\bar{N}_{y\nu} - h\Phi m \right) ds$$

$$- E\int_{\Gamma_i} \left[m\left(yw_{,x} w_{,xy} + xw_{,x} w_{,xx} \right) - \ell \left(yw_{,x} w_{,yy} + xw_{,x} w_{,xy} \right) \right] ds \quad ,$$

and

$$\int_{\Gamma_i} \left[y \frac{\partial(\nabla^2 F)}{\partial s} + x \frac{\partial(\nabla^2 F)}{\partial \nu} \right] ds = - E\left(b_i - x_i\, c_i\right) \qquad (58)$$

$$- (1 - \mu) \int_{\Gamma_i} \left(y \frac{\partial \Phi}{\partial s} + x \frac{\partial \Phi}{\partial \nu} \right) ds \; - E\alpha \int_{\Gamma_i} \left(y \frac{\partial T}{\partial s} + x \frac{\partial T}{\partial \nu} \right) ds$$

$$- \frac{(1 + \mu)}{h} \int_{\Gamma_i} \left(\bar{N}_{x\nu} - h\Phi \ell \right) ds$$

$$- E \int_{\Gamma_i} \left[m\left(y w_{,y} w_{,xy} + x w_{,y} w_{,xx} \right) - \ell \left(x w_{,y} w_{,xy} + y w_{,y} w_{,yy} \right) \right] ds \quad ,$$

where (56), (57) and (58) are for i = 1, 2, ...,n. The form of Equations (56), (57) and (58) could be shortened slightly by rewriting the last term in each of them. The last term of (56) becomes

$$- \frac{E}{2} \int_{\Gamma_i} \left(w_{,x} \right)^2 \left(\frac{w_{,y}}{w_{,x}} \right)_{,s} ds \quad ,$$

that of (57) becomes

$$- E \int_{\Gamma_i} \left(w_{,x} \right) \left[x \left(w_{,x} \right)_{,s} + y \left(w_{,y} \right)_{,s} \right] ds \quad ,$$

and finally the last term of (58) becomes

$$+ E \int_{\Gamma_i} w,_y \left[x\left(w,_x\right),_s + y\left(w,_y\right),_s \right] ds \quad .$$

The total stress formulation of the coupled nonlinear plate problem is now complete. By studying the governing equations, the boundary conditions and the auxiliary conditions, it can be seen that the solution of a particular problem can involve a substantial amount of effort.

Modeling and Nondimensionalization

The possibility of deducing information of a general nature from tests or experiments performed on specimens of a particular material is of practical interest. To make use of test results, however, an experiment must be properly designed, i.e., all parameters which influence the behavior of interest must be properly taken into account. In structural mechanics the parameters usually include the specimen geometry, the nature of the loading, and the material properties.

J. N. Goodier and W. T. Thomson [59] have presented a thorough discussion of the application of modeling or similarity principles to structural models. They point out in this reference that the use of similarity principles is not limited to simple linear systems. It is significant that the model chosen for examination in this reference was a thin sheet with a central hole. The models which were, of course, multiply connected were loaded into the large deformation range by shear tractions on the outer boundary. Goodier and Thomson used similarity principles to analyze their test results. It is of interest to note that they were able to deduce from dimensional analysis

considerations that although materials with different values of Young's modulus could be modeled, the values of Poisson's ratio could not differ.

Although modeling laws can be deduced by use of dimensional analysis, an examination of the governing differential equations can provide additional understanding of behavior which leads to modeling restrictions.

In order to examine the governing equations for the plate problem it is convenient to introduce the following set of nondimensional parameters:

$$\bar{\nabla}^2 = a^2 \nabla^2 \qquad \bar{x} = \frac{x}{a} \qquad \bar{w} = \frac{w}{h}$$

$$\bar{F} = \frac{F}{Eh^2} \qquad \bar{y} = \frac{y}{a} \qquad \bar{\alpha}_i = \frac{a}{Eh^2}\alpha_i$$

$$\bar{T} = \alpha\left(\frac{a}{h}\right)^2 T \qquad \bar{s} = \frac{s}{a} \qquad \bar{\beta}_i = \frac{a}{Eh^2}\beta_i$$

$$\bar{\Phi} = \frac{a^2}{Eh^2}\Phi \qquad \bar{\nu} = \frac{\nu}{a} \qquad \bar{\gamma}_i = \frac{a^2}{Eh^2}\gamma_i$$

$$\bar{A}_i = \frac{a}{Eh^2}A_i \qquad \bar{B}_i = \frac{a}{Eh^2}B_i \qquad \bar{r} = \frac{r}{a}$$

$$\bar{b}_i = \frac{a}{h^2}b_i \qquad \bar{a}_i = \frac{a}{h^2}a_i \qquad \bar{c}_i = \frac{a^2}{h^2}c_i$$

$$\bar{\bar{N}}_{x\nu} = \frac{a^2}{Eh^3}\bar{N}_{x\nu} \qquad \bar{\bar{N}}_{y\nu} = \frac{a^2}{Eh^3}\bar{N}_{y\nu}$$

In these relations "a" is a characteristic length in the problem and "h" is the plate thickness. Use of the above relations enables the governing equations to be written in a nondimensional form. The compatibility equation becomes

$$\bar{\nabla}^4 \bar{F} = - \bar{\nabla}^2 \bar{T} - (1 - \mu)\, \bar{\nabla}^2 \bar{\Phi} + \left(\bar{w}_{,\bar{x}\bar{y}}\right)^2 - \bar{w}_{,\bar{x}\bar{x}}\, \bar{w}_{,\bar{y}\bar{y}} \quad . \tag{60}$$

The in-plane boundary conditions in nondimensional form are

$$\left.\begin{aligned} \bar{F}\,\big|_{\Gamma_i} &= \int_0^{\bar{s}} \left(\bar{B}_i \ell - \bar{A}_i m\right) d\bar{s} + \bar{\alpha}_i\, \bar{x} + \bar{\beta}_i \bar{y} + \bar{\gamma}_i \quad , \\ \text{and} \qquad & \\ \bar{F}_{,\bar{\nu}}\,\big|_{\Gamma_i} &= \bar{A}_i \ell + \bar{B}_i m + \bar{\alpha}_i \ell + \bar{\beta}_i m \quad , \end{aligned}\right\} \tag{61}$$

where i = 0, 1, 2, ...,n in Equation (61). Similarly, the auxiliary conditions becomes

$$\int_{\Gamma_i} \frac{\partial(\bar{\nabla}^2 \bar{F})}{\partial \bar{\nu}}\, d\bar{s} = \bar{c}_i - (1 - \mu) \int_{\Gamma_i} \frac{\partial \bar{\Phi}}{\partial \bar{\nu}}\, d\bar{s} - \int_{\Gamma_i} \frac{\partial \bar{T}}{\partial \bar{\nu}}\, d\bar{s} \tag{62}$$

$$- \int_{\Gamma_i} \left(\bar{w}_{,\bar{x}}\right)^2 \left(\frac{\bar{w}_{,\bar{y}}}{\bar{w}_{,\bar{x}}}\right)_{,\bar{s}}\, d\bar{s} \quad ,$$

$$\int_{\Gamma_i} \left[\bar{y} \frac{\partial(\bar{\nabla}^2 \bar{F})}{\partial \bar{\nu}} - \bar{x} \frac{\partial(\bar{\nabla}^2 \bar{F})}{\partial \bar{s}} \right] d\bar{s} = \left(\bar{a}_i + \bar{y}_i \bar{c}_i \right) \tag{63}$$

$$- (1 - \mu) \int_{\Gamma_i} \left(\bar{y} \frac{\partial \bar{\Phi}}{\partial \bar{\nu}} - \bar{x} \frac{\partial \bar{\Phi}}{\partial \bar{s}} \right) d\bar{s} - \int_{\Gamma_i} \left(\bar{y} \frac{\partial \bar{T}}{\partial \bar{\nu}} - \bar{x} \frac{\partial \bar{T}}{\partial \bar{s}} \right) d\bar{s}$$

$$- (1 + \mu) \int_{\Gamma_i} \left(\bar{\bar{N}}_{y\nu} - \bar{\Phi} m \right) d\bar{s} - \int_{\Gamma_i} \left(\bar{w}, \bar{x} \right) \left[\bar{x} \left(\bar{w}, \bar{x} \right), \bar{s} + \bar{y} \left(\bar{w}, \bar{y} \right), \bar{s} \right] d\bar{s} \quad ,$$

and finally,

$$\int_{\Gamma_i} \left[\bar{y} \frac{\partial(\bar{\nabla}^2 \bar{F})}{\partial \bar{s}} + \bar{x} \frac{\partial(\bar{\nabla}^2 \bar{F})}{\partial \bar{\nu}} \right] d\bar{s} = - \left(\bar{b}_i - \bar{x}_i \bar{c}_i \right) \tag{64}$$

$$- (1 - \mu) \int_{\Gamma_i} \left(\bar{y} \frac{\partial \bar{\Phi}}{\partial \bar{s}} + \bar{x} \frac{\partial \bar{\Phi}}{\partial \bar{\nu}} \right) d\bar{s} - \int_{\Gamma_i} \left(\bar{y} \frac{\partial \bar{T}}{\partial \bar{s}} + \bar{x} \frac{\partial \bar{T}}{\partial \bar{\nu}} \right) d\bar{s}$$

$$- (1 + \mu) \int_{\Gamma_i} \left(\bar{\bar{N}}_{x\nu} - \bar{\Phi} \ell \right) d\bar{s} + \int_{\Gamma_i} \left(\bar{w}, \bar{y} \right) \left[\bar{x} \left(\bar{w}, \bar{x} \right), \bar{s} + \bar{y} \left(\bar{w}, \bar{y} \right), \bar{s} \right] d\bar{s} \quad ,$$

where i = 1, 2, ..., n in Equations (62), (63), and (64). Nondimensionalization of the transverse equilibrium Equation (10) yields

$$\frac{1}{12(1 - \mu^2)} \bar{\nabla}^4 \bar{w} = \bar{F}, \bar{\bar{y}}\bar{\bar{y}} \, \bar{w}, \bar{\bar{x}}\bar{\bar{x}} + \bar{F}, \bar{\bar{x}}\bar{\bar{x}} \, \bar{w}, \bar{\bar{y}}\bar{\bar{y}} - 2\bar{F}, \bar{\bar{x}}\bar{\bar{y}} \, \bar{w}, \bar{\bar{x}}\bar{\bar{y}} \tag{65}$$

$$+ \left(\bar{\Phi} \bar{w}, \bar{x} \right), \bar{x} + \left(\bar{\Phi} \bar{w}, \bar{y} \right), \bar{y}$$

The possible boundary conditions on $\bar{w}$ are

$$\bar{w} = 0$$

$$\frac{\partial \bar{w}}{\partial \bar{\nu}} = 0 \tag{66}$$

$$- \frac{1}{12(1 - \mu^2)} \left[\frac{\partial^2 \bar{w}}{\partial \bar{\nu}^2} + \mu \left(\frac{\partial^2 \bar{w}}{\partial \bar{s}^2} + \frac{1}{\bar{r}} \frac{\partial \bar{w}}{\partial \bar{\nu}} \right) \right] = 0 \quad ,$$

and

$$- \frac{1}{12(1 - \mu^2)} \left\{ \frac{\partial}{\partial \bar{\nu}} \left(\bar{\nabla}^2 \bar{w} \right) + \left(1 - \mu \right) \frac{\partial}{\partial \bar{s}} \left[\frac{\partial}{\partial \bar{\nu}} \left(\frac{\partial \bar{w}}{\partial \bar{s}} \right) \right] \right\} + \left(\bar{\bar{N}}_{x\nu} \frac{\partial \bar{w}}{\partial \bar{x}} + \bar{\bar{N}}_{y\nu} \frac{\partial \bar{w}}{\partial \bar{y}} \right) = 0 \ .$$

The complete coupled problem has thus been formulated in nondimensional form in Equations (60) through (66). It is now possible to examine the relationship between model and prototype stresses and deflections. Assuming that the conditions of similarity expressed by Goodier and Thomson [59] have been satisfied, the solution satisfying Equations (60) through (66) require that μ be the same for both the model and the prototype in order that they both yield the same solutions for the nondimensionalized, dependent variables. Under certain circumstances the dependence on Poisson's ratio can be eliminated from Equations (60) through (64). It cannot, however, be eliminated from (65) and (66). It may also be seen that the presence of the terms involving $\bar{w}$ in Equations (60) through (64) comes about from the

nonlinearity of the kinematic relations (1). These assumed kinematic relations take into account the possibility of stretching due to large lateral deflections.

If the lateral deflection is small, then the theory reduces to the linear uncoupled theory. That is, the stress state can be determined without a knowledge of the deflection function by Equations (60) through (64) with the $\bar{w}$ terms omitted. The stress will then be independent of Poisson's ratio under the same conditions as those specified by Mindlin and Salvadori [58] for the linear plane stress problem. That is, if all of the following integrals vanish or at least vanish in the combination in which they appear in Equations (60) through (64):

$$\int_{\Gamma_i} \bar{\bar{N}}_{x\nu}\, d\bar{s} \quad ; \quad \int_{\Gamma_i} \bar{\bar{N}}_{y\nu}\, d\bar{s} \quad ;$$

$$\int_{\Gamma_i} \frac{\partial \bar{\Phi}}{\partial \bar{\nu}}\, d\bar{s} \quad ; \quad \int_{\Gamma_i} \bar{\Phi}\ell\, d\bar{s} \quad ; \quad \int_{\Gamma_i} \bar{\Phi} m\, d\bar{s} \quad ;$$

$$\int_{\Gamma_i} \left(\bar{y}\, \frac{\partial \bar{\Phi}}{\partial \bar{\nu}} - \bar{x}\, \frac{\partial \bar{\Phi}}{\partial \bar{s}}\right) d\bar{s} \quad ; \quad \int_{\Gamma_i} \left(\bar{y}\, \frac{\partial \bar{\Phi}}{\partial \bar{s}} + \bar{x}\, \frac{\partial \bar{\Phi}}{\partial \bar{\nu}}\right) d\bar{s} \quad .$$

The first two integrals represent the x and y components of the resultant force on an internal boundary. Mindlin and Salvadori observe that the last two integrals are nonvanishing only if the body force potential has singularities inside Γ_i of the order of a doublet or less.

For the purpose of modeling there are some subtleties of the nondimensionalized relations which should be noted. For instance, if dislocations are introduced into a model, then the corresponding dislocation in the prototype depends not only upon "a" but also upon "h". All other geometric parameters depend only upon "a". It is also noted that body force potential and the boundary tractions depend not only on "a" and "h" in scaling also upon E. The overall result is that the modeling of even fairly simple multiply connected plates is complex.

It should be realized that the restrictions and difficulties of modeling plates, which have been presented through a stress formulation, would have been no less severe if a displacement formulation had been presented. Poisson's ratio appears in the same fashion in each formulation.

Summary

The preceding development demonstrates the complexity of problems involving multiply connected plates. A complete solution would be one in which both the stress fields and the deflection fields are determined. The presence of nonlinearities in the kinematic relations introduces complications which cause the governing equations to be nonlinear and coupled. The compatibility requirements provide a set of three conditions on each internal boundary which must be satisfied in addition to the usual compatibility equation.

By nondimensionalizing the governing equations and boundary conditions, relations are obtained which reveal what requirements must be satisfied in the use of models. In the case in which the temperature is constant throughout the plate and the potential Φ may be omitted, it is possible to use a model constructed of a material which has a different value of Young's modulus than the prototype. The value of Poisson's ratio must, however, be the same for both model and prototype. This is true whether the plate is multiply connected or not. This is not too severe a restriction, however, because it is often possible to select two materials which have the same, or almost the same, value of Poisson's ratio in spite of the fact that the values of Young's modulus are substantially different.

The results to be presented in subsequent chapters were obtained from an analytical and experimental investigation of a problem which is within the class of problems described by the developments of this chapter. Applications and discussions of the results of this chapter will, therefore, be made at appropriate places in this dissertation.

CHAPTER III

STRESS DISTRIBUTIONS AROUND HOLES IN THIN PLATES

In the previous chapter an analysis of the moderately large deflection of a thin sheet with holes was presented. This chapter will examine the stress distributions in thin plates with holes. The development will be based on the assumption that the plate remains flat during tensile loading and thus the stresses can be obtained from the governing equations with w and its derivatives set equal to zero. Body forces and temperature effects will not be included.

For the case of uniaxial tension applied to a plate with traction free holes, it is shown in Chapter II that because the resultant force on each boundary is zero, Poisson's ratio does not appear in the governing equations. It is of interest to note that J. S. Brock [60] has shown that the in-plane boundary displacements around a hole will be independent of Poisson's ratio. Displacements at any other point still depend on the elastic constants. As noted above, however, the stresses in any case can be modeled from one material to another.

The analytic determination of stresses in finite plates is extremely difficult. The stress distribution in finite plates can be determined by the use of photoelastic techniques. It is possible to determine the stress distribution in infinite plates by use of a complex variable formulation of elasticity. Both techniques have been used in this investigation. The presentation of analytic results for

infinite plates and experimental results for finite plates illustrates the features of each method.

Analytic Determination of Stresses in an Infinite Plate with a Hole

The determination of the stresses around a hole in an infinite plate subjected to a uniaxial tension at infinity is most easily accomplished by the method of complex variable stress functions. The development presented follows the work of Sobey [61], and with reference to Milne-Thomson [62] the procedure is straightforward in its approach.

It should be noted that certain simplifications have occurred due to the doubly-symmetric geometry of the hole and the direction of the uniaxial loading being considered. For more general problems the procedure would parallel that presented here, but it would be quite a bit more complicated. The simplifications are pointed out as they occur in the development.

One of the most difficult problems encountered in the complex variable solution is the construction of an acceptable mapping function. Sobey's application of Melentiev's iterative procedure greatly simplifies this task. The mapping function can be taken with as many terms as are necessary to obtain a good representation of the hole shape. This procedure can be easily programmed and it is limited only by the capacity of the computer.

Development of Complex Variable Mapping Function

It is desired to obtain a function

$$Z = m(\zeta) \tag{1}$$

which continuously and uniquely transforms each point in the ζ-plane onto a point in the Z-plane. Furthermore, this function must transform the unit circle in the ζ-plane to a specified closed curve in the Z-plane.

The specified closed curve in the Z-plane represents the boundary of a hole. The hole considered in this development is a slot which is constructed by putting semi-circular ends on a rectangle. Figure 4 shows a typical slot geometry. It is seen from this figure that the slot geometry is completely specified by the end radius, R, and the slot half length, H. The origin of the Z-plane is taken at the geometric center of the slot. The development presented will be valid for any shape hole which is symmetric about the origin and does not contain sharp corners. Since the boundary in the Z-plane has a continuously turning tangent, the transformation $m(\zeta)$ is free of singularities on the boundary and can be represented as a power series in the form

$$Z = m(\zeta) = \sum_{I=1}^{N} B(I)\, \zeta^{3-2I} \quad . \tag{2}$$

The upper limit, N, is in general infinite, but the series can be truncated to give an approximate representation. It should be noted that limiting the highest positive power of ζ to be unity permits the Z- and ζ- planes to be brought into coincidence at infinity. It may also be noted that only odd powers of ζ are permitted in order to

satisfy the symmetry characteristic of the hole.

The significance of mapping from the unit circle is that the transformation to the boundary will be a function only of the angle θ in the ζ-plane. That is, if the boundary is designated as Z_c then

$$Z_c = \sum_{I=1}^{N} \left\{ B(I) \left[\cos(3-2I)\theta + i \sin(3-2I)\theta \right] \right\} \quad . \tag{3}$$

Since

$$\left.\begin{aligned} Z_c &= x_c + i\, y_c \quad , \\ x_c(\theta) &= \sum_{I=1}^{N} B(I) \cos(3-2I)\theta \quad , \\ \text{and} \qquad y_c(\theta) &= \sum_{I=1}^{N} B(I) \sin(3-2I)\theta \quad . \end{aligned}\right\} \tag{4}$$

The coefficients of the mapping function can be obtained by solving a set of 2N equations developed directly from Equations (4) by choosing N points along the boundary of the first quadrant in the Z-plane. For the two points corresponding to the x and y axis intercepts of the boundary, the values of θ must be zero and ninety degrees, respectively. For any other point the corresponding value of θ is an unknown. The B(I)'s are also unknowns. Thus there are

(2N-2) unknowns and the same number of equations (note $y(0) = 0$ and $x(\frac{\pi}{2}) = 0$ are automatically satisfied). This system of equations could be solved but it is an extremely tedious chore since so many of the unknowns are in transcendental functions. An iterative procedure is usually used to solve this set of equations. Heller, Brock, and Bart [36] simplify the procedure somewhat by choosing some of the values of θ and having the x's or y's as unknowns. This simplifies the task somewhat, but it is still a formidable task to solve them if N is very large.

Melentiev's procedure is to transform the original coordinates to a new set which behaves quite differently from the (x,y) set of coordinates. The new complex variable is obtained from the relation

$$\left(\frac{Z}{\zeta}\right)_c = u(\theta) + i\, v(\theta) \tag{5}$$

$$= \sum_{I=1}^{N} B(I) \left[\cos(2-2I)\theta + i \sin(2-2I)\theta\right] \quad .$$

Thus,

$$\left.\begin{aligned} u(\theta) &= \sum_{I=1}^{N} B(I) \cos(2-2I)\theta \\ \text{and} \\ v(\theta) &= \sum_{I=1}^{N} B(I) \sin(2-2I)\theta \quad . \end{aligned}\right\} \tag{6}$$

It should also be noted that

$$\left(\frac{Z}{\zeta}\right)_c = \left(\frac{x + i\,y}{\zeta}\right)_c \tag{7}$$

$$= \left[x_c(\theta) + i\,y_c(\theta)\right]e^{-i\theta}$$

$$= \left[x_c(\theta) + i\,y_c(\theta)\right]\left[\cos\theta - i\sin\theta\right]$$

$$= \left[x_c(\theta)\cos\theta + y_c(\theta)\sin\theta\right]$$

$$+ i\left[y_c(\theta)\cos\theta - x_c(\theta)\sin\theta\right] \quad .$$

Thus,

$$\left.\begin{aligned} u(\theta) &= x_c(\theta)\cos\theta + y_c(\theta)\sin\theta \\ \text{and} \\ v(\theta) &= y_c(\theta)\cos\theta - x_c(\theta)\sin\theta \quad . \end{aligned}\right\} \tag{8}$$

The sketch in Figure 4 illustrates the new set of coordinates.

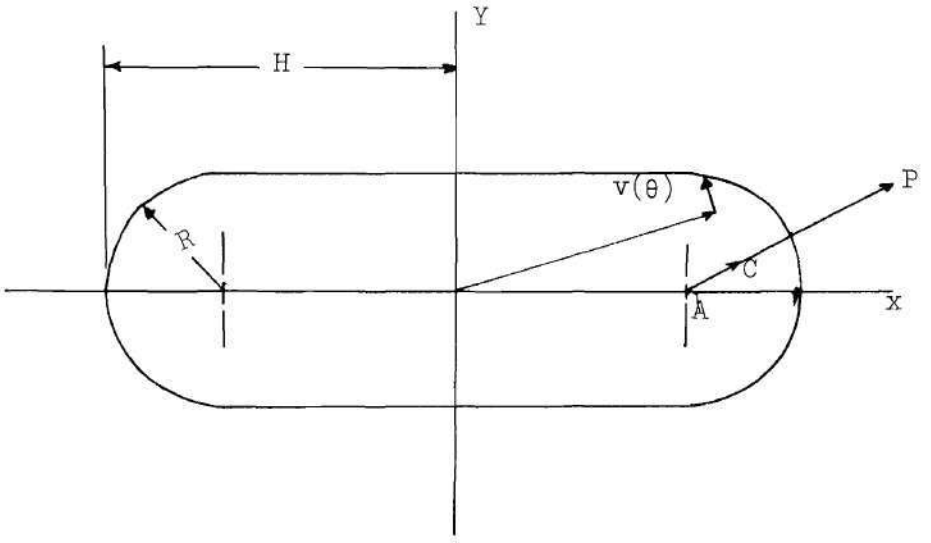

Figure 4. Melentiev Coordinates and Slot Geometry

It can be seen from an examination and Equations (8) that for the slots, $u(\theta)$ remains positive around the contour while $v(\theta)$ changes sign. In any case the magnitude of $v(\theta)$ is usually small compared to the magnitude of $u(\theta)$. If a set of values of θ is chosen then fairly accurate starting values of $u(\theta)$ can be chosen from a direct correspondence of position. That is, the $v(\theta)$ coordinate is ignored completely and the angle θ is assumed to be measured in the Z-plane. Thus, from the first of Equations (6) a set of linear equations in the B(I)'s can be generated. This set of equations is then solved to obtain the first approximation to the mapping function. The mapping function will, in general, represent some curve C′ different from the original curve C. Corrections can now be made to the originally assumed values of $u(\theta)$ and the process can be repeated until the curve C′ is as

close to C as desired.

It is convenient to take equally spaced intervals of θ even though this is not the most accurate procedure (for accuracy the θ intervals should be smaller in the vicinity of a discontinuity in curvature). The convenience of picking equal spacings is that a closed form solution for the B(I)'s can be generated without using matrix inversion (see Whittaker and Robinson [63]). Thus the equation for the θ's is

$$\theta(I) = \frac{\pi}{2}\left(\frac{I-1}{N-1}\right) \qquad (I = 1, 2,\ldots,N) \qquad (9)$$

The equations for the B(I)'s are

$$\left.\begin{aligned}
B(1) &= \frac{1}{2(N-1)}\left\{u(1) + 2u(2) + \ldots + 2u(N-1) + u(N)\right\} \quad , \\
B(I) &= \frac{1}{2(N-1)}\left\{2u(1) + \sum_{K=2}^{N-1} 4u(K)\cos\left[\frac{(I-1)\,(K-1)\pi}{(N-1)}\right]\right. \\
&\qquad \left. + 2(-1)^{I-1}\,u(N)\right\} \qquad (I = 2, 3,\ldots,N-1) \\
B(N) &= \frac{1}{2(N-1)}\left\{u(1) - 2u(2) + 2u(3) + \ldots\right. \\
&\qquad \left. + 2(-1)^{N-2}\,u(N-1) + (-1)^{N-1}\,u(N)\right\} \quad .
\end{aligned}\right\} \qquad (10)$$

In order to make improvements in the values of the assumed $u(I)$'s the cartesian coordinates corresponding to the $\theta(I)$'s and $B(I)$'s are computed from Equation (4). If the computed value of the x-coordinate of a point is less than (H-R), a perpendicular is drawn from the point to the line $y=R$ and the corrections to the coordinates are designated as $\delta y(I)$ and $\delta x(I)$,

$$\left.\begin{aligned} &\text{where} && \delta y(I) = -\left[y(I) - R\right] \\ &\text{and} && \delta x(I) = 0 \quad . \end{aligned}\right\} \qquad (11)$$

If, on the other hand, the computed value of the x-coordinate of a point is greater than (H-R) then the midpoint of a line drawn between the point and its inverse with respect to the circular arc is chosen as the corrected position. The inverse of the point with respect to the circular arc is defined from Figure 4 such that

$$\frac{|\vec{AC}|}{R} = \frac{R}{|\vec{AP}|} \quad .$$

In this case

$$\left.\begin{aligned} \delta x(I) &= \lambda \left[x(I) - (H-R)\right] \quad , \\ \delta y(I) &= \lambda \left[y(I)\right] \quad , \\ \lambda &= \frac{1}{2}\left\{ \frac{R^2}{\left[x(I) - (H-R)\right]^2 + \left[y(I)\right]^2} \right\} \quad . \end{aligned}\right\} \qquad (12)$$

Whether Equations (11) or (12) are used to compute the corrections to the cartesian coordinates, the correction to $u(I)$ can be computed by using Equation (8).

Thus,

$$\delta u(I) = [\cos \theta(I)]\ \delta x(I) + [\sin \theta(I)]\ \delta y(I) \quad .$$

The new value of $u(I)$ is then

$$u(I)\big|_{new} = u(I)\big|_{old} + \delta u(I) \quad .$$

A new set of values for $B(I)$ is computed from the first of Equations (6) and the procedure is continued until satisfactory convergence has been obtained. A good measure of the discrepancy between C and C' is the quantity

$$\delta = \sum_{I=1}^{N} \left\{ \left[\delta x(I) \right]^2 + \left[\delta y(I) \right]^2 \right\}^{\frac{1}{2}} \quad . \tag{13}$$

Sobey [61] reports that if δ is reduced to about 10^{-5} no significant variations in the curvature of C' occur with further iterations.

The final form of the iterated mapping function is taken as

$$Z = m(\zeta) = \sum_{I=1}^{N} B(I)\ \zeta^{3-2I} \quad ,$$

where the $B(I)$'s have been normalized by the last value of $B(1)$.

That is

$$B(I)\Big|_{final} = \frac{B(I)}{B(1)}\Big|_{\substack{last \\ interation}} \quad . \tag{14}$$

This last step of normalizing the mapping function is done in order to bring the Z- and ζ-planes into coincidence at infinity.

It should be noted that normalization of the mapping function is equivalent to multiplying the coordinates in the Z-plane by a linear scale factor. In other words, the hole in the Z-plane is adjusted in size so that the mapping function begins with unity. This procedure is possible since the stress distributions around geometrically similar holes in infinite sheets loaded at infinity are the same.

Development of Stress Functions

The stresses in a flat plate are determined by the Kolosov equations. Milne-Thomson [62] expresses these equations in the form

$$\left.\begin{aligned} \sigma_x + \sigma_y &= W_0(Z) + \bar{W}_0(Z) \quad , \\ \text{and} \qquad \sigma_y - \sigma_x + 2i\,\tau_{xy} &= \bar{Z}W_0'(Z) + w_0(Z) \quad . \end{aligned}\right\} \tag{15}$$

where Z is the complex variable,

$$Z = x + iy \quad ,$$

and W_0 and w_0 are complex stress functions to be determined by the

loading at infinity and by the boundary conditions around the hole. The overbar, (-), denotes the complex conjugate.

From the preceding development it is clear that a function can be constructed which maps the ζ-plane onto the Z-plane for a given problem. Substituting this function into Equations (15) gives

$$\left.\begin{aligned} \sigma_x + \sigma_y &= W(\zeta) + \bar{W}(\zeta) \quad , \\ \sigma_y - \sigma_x + 2i\,\tau_{xy} &= \frac{\bar{m}(\zeta)W'(\zeta)}{m'(\zeta)} + w(\zeta) \quad , \end{aligned}\right\} \tag{16}$$

where

$$\left.\begin{aligned} W_0(Z) &= W_0(m(\zeta)) = W(\zeta) \quad , \\ w_0(Z) &= w_0(m(\zeta)) = w(\zeta) \quad , \end{aligned}\right\}$$

and

$$\frac{dW_0(Z)}{dZ} = \frac{\dfrac{dW_0(m(\zeta))}{d\zeta}}{\dfrac{dZ}{d\zeta}} = \frac{W'(\zeta)}{m'(\zeta)} \quad .$$

At this point it is helpful to examine one property of a power series representation of a function in the complex plane. If

$$f(\xi) = \ldots + a_N\xi^N + \ldots + a_1\xi + a_0 + a_{-1}\xi^{-1} \ldots + a_{-N}\xi^{-N} + \ldots \quad ,$$

then the complex conjugate of f, denoted either as $\overline{f(\xi)}$ or $\bar{f}(\bar{\xi})$ is given by

$$\bar{f}(\bar{\xi}) = \ldots + \bar{a}_N \bar{\xi}^N + \ldots + \bar{a}_1 \bar{\xi} + \bar{a}_0 + \bar{a}_{-1} \bar{\xi}^{-1} + \ldots + \bar{a}_{-N} \bar{\xi}^{-N} + \ldots$$

Noting that if

$$\xi \, \bar{\xi} = |\xi|^2 = A$$

then

$$\bar{\xi} = \frac{A}{\xi} \quad .$$

Thus

$$\bar{f}(\bar{\xi}) = \ldots + \bar{a}_N \frac{A^N}{\xi^N} + \bar{a}_{N-1} \frac{A^{N-1}}{\xi^{N-1}} + \ldots + \bar{a}_1 \frac{A}{\xi} + \bar{a}_0 + \bar{a}_{-1} \frac{\xi}{A} + \ldots + \bar{a}_{-N} \frac{\xi^N}{A^N} + \ldots$$

The above relation will be used throughout the rest of this development with the understanding that under the conditions of this problem the a_i's will be real for all functions developed herein and thus $\bar{a}_i = a_i$.

For a tension, σ, applied at infinity and making an angle Ψ with the x-axis, the stress functions must have the form, <u>for large Z or large ζ</u>.

$$W_0(Z) = W(\zeta) = \frac{1}{2} \sigma + O(\zeta^{-2}) \quad ,$$

and

$$w_0(Z) = w(\zeta) = - \sigma e^{-2i\Psi} + O(\zeta^{-2}) \quad .$$

The above two equations represent the traction boundary conditions at infinity. This dissertation is limited to studies of the stress

distributions resulting from uniaxial tractions applied at $\Psi = \frac{\pi}{2}$.

In this case

$$\left.\begin{aligned} W(\zeta) &= \frac{1}{2}\sigma + O(\zeta^{-2}) \quad , \\ \text{and} \qquad & \\ w(\zeta) &= \sigma + O(\zeta^{-2}) \quad . \end{aligned}\right\} \tag{17}$$

The complex displacement $(u + iv)$ is given by

$$4G(u + iv) = S \int W_0(Z)dZ - Z\,\bar{W}_0(\bar{Z}) - \int \bar{w}_0(\bar{Z})\,dZ \tag{18}$$

where S is $(3 - 4\mu)$ for plane strain and $\left(\frac{3 - \mu}{1 + \mu}\right)$ for generalized plane stress, μ is Poisson's ratio, and G is the shear modulus.

The requirement that the displacements given by Equation (18) are single valued permits the stress field to be developed in terms of a single function of ζ. By introducing the analytic continuation of $W(\zeta)$ across the stress free boundary (Milne-Thomson, sec 6.21), it is possible to express the stress function $w(\zeta)$ in the form

$$m'(\zeta)\, w(\zeta) = -\frac{d}{d\zeta}\left[\bar{m}\left(\frac{1}{\zeta}\right) W(\zeta)\right] + \frac{1}{\zeta^2}\,\bar{m}'\left(\frac{1}{\zeta}\right)\bar{W}\left(\frac{1}{\zeta}\right) \quad . \tag{19}$$

Equation (19) is a relation between the two complex potential functions $w(\zeta)$ and $W(\zeta)$. In essence, this equation is obtained by requiring that $W(\zeta)$ be analytic throughout the entire ζ-plane. Implicitly contained in the form of the continuation as given in Equation (19) is the traction free condition of the hole boundary. It is observed that if an

expression can be obtained for $W(\zeta)$ then it is possible to solve for $w(\zeta)$ by making use of Equation (19). Recall that the mapping function is derived as indicated in the previous section.

The general procedure to follow is to obtain explicit expressions for all the terms on the right-hand side of Equation (19). The final form of the interated mapping function as given by Equation (2) is such that $B(1) = 1$ and all the $B(I)$'s are real. Then

$$\bar{m}\left(\frac{1}{\zeta}\right) = \sum_{I=1}^{N} B(I)\zeta^{2I-3} \quad , \tag{20}$$

and

$$m'(\zeta) = \sum_{I=1}^{N} (3-2I)\, B(I)\zeta^{2-2I} \quad . \tag{21}$$

An investigation of the singularities of $m'(\zeta)\, W(\zeta)$ (Milne-Thomson, section 6.22) enables one to write

$$m'(\zeta)\, W(\zeta) = \sum_{I=1}^{N} A(I)\zeta^{2-2I} \tag{22}$$

It is noted that for uniaxial loading (tension or compression) along the x or y axes all of the $A(I)$ are real. Also note that it is possible to find a function

$$\left[m'(\zeta)\right]^{-1} = \sum_{I=1}^{N-1} BB(I)\zeta^{2-2I} \tag{23}$$

such that

$$\left[m'(\zeta)\right]^{-1}\left[m'(\zeta)\right] = 1 + O\left(\zeta^{2-2N}\right) \quad . \tag{24}$$

The coefficients BB(I) can be obtained in a straight-forward manner by substitution of Equation (21) and (23) into Equation (24). The product of the two summations is then expanded and the coefficient of ζ^0 is set equal to unity while the coefficients of all other powers of ζ are set equal to zero. The following set of linear equations is obtained.

$$\left.\begin{aligned} BB(1)\ B(1) &= 1 \\ BB(2)\ B(1) - BB(1)\ B(2) &= 0 \\ BB(3)\ B(1) - BB(2)\ B(2) - 3BB(1)\ B(3) &= 0 \\ &\vdots \\ BB(N-1)\ B(1) - BB(N-2)\ B(2) + \ldots + (5-2N)\ BB(1)\ B(N-1) &= 0 \end{aligned}\right\} \tag{25}$$

Since all the B(I)'s are known, Equations (25) can be solved consecutively for the BB(I)'s. It should be noted that terms of $O(\zeta^{2-2N})$ are neglected in the product. In the computational procedure it proves convenient to write a general expression for the value of BB(I). The value of B(1) as previously stated is unity. Thus

$$
\left.
\begin{aligned}
&BB(1) = 1 \quad , \\
&\text{and for} \qquad I = 2, 3, \ldots N-1 \quad , \\
&BB(I) = \sum_{J=1}^{I-1} \left[2(I-J) - 1\right] BB(J) \;\; B(I-J+1) \quad .
\end{aligned}
\right\} \tag{26}
$$

The coefficients A(I) can be determined by making use of the traction boundary conditions at infinity, Equations (17), and the continuation relation, Equation (19). For large values of ζ it is noted that

$$m'(\zeta) = 1 \quad .$$

Thus, from Equations (17)

$$m'(\zeta)\; w(\zeta) = \sigma + 0(\zeta^{-2}) \tag{27}$$

and

$$m'(\zeta)\; W(\zeta) = \frac{1}{2}\sigma + 0(\zeta^{-2}) \quad . \tag{28}$$

By equating relations (22) and (28) it can be seen that

$$A(1) = \frac{1}{2}\sigma \quad . \tag{29}$$

It is observed from Equation (22) that for the case where all of the A(I)'s are real,

$$\frac{1}{\zeta^2}\,\bar{m}'\left(\frac{1}{\zeta}\right)\,\bar{W}\left(\frac{1}{\zeta}\right) = \sum_{I=1}^{N} A(I)\,\zeta^{2I-4} \tag{30}$$

$$= A(1)\,\zeta^{-2} + \sum_{I=1}^{N-1} A(I+1)\,\zeta^{2I-2} \quad .$$

Also, from Equations (20), (22) and (24)

$$\bar{m}\left(\frac{1}{\zeta}\right)\,W(\zeta) = \bar{m}\left(\frac{1}{\zeta}\right)\left[m'(\zeta)\right]^{-1}\left[m'(\zeta)\,W(\zeta)\right] \quad ,$$

or

$$\bar{m}\left(\frac{1}{\zeta}\right)\,W(\zeta) = \left(\sum_{I=1}^{N} B(I)\,\zeta^{2I-3}\right)\left(\sum_{I=1}^{N-1} BB(I)\,\zeta^{2-2I}\right)\left(\sum_{I=1}^{N} A(I)\,\zeta^{2-2I}\right) \tag{31}$$

Note that Equation (31) is valid only for large ζ. Expanding the first two summations in Equation (31), and carrying out the indicated multiplication yields

$$\left.\begin{aligned} \bar{m}\left(\frac{1}{\zeta}\right)\left[m'(\zeta)\right]^{-1} &= \left(\sum_{I=1}^{N-1} CP(I)^{2I-1}\right) + \left(\sum_{I=1}^{N-1} CN(I)\,\zeta^{1-2I}\right) \\ \text{where} \qquad CP(1) &= \sum_{J=1}^{N-I} BB(J)\,B(I+J) \\ \text{and} \qquad CN(I) &= \sum_{J=1}^{N-I} B(J)\,BB(I+J-1) \quad . \end{aligned}\right\} \tag{32}$$

In a similar manner substituting Equation (32) into (31) and expanding the products yields,

$$\bar{m}\left(\frac{1}{\zeta}\right) W(\zeta) = \left\{\left(\sum_{I=1}^{N-1} CQ(I)\ \zeta^{2I-1}\right) + \left(\sum_{I=1}^{N-1} CR(I)\ \zeta^{1-2I}\right)\right. \tag{33}$$

$$\left. + \left(\sum_{I=1}^{N-1} CS(I)\ \zeta^{1-2I}\right)_m + \left(\sum_{I=1}^{N-1} CT(I)\ \zeta^{3-2(N+I)}\right)\right\}$$

where $$CQ(I) = \sum_{J=1}^{N-1} A(J)\ CP(I + J - 1) \quad ,$$

$$CR(I) = \sum_{J=1}^{N-1} CP(J)\ A(I + J) \quad ,$$

$$CS(I) = \sum_{J=1}^{I} A(J)\ CN(I + 1 - J) \quad ,$$

$$CT(I) = \sum_{J=1}^{N-1} CN(J)\ A(N + 1 - J) \quad .$$

The last three summations of Equation (33) may be neglected since (33) is valid and used only for large ζ. Differentiation then gives

$$-\frac{d}{d\zeta}\left[\bar{m}\left(\frac{1}{\zeta}\right) W(\zeta)\right] = -\sum_{I=1}^{N-1} (2I-1)\ CQ(I)\zeta^{2I-2} \quad . \tag{34}$$

Equations (30) and (34) are now substituted

$$m'(\zeta)\ w(\zeta) = \left\{A(1)\zeta^{-2} + \sum_{I=1}^{N-1} \left[A(I+1) - (2I-1)\ CQ(I)\right]\zeta^{2I-2}\right\} \quad . \tag{35}$$

Then, equating the right-hand sides of Equations (27) and (35) gives

$$\sum_{I=1}^{N-1} \left[A(I+1) - 2(I-1)\ CQ(I)\right] \zeta^{2I-2} + O(\zeta^{-2}) = \sigma + O(\zeta^{-2}) \tag{36}$$

Using the definition of the CQ(I)'s, as given in Equation (33), and equating like coefficients of ζ in Equation (36), a set of (N-2) non-homogeneous equations linear in the A(I)'s is generated. This set is

$$\begin{bmatrix} 1 - CP(2) \ldots & -CP(N-2) & -CP(N-1) \\ -3CP(3) \ldots & -3CP(N-1) & 0 \\ -5CP(4) & 0 & 0 \\ \vdots & \vdots & \vdots \\ -(2N-7)CP(N-1)\ldots & 1 & 0 \\ -(2N-5)CP(N-1)\ldots & 0 & 1 \end{bmatrix} \begin{bmatrix} A(2) \\ A(3) \\ A(4) \\ \vdots \\ A(N-2) \\ A(N-1) \end{bmatrix} = \sigma \begin{bmatrix} 1 + \frac{1}{2} CP(1) \\ \frac{3}{2} CP(2) \\ \frac{5}{2} CP(3) \\ \vdots \\ \frac{2N-7}{2} CP(N-3) \\ \frac{2N-5}{2} CP(N-2) \end{bmatrix}$$

The equation for A(N) may be written

$$A(N) = \sigma \left(\frac{2N-3}{2}\right) CP(N-1) \quad . \tag{37b}$$

The matrix equation can be solved by inversion of the matrix of coefficients of the A(I)'s.

The analysis for the determination of the stress functions is now essentially completed. Equation (19) is written in the form

$$m'(\zeta)\, w(\zeta) = \frac{1}{\zeta^2}\, \bar{m}'\left(\frac{1}{\zeta}\right)\left[W(\zeta) + \bar{W}\left(\frac{1}{\zeta}\right)\right] - \bar{m}\left(\frac{1}{\zeta}\right) W'(\zeta) \quad . \tag{38}$$

It may also be observed that

$$\left[m'(\zeta)\, W(\zeta)\right]' = m''(\zeta)\, W(\zeta) + m'(\zeta)\, W'(\zeta) \quad .$$

Thus, solving for $W'(\zeta)$ yields

$$W'(\zeta) = \frac{[m'(\zeta)\, W(\zeta)]' - m''(\zeta)\, W(\zeta)}{m'(\zeta)} \quad . \tag{39}$$

Differentiation of Equations (21) and (22) yields

$$m''(\zeta) = \sum_{I=1}^{N} (2-2I)\, A(I)\zeta^{1-2I} \quad . \tag{40}$$

and

$$\left[m'(\zeta)\, W(\zeta)\right]' = \sum_{I=1}^{N} (2-2I)\, A(I)\zeta^{(1-2I)} \tag{41}$$

Equations (16) can be solved for the stress components. These can be written in the form

$$\sigma_y = \mathrm{Re}\left[W(\zeta)\right] + \frac{1}{2}\,\mathrm{Re}\left[\frac{\bar{m}(\bar{\zeta})\,W'(\zeta)}{m'(\zeta)} + w(\zeta)\right]$$

$$\sigma_x = \mathrm{Re}\left[W(\zeta)\right] - \frac{1}{2}\,\mathrm{Re}\left[\frac{\bar{m}(\bar{\zeta})\,W'(\zeta)}{m'(\zeta)} + w(\zeta)\right] \quad . \tag{42}$$

and $$\tau_{xy} = \frac{1}{2}\,\mathrm{Im}\left[\frac{\bar{m}(\zeta)\,W'(\zeta)}{m'(\zeta)} + w(\zeta)\right] \quad .$$

In the above equations $\mathrm{Re}\left[\ \right]$ is the real part of the quantity in brackets as $\mathrm{Im}\left[\ \right]$ is the imaginary part. The principal stresses at a point can be determined by use of the equation

$$\begin{matrix}\sigma_1 \\ \sigma_2\end{matrix} = \left(\frac{\sigma_x + \sigma_y}{2}\right) \pm \left[\left(\frac{\sigma_x - \sigma_y}{2}\right)^2 + \tau_{xy}^2\right]^{\frac{1}{2}} \quad . \tag{43}$$

The state of stress at any point in the plate is thus determined as a function of ζ .

Algebraic Considerations for Computer Programs

The stresses given by Equations (42) may easily be expressed in terms of explicit functions of ζ . It is not easy, however, to obtain a solution in terms of the coordinates (x, y) of the Z-plane. If the stresses at a point (x,y) are required, a value of ζ may be assumed and an interation process which converges to the proper ζ can be initiated.

For computational purposes the variable ζ is written in polar form as

$$\zeta = \eta \left[\cos\theta + i \sin \theta \right] \quad .$$

Then from DeMoivre's Theorem

$$\zeta^n = \eta^n \left[\cos n\theta + i \sin n\theta \right]$$

for any integer n. Thus any summation of the form $\sum_n b_n \zeta^n$ can be written as

$$\sum_n b_n \zeta^n = \sum_n b_n (\cos n\theta)\, \eta^n + i \sum_n b_n (\sin n\theta) \eta^n \quad . \qquad (44)$$

The following definitions can now be made:

$$m(\zeta) = X + iY = \sum_{I=1}^{N} B(I) \zeta^{3-2I}$$

$$m'(\zeta) = XP + iYP = \sum_{I=1}^{N} (3-2I)\, B(I) \zeta^{2-2I}$$

$$m''(\zeta) = XPP + iYPP = \sum_{I=1}^{N} (3-2I)\, (2-2I)\, B(I) \zeta^{1-2I}$$

$$m'(\zeta) = VR + iVI = \sum_{I=1}^{N} A(I)\, \zeta^{2-2I}$$

$$\left.\begin{aligned}
\left[m'(\zeta)\ W(\zeta)\right]' &= VRP + iVIP = \sum_{I=1}^{N} (2-2I)\ A(I)\zeta^{1-2I} \\
\frac{1}{\zeta^2}\,\bar{m}'\left(\frac{1}{\zeta}\right)\ W\left(\frac{1}{\zeta}\right) &= RR + iRI = \sum_{I=1}^{N} A(I)\zeta^{2I-4} \\
\frac{1}{\zeta^2}\,\bar{m}'\left(\frac{1}{\zeta}\right) &= HR + iHI = \sum_{I=1}^{N} (3-2I)\ B(I)\zeta^{2I-4} \\
\bar{m}\left(\frac{1}{\zeta}\right) &= GR + iGI = \sum_{I=1}^{N} (B(I)\zeta^{2I-3}\ .
\end{aligned}\right\} \quad (45)$$

Use of Equation (44) enables the real and imaginary parts of Equations (45) to be computed in terms of η and θ. To proceed further a number of other quantities must be defined:

$$\left.\begin{aligned}
ZMAG &= \left|m'(\zeta)\right|^2 \quad ; \\
W(\zeta) &= UR + iUI \quad ; \\
m'(\zeta)\ w(\zeta) &= TR + iTI \quad ; \\
m''(\zeta)\ W(\zeta) &= SR + iSI \quad ; \\
W'(\zeta) &= PR + iPII \quad ; \\
w(\zeta) &= WR + iWI \quad .
\end{aligned}\right\} \quad (46)$$

Then, from Equations (45) it can be shown that (note that an asterisk * will be used to indicate multiplication),

$$
\begin{aligned}
\text{ZMAG} &= (\text{XP})^2 + (\text{YP})^2 \\
\text{UR} &= (\text{VR} * \text{XP} + \text{VI} * \text{YP})/\text{ZMAG} \\
\text{UI} &= (\text{VI} * \text{XP} - \text{VP} * \text{YP})/\text{ZMAG} \\
\text{TR} &= \text{RR} + \text{HR} * \text{UR} - \text{HI} * \text{UI} \\
&\quad - [(\text{GR} * \text{XP} + \text{GI} * \text{YP}) \\
&\qquad * (\text{VRP} - \text{UR} * \text{PP} + \text{UI} * \text{YPP}) \\
&\quad - (\text{GI} * \text{XP} - \text{GR} * \text{YP}) \\
&\qquad * (\text{VIP} - \text{UR} * \text{YPP} - \text{UI} * \text{XPP}]/\text{ZMAG} \\
\text{TI} &= \text{RI} + \text{HR} * \text{UI} + \text{HI} * \text{UR} \\
&\quad - [(\text{GI} * \text{XP} - \text{GR} * \text{YP}) \\
&\qquad * (\text{VRP} - \text{UR} * \text{XPP} + \text{UI} * \text{YPP}) \\
&\qquad + (\text{GR} * \text{XP} + \text{GI} * \text{YP}) \\
&\qquad * (\text{VIP} - \text{UR} * \text{YPP} - \text{UI} * \text{XPP})]/\text{ZMAG} \\
\text{SR} &= \text{UR} * \text{XPP} - \text{UI} * \text{YPP} \\
\text{SI} &= \text{UI} * \text{XPP} + \text{UR} * \text{YPP} \\
\text{PR} &= [(\text{VRP} - \text{SR}) * \text{XP} + (\text{VIP} - \text{SI}) * \text{YP})]/\text{ZMAG} \\
\text{PII} &= [(\text{VIP} - \text{SI}) * \text{XP} - (\text{VRP} - \text{SR}) * \text{YP})]/\text{ZMAG} \\
\text{WR} &= (\text{TR} * \text{XP} + \text{TI} * \text{YP})/\text{ZMAG} \\
\text{WI} &= (\text{TI} * \text{XP} - \text{TR} * \text{YP})/\text{ZMAG}
\end{aligned}
\qquad (47)
$$

It is now apparant that by use of Equations (45), (46) and (47), the computation of the stresses follows from Equations (42). The results of these computations can finally be expressed in terms of the stress components as

$$
\begin{aligned}
\sigma_x &= \text{UR} - 0.5 \left\{ \left[(\text{PR} * \text{X} + \text{PII} * \text{Y}) * \text{XP} \right.\right. \\
&\qquad \left.\left. + (\text{PII} * \text{X} - \text{PR} * \text{Y}) * \text{YP} \right]/\text{ZMAG} + \text{WR} \right\} \\
\sigma_y &= \text{UR} + 0.5 \left\{ \left[(\text{PR} * \text{X} + \text{PII} * \text{Y}) * \text{XP} \right.\right. \\
&\qquad \left.\left. + (\text{PII} * \text{X} - \text{PR} * \text{Y}) * \text{YP} \right]/\text{ZMAG} + \text{WR} \right\}
\end{aligned}
\qquad (48)
$$

and

$$\tau_{xy} = 0.5 \left\{ \left[(PII * X - PR * Y) * XP - (PR * X + PII * Y) * YP \right] / ZMAG + WI \right\} .$$

Computational difficulties arise throughout the development due to the large powers of ζ which are required. It is, therefore, necessary to use double precision in order to increase the capability of the program. Very good mapping functions can be obtained using $N = 41$ for ratios of hole height to hole length greater than or equal to 0.40 ($\rho \geq 0.40$). For $\rho < 0.40$ it is necessary to increase the size of N. Good results can be obtained with $N = 91$ for ρ as small as 0.05.

If only the boundary stresses are required, they can be obtained from a computation of only $W(\zeta)$. In this case $N = 41$ will provide good results for $\rho = 0.05$. The necessity for increasing the number of terms in the solution arises in the computation of $w(\zeta)$ which requires differentiation of many of the series.

The stresses as computed by this method for values of ρ from $1.0 \rightarrow 0.05$ have been shown in Figures 10, 11, and 12 as dashed lines. The stresses for $\rho = 0.5$ have been checked with those of Heller, Brock, and Bart [36] and the agreement is excellent.

Photoelastic Determination of Stresses in Plates with Holes

In the previous section a method for determining the stress distribution in an infinite plate with a hole was presented. Naturally, it is desirable to determine the effect of finite width on this distribution. The analytic determination of the stress distribution in

finite width plates is extremely difficult. Howland [26] has obtained a solution for finite width plates containing circular holes. Savin [35] has suggested the use of an iterative scheme in a complex variable solution to solve this problem for any shape hole. In problems of this type, however, experimental techniques are usually used to determine stress distributions.

The determination of the stress distribution in a thin plate made of birefringent material is accomplished by the techniques of two-dimensional photoelasticity. The isochromatic fringe pattern produced in these techniques represents lines of constant magnitude of the principal stress difference. Thus, obtaining the fringe order at a point is equivalent to obtaining the difference in the principal stresses at the point. In order to find the individual stresses, however, some additional information must be obtained. This additional information can be obtained from a numerical solution for the sum of the principal stresses. The details of this solution will be discussed in a subsequent section.

It should be pointed out that although the region of compressive stress is of primary interest for the study of buckling, the complete stress distribution in the plate is obtained. Thus, a great deal of information has been obtained about the effects of finite plate width and of hole geometry on the stress distribution. This includes, of course, determinations of stress concentration factors. This information is useful design data and adds to the stress concentration data given by Frocht and Leven [37].

Models and Apparatus

The apparatus used for the photoelastic part of this study was relatively simple. A standard transmission polariscope with a twelve inch diameter field was used. Because of the size of the model and the associated end grips, the straining frame normally used with this polariscope was not satisfactory. Instead, the polariscope was placed in an Instron Universal Testing Machine. The testing machine was then used in place of the straining frame.

An x-y micrometer traveling table was mounted in front of the polariscope analyzer. The table was mounted to provide a capability for travel in a plane parallel to the analyzer. To increase the accuracy of the measurements a telemicroscope with a zoom-lens attachment was positioned on the x-y table perpendicular to the plane of the analyzer. This system provided the capability of accurate fringe measurements in regions of high stress gradients. It also permitted the use of a smaller grid size.

The models used in this study were made of a clear polyester sheet, PSM-1, produced by Photolastic, Inc. Special care had to be taken on the machining of this material to prevent machining stresses. This material is excellent for two-dimensional models since it does not exhibit any time edge effects, and it is virtually free of creep. It has a relatively high Young's modulus (340,000 psi) and a high photoelastic sensitivity (stress optic constant of 40 psi/fringe in a one inch thick plate). The sheet thickness of 0.125 inch was selected and all models were machined to size from standard ten inch square

sheets.

A set of end fixtures was manufactured from one inch thick aluminum plate stock. A slot 0.75 inch deep was machined in the end of the fixture and a row of 0.25 inch diameter holes was drilled with a 0.75 inch spacing between centers. Figure 5 illustrates the details of the fixture.

The models were connected to the end fixtures with 0.25 inch diameter bolts. It was found that very good distributions of load into the models could be achieved if the bolts were adjusted for each hole by filing them as needed. The adjustment continued until a satisfactory distribution of end traction was developed. The models were machined with the centerline as a reference in order to minimize eccentric loading effects. Figure 6 illustrates a typical model configuration. Table 1 gives the model nomenclature and the exact dimensions of each model configuration. It should be noted that the parameters examined were the hole length to plate width ratio, γ , and the hole height to hole length ratio, ρ .

The plate length was generally found to be long enough to have little effect on the stresses in the vicinity of the hole. Naturally, a fringe pattern associated with the bolts used for loading was evident in the vicinity of the end fixtures. There was also a fringe pattern which could be associated with the redistribution of stresses due to the presence of the hole. For models less than six inches wide these patterns were distinctly separated by a large region of uniform color. That is, local effects due to the loading bolts and the hole were not present in this uniform region. The plate could thus be thought of as

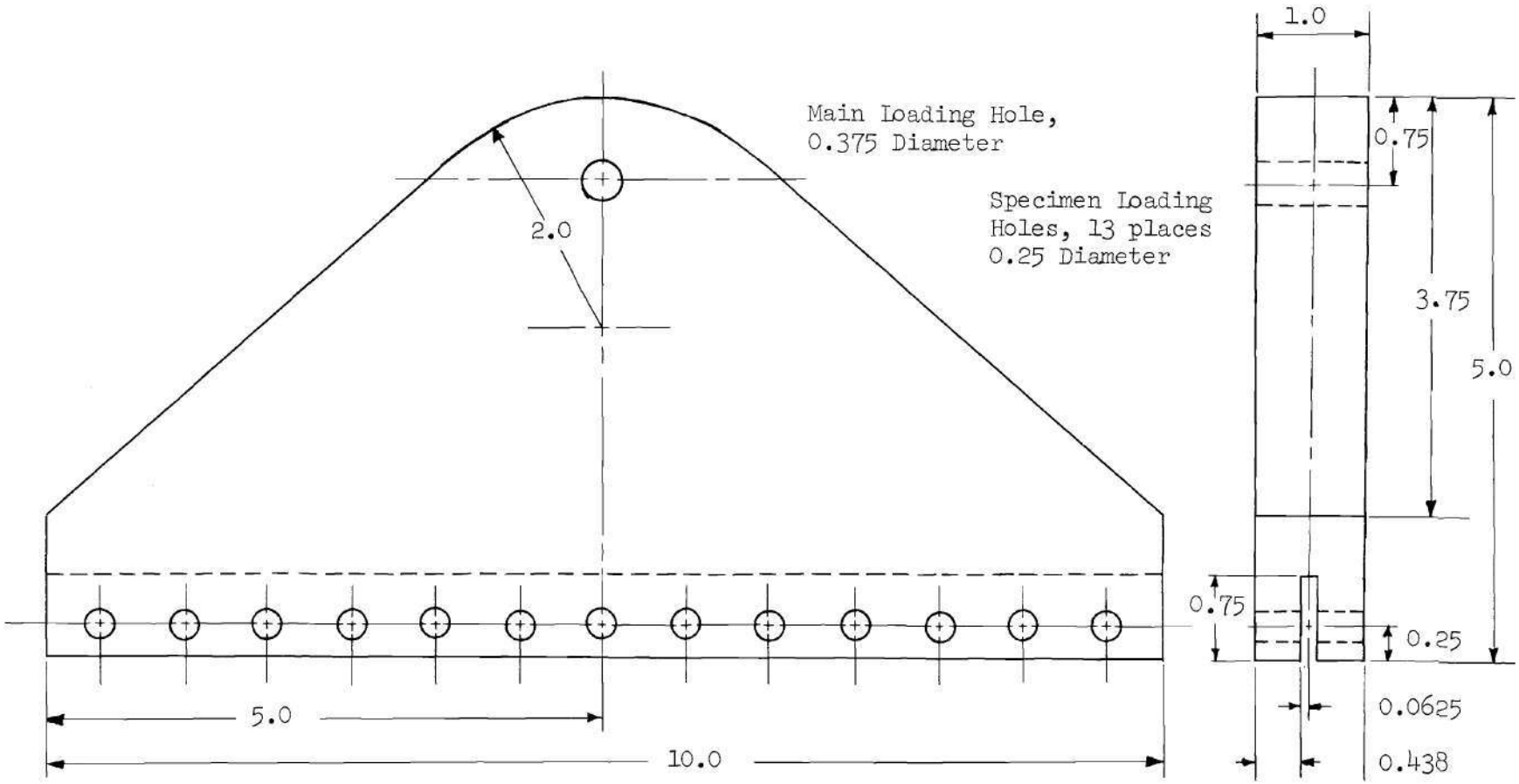

All Dimensions in Inches

Figure 5. End Fixture for Photoelastic Models

Table 1. Photoelastic Model Designations and Dimensions

Series	Height of Slot = 2R	Length of Slot = 2H	$\rho = \frac{2R}{2H}$	Model 1 $\widetilde{W}$	Model 2 $\widetilde{W}$	Model 3 $\widetilde{W}$	Model 4 $\widetilde{W}$	Model 5 $\widetilde{W}$
D	0.250	0.312	0.80	3.12	1.56	1.04	0.782	0.625
E	0.250	0.417	0.60	4.17	2.08	1.39	1.04	0.834
F	0.250	0.500	0.50	5.00	2.50	1.67	1.25	1.00
G	0.250	0.625	0.40	6.25	3.12	2.08	1.56	1.25
H	0.250	1.25	0.20	___	6.25	4.17	3.12	2.50
I	0.250	2.50	0.10	___	___	8.33	6.25	5.00
J	0.250	5.00	0.05	___	___	___	___	10.00

being subjected to a uniform traction along a line perpendicular to the direction of loading and lying in the region of uniform color.

If the model was over six inches wide it was difficult to obtain this region of uniform color. There was then some question as to whether or not the distribution of load into the plate was representative of the uniaxial stress which was desired. To answer this question, several of the loading bolts were completely removed and the fringe pattern in the vicinity of the end fixtures was distorted. Under these conditions very little change in the fringe orders in the vicinity of the hole was observed. A maximum of about 0.05 of a fringe order change was observed in low stress regions and about 0.20 of a fringe order in high stress regions. In either case the change was less than five percent of the total fringe order.

Another indication that the end fixtures were providing a uniform loading distribution was the symmetric nature of the pattern developed. Also, the zero degree isoclinics fell without exception on the geometric lines of symmetry of the models.

A rectangular grid pattern was selected as being the most convenient for rapid analysis of the models. The segment of circular boundaries was small in comparison with the total boundary length for most models investigated so the use of a polar system was not warranted. The grid pattern was scribed onto the models with the tip of a height gage which was accurate to within 0.001 inch. The spacing of the grid was changed four times on each model. The spacing was finest near the hole and became progressively more coarse away from the hole. A typical model and grid pattern is shown in Figure 6.

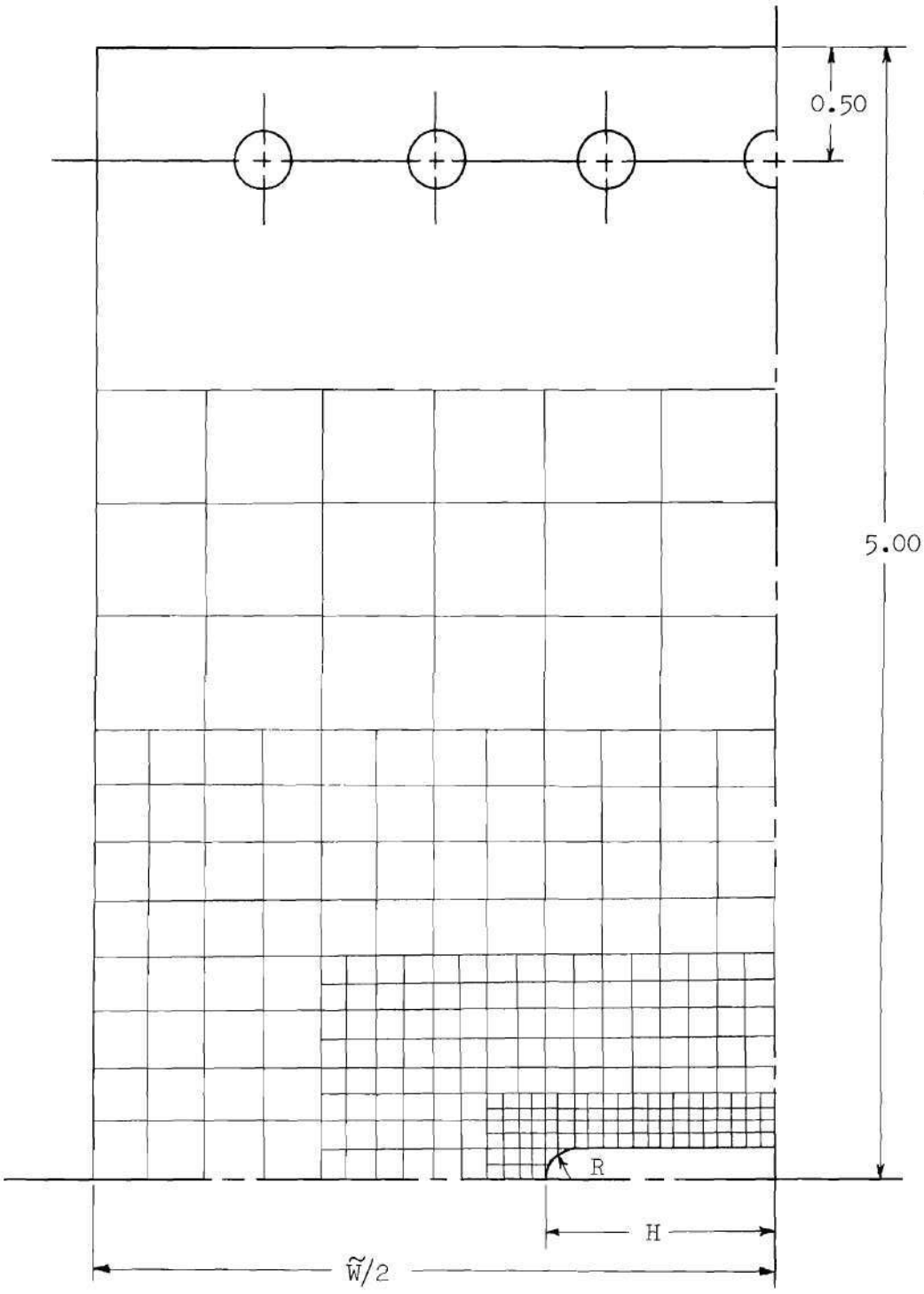

Array A ~ 0.50 inch Mesh
Array B ~ 0.25 inch Mesh
Array C ~ 0.125 inch Mesh
Array D ~ 0.0625 inch Mesh

Figure 6. Quadrant of a Typical Photoelastic Model

Photoelastic Analysis

Photoelastic readings were obtained for each grid point on a model. Depending on the size of the model, it took from one to four hours to complete the analysis. At each point, the angle of the principal stresses was determined. The fringe order, which is linearly proportional to the difference in the principal stresses, was then obtained by Tardy compensation. This method of obtaining fractional fringe orders is rapid, and if used properly, provides very accurate results.

The total load applied to a model was approximately that which was necessary to produce a uniform field of one fringe order. The exact load necessary to produce this fringe order could not always be established with accuracy. For calculations all of the fringe orders were normalized with reference to an average of the fringe orders along a horizontal line far above the hole.

As noted previously, the fringe order is linearly proportional to the difference of the principal stresses at a point. For all traction free boundaries one of the principal stresses is normal and the other is tangential to the boundary. The normal principal stress is then zero and the photoelastic reading on a boundary represents the magnitude of the boundary tangential stress. The sign of the stress (i.e., tensile or compressive) can be determined from an apriori knowledge of the problem or by use of a compensating wedge. The above property is used in the solution of the complete stress distribution problem. References to negative values of fringe order are often found in the literature. These, however, are simply conventions adopted to illustrate

specific problems and they convey an erroneous impression regarding the possible character of the fringe order.

The difference of the principal stresses (normalized to a uniform tensile field of one) is given by

$$U = \sigma_p - \sigma_q \quad , \tag{49}$$

where σ_p and σ_q are the normalized principal stresses at a point and

$$\sigma_p \geq \sigma_q \quad .$$

Thus, U will always be positive or zero. The sum of the principal stresses, on the other hand, may have either a positive or a negative value. If V denotes the sum of the principal stresses then on a traction free boundary

$$\left.\begin{aligned} V = U \quad \text{if} \quad \sigma_p \neq 0 \quad \text{and} \quad \sigma_q = 0 \quad , \\ \text{and} \\ V = -U \quad \text{if} \quad \sigma_p = 0 \quad \text{and} \quad \sigma_q \neq 0 \quad . \end{aligned}\right\} \tag{50}$$

If body forces and temperature effects are absent and if the plate remains flat and is free of dislocations then the compatibility requirements from the formulation presented in Chapter II are

$$\nabla^4 F = 0 \quad ,$$

$$\int_{\Gamma_i} \frac{\partial(\nabla^2 F)}{\partial \nu} ds = 0 \quad ,$$

$$\int_{\Gamma_i} \left[y \frac{\partial(\nabla^2 F)}{\partial \nu} - x \frac{\partial(\nabla^2 F)}{\partial s} \right] ds = 0$$

and

$$\int_{\Gamma_i} \left[y \frac{\partial(\nabla^2 F)}{\partial s} + x \frac{\partial(\nabla^2 F)}{\partial \nu} \right] ds = 0 \quad .$$

In general, the above relations along with the in-plane boundary conditions can be used to solve for F. Since, however, the present solution makes use of experimental results the problem is partially solved. With the aid of the experimental results, a new problem can be posed which is mathematically complete.

Note that

$$\nabla^2 F = (F,_{xx} + F,_{yy}) = \sigma_x + \sigma_y \quad .$$

The sum of the normal stresses, however, is an invariant thus

$$\sigma_x + \sigma_y = \sigma_p + \sigma_q = V \quad .$$

Thus, the compatibility equation can be written as

$$\nabla^2 V = 0 \quad . \tag{51}$$

The domain of Equation (51) is the portion of the photoelastic models indicated in Figure 6. It is seen that only one quadrant of the plate had to be used since symmetry conditions were imposed along the axes. The boundary conditions used with Equation (51) are obtained from the photoelastic readings.

For properly specified boundary conditions the solution of Equation (51) is unique. It is of interest to note that the solution is obtained without the application of the auxiliary equations. An interative procedure is used to obtain a numerical solution of V. The inputs necessary for this solution are the boundary values of V as obtained from Equation (50). The general two dimensional finite difference formula given by Frocht [64] for solution of Equation (51) is

$$\left(\frac{1}{ac} + \frac{1}{bd}\right) V_O = \frac{1}{a(a + c)} V_A + \frac{1}{b(b + d)} V_b \qquad (52)$$

$$+ \frac{1}{c(c + a)} V_C + \frac{1}{d(b + d)} V_D \quad ,$$

where V_O, V_A, V_B, V_C, and V_D are values of V at the subscripted points. The quantities a, b, c, and d are the distance from point O to the corresponding points. The geometric relationship of the points to one another is illustrated in Figure 7.

Using Equation (52), equations can be written for each interior point (points not on the boundary) and four neighboring points. The resulting system of equations was solved by use of the Gauss-Seidel iteration method. In the use of this method the initial value of V

at the interior points can be arbitrarily selected. Convergence to the correct values will be faster, however, of the initial values are approximately correct. In the calculations of V for these models it was found that setting all interior values equal to unity was satisfactory.

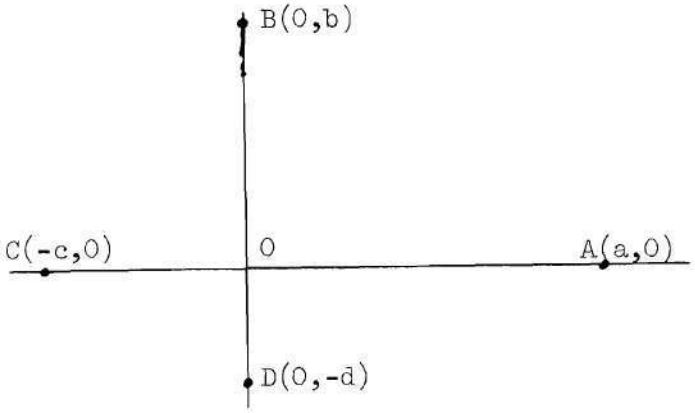

Figure 7. Relationship of Finite Difference Points

The iterative procedure was terminated when the sum of the absolute values of all changes from one iteration to the next was less than 0.01. That is,

$$\text{Error} = \sum_{i=1}^{N} \left| V_i^{(s)} - V_i^{(s+1)} \right| < 0.01 \quad .$$

In the above relation N is the number of interior points, V_i is the value of V at a point i, and s is the number of the iteration. The number of iterations necessary for convergence varied from about 60 for the smaller models to over 4000 for the larger ones.

When the function V has been determined to sufficient accuracy, it is a simple matter to determine the individual principal stresses from

$$\left.\begin{aligned} \sigma_p &= \frac{1}{2}(V + U) \quad , \\ \text{and} \qquad \sigma_q &= \frac{1}{2}(V - U) \quad . \end{aligned}\right\} \tag{53}$$

If the stress components in the x and y directions are required, they can be found by making use of the principal stress angle determined photoelastically. For the purposes of this study it was sufficient to express the stresses in terms of the principal values.

Discussion of Stress Distribution

As indicated in Table 1, a total of 28 model configurations were examined in the photoelastic part of this study. Seven different hole geometries and five different hole length to plate width ratios were included. Supplementing these were the results from the complex variable solution for infinitely wide plates. Also included are results for circles in finite width plates. These were obtained from Howland's paper [26].

In Figures 8 and 9 the stress concentration factor has been plotted as a function of the hole length to plate width ratio, γ . The solid lines connecting points between $\gamma = 0.1$ and $\gamma = 0.5$ represent finite width plates. The dashed lines connect these results for finite width plates with the complex variable results for infinitely wide plates. The finite plate width results for circular holes ($\rho = 1.0$)

were obtained from Howland. All other results for finite plate widths are from the photoelastic experiments. In Figure 8 the stress concentration factor is based on the average stress in a section far above the slot. In Figure 9 the stress concentration factor is based on the stress in the net section through the slot. Figure 8 indicates that the maximum stress increases as plate width decreases; however, Figure 9 indicates a decrease in the stress concentration factor based on the net stress.

For the type of problem involved it would be expected that the dashed curves in Figure 8 would have a positive slope rather than the negative slope indicated. The probable cause for the discrepancy is the difficulty associated with taking photoelastic readings in regions of high stress gradients. There is a natural tendency to average readings over small areas, and this accounts for the low photoelastic readings.*

Figures 10(a) through 10(h) give the distributions of σ_y along the x-axes of the plates. Each figure in this sequence represents a particular hole geometry. The plate half width in each case is taken to be unity. The dashed lines represent the complex variable solution. The complex variable solution in some cases coincides with the photoelastic solution. In these instances only the dashed curve is shown. Where differences exist, both dashed and solid lines are presented. Note that the complex variable solution was carried out to only four

*It should be noted that a number of workers have shown that an analysis including couple stress effects can result in a reduction in the computed stress concentration factor.

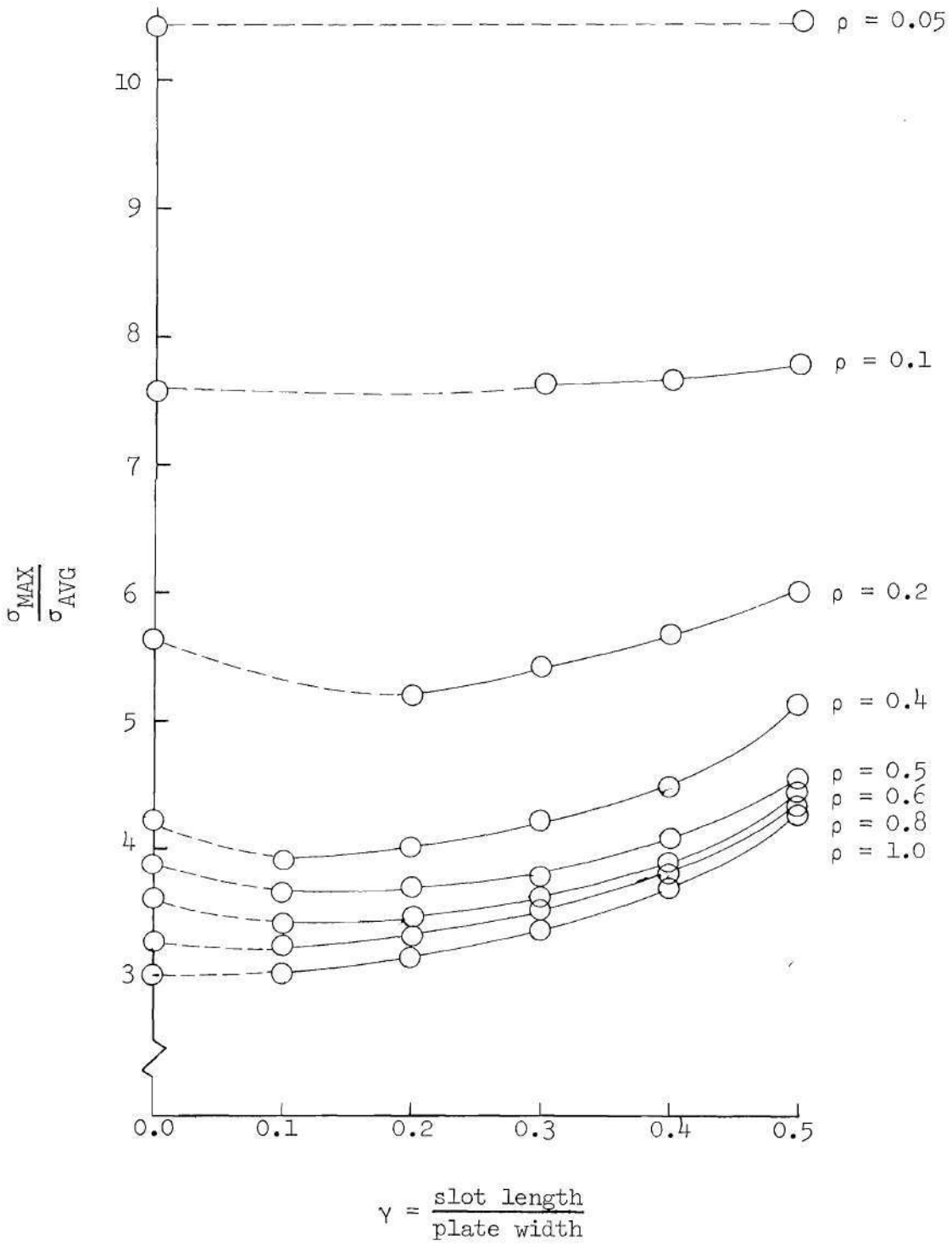

Figure 8. Stress Concentration Factor Based on Total Plate Area

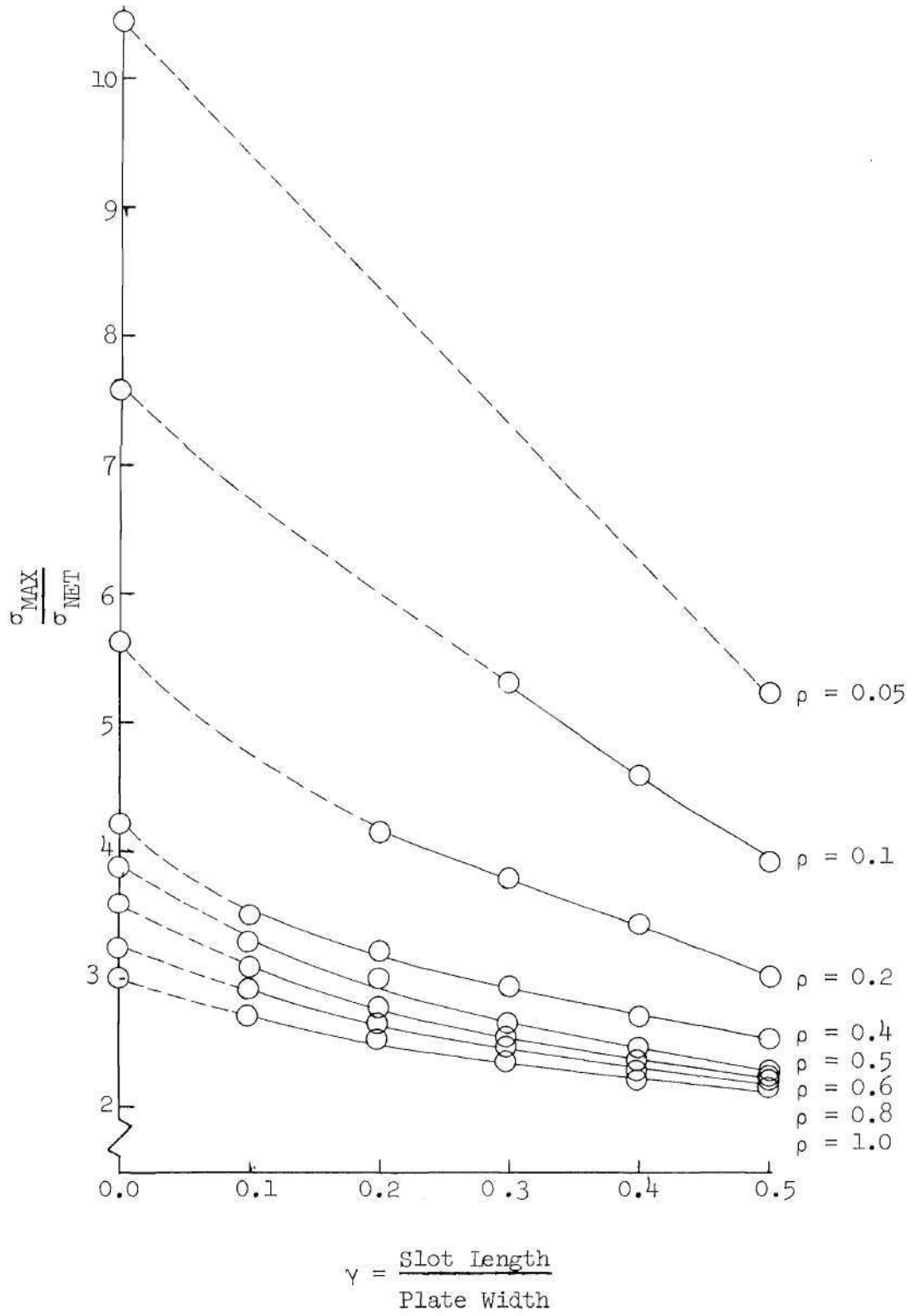

Figure 9. Stress Concentration Factor Based on Net Plate Area at Slot

times the hole length.

Figures 11(a) through 11(h) give the distributions of σ_x along the y-axes of the plates. Once again each figure represents a particular hole geometry and it is assumed that the plate half width is always unity. The complex variable result is again presented in dashed curves. The complex variable solution appears lower in magnitude than the photoelastic solution at the edge of the hole. An explanation of this deviation is the "swayback" shape which the mapping function gives to a hole with a straight line. This "swayback" effect is less accentuated as the length of the hole increases and it is seen that the complex variable solution for the maximum compressive stress approaches the expected value of minus one.

The photoelastic results indicate a gradual increase in the magnitude of the maximum compressive stress as the hole length to plate width ratio, γ , increases. It should be noted that as ρ decreases from 1.0 to 0.2 the difference in the maximum compressive stresses from $\gamma = 0.1$ to $\gamma = 0.5$ decreases. The increases in the magnitude of this stress shown in Figures 11(g) and 11(h) for values of ρ equal to 0.1 and 0.05 are contrary to the above noted behavior and are difficult to explain. An examination of these two models revealed that the slots were slightly wider at the center than they were at the ends; i.e., they tend toward elliptical shapes. It has been shown by Durelli, Parks, and Feng [39] that the maximum compressive stresses for elliptical holes can be much greater than minus one for plates of finite width. Thus, it is conceivable that in a loaded condition, the long slots could behave to a small extent like ellipses.

Another sequence of stress distributions is given in Figures 12(a) through 12(h). This set of figures represents the tangential boundary stress around the holes. Stresses plotted exterior to the boundary are tensile while those interior are compressive. Again each figure represents a particular slot geometry. For clarity of presentation, only representative photoelastic results have been presented on these figures. In each figure the complex variable solution is shown as a dashed curve. In Figure 12(a) no complex variable solution is shown since it coincides so closely with the result for $\gamma = 0.1$. All of the correlations between the complex variable solutions and the results for finite width plates which were discussed for Figures 10 and 11 can also be seen in Figure 12.

The nature and size of the region of compressive stresses is of special importance. The type of plot which illustrates these features of the stress distributions is shown in Figure 13. Figure 13 is a plot of constant value of compressive principal stress magnitude. The trends which are evident from a study of plots such as Figure 13 are referred to in the next chapter. These trends are the basis for important decisions concerning the buckling behavior. Although no other figures such as Figure 13 will be given, any trends discussed can also be observed from a study of Figures 11 and 12.

In the preceding sections comparisons were made between results from the complex variable analysis and the photoelastic analysis. Both methods of analysis possess inherent limitations which restrict their use in stress analysis. Fortunately, the specific limitations differ

and as a result, the two methods may be used to supplement one another. This has been clearly illustrated in the results which have been presented. The use of both methods of analysis has, in fact, made it possible to gain a more thorough and complete knowledge of the problem studied here.

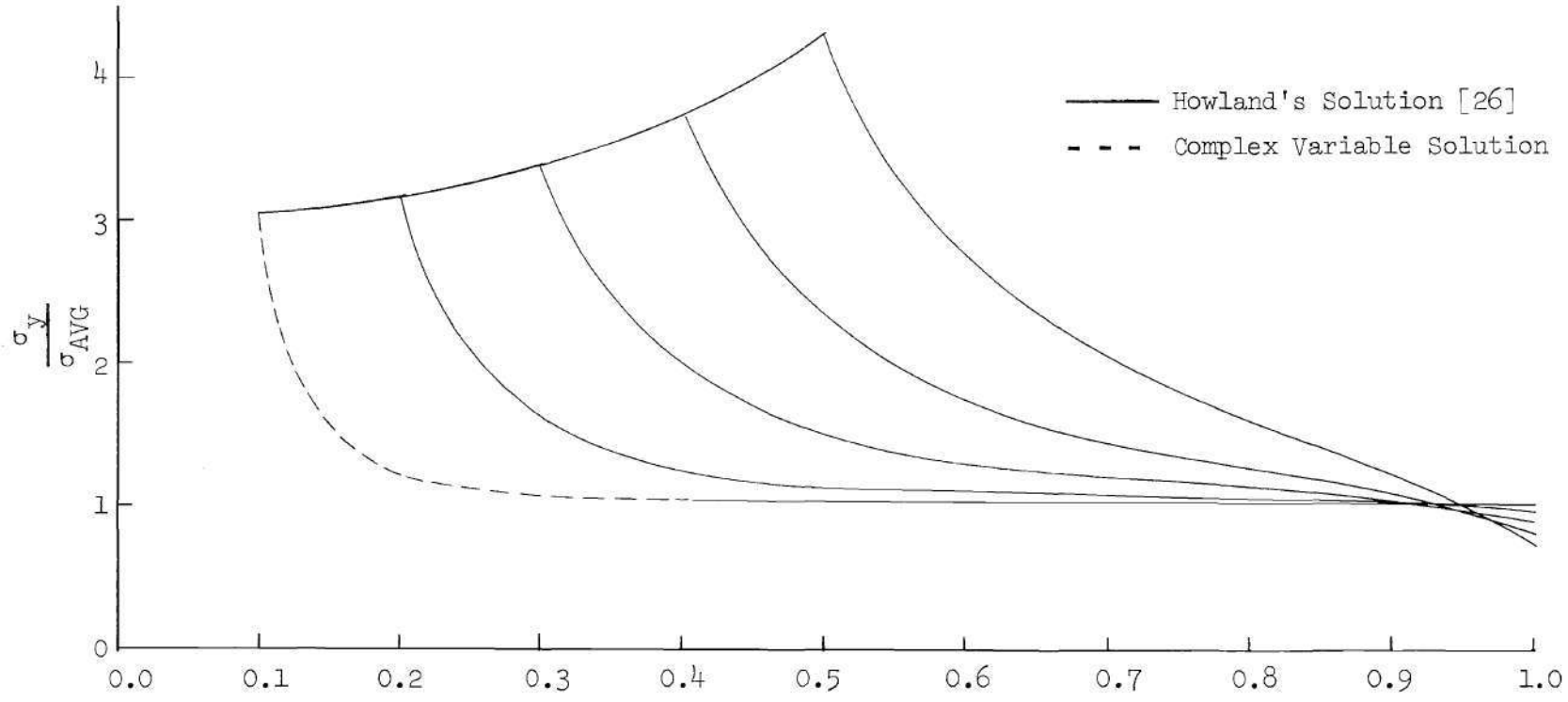

Figure 10(a) σ_y Along x-Axis for $\rho = 1.0$

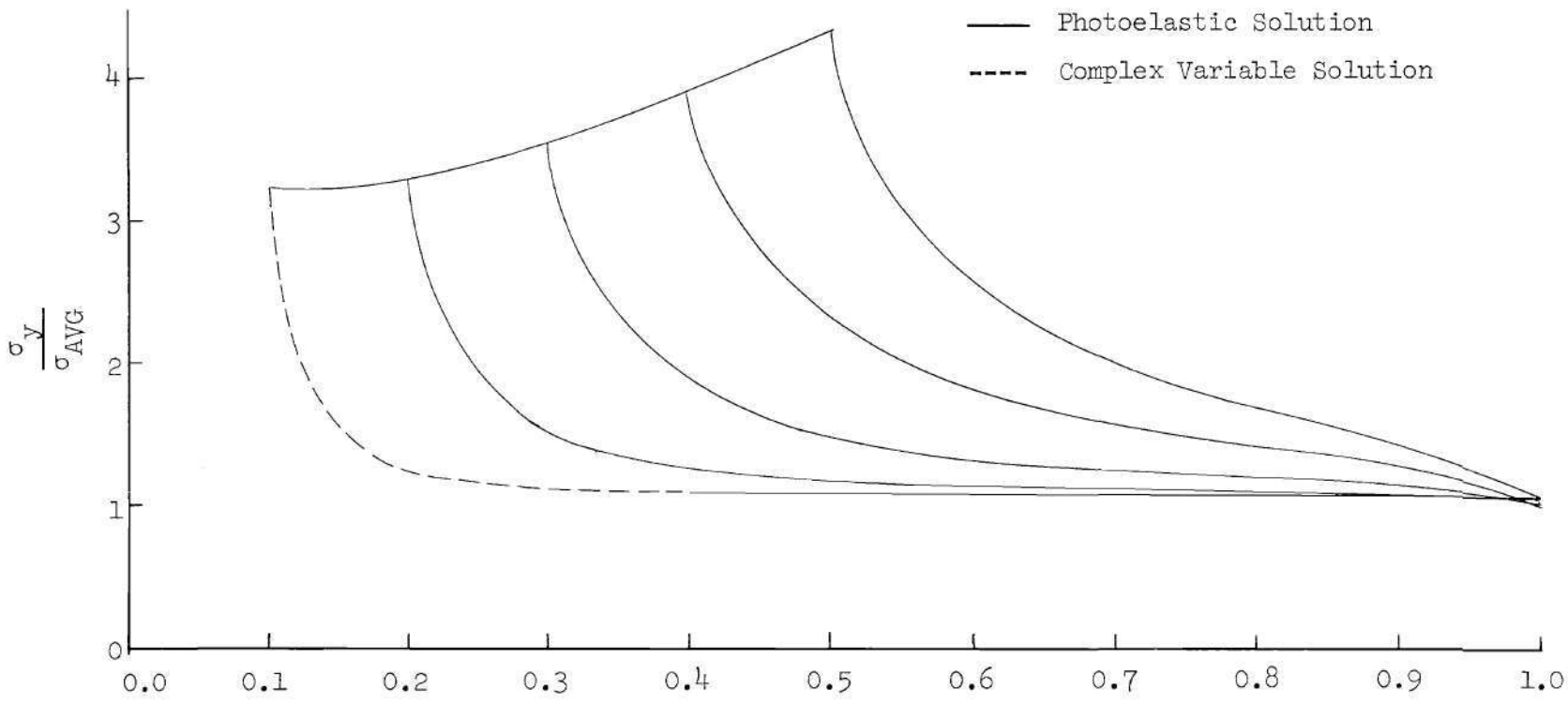

Figure 10(b). σ_y Along x-Axis for $\rho = 0.8$

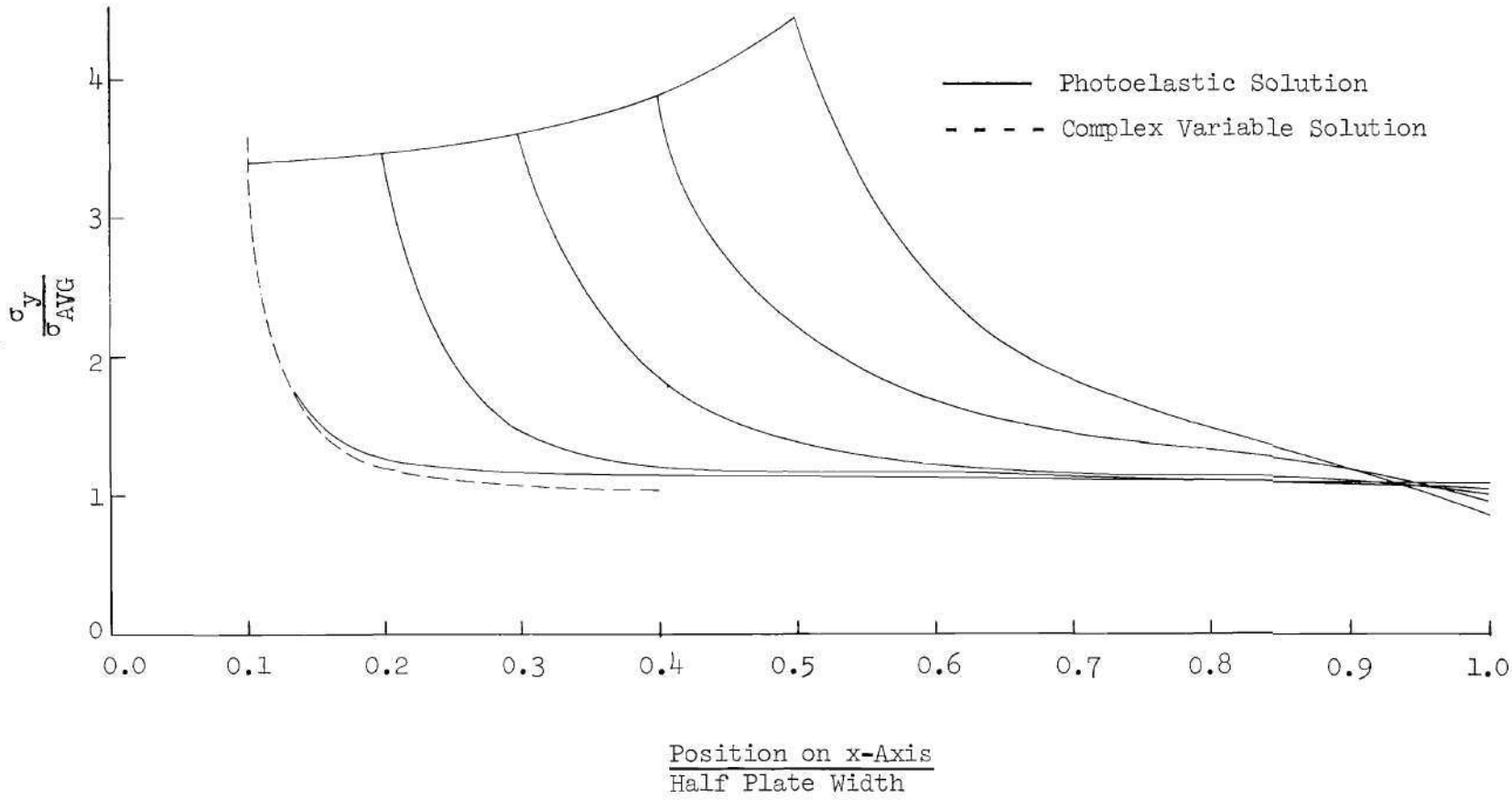

Figure 10(c) σ_y Along x-Axis for $\rho = 0.6$

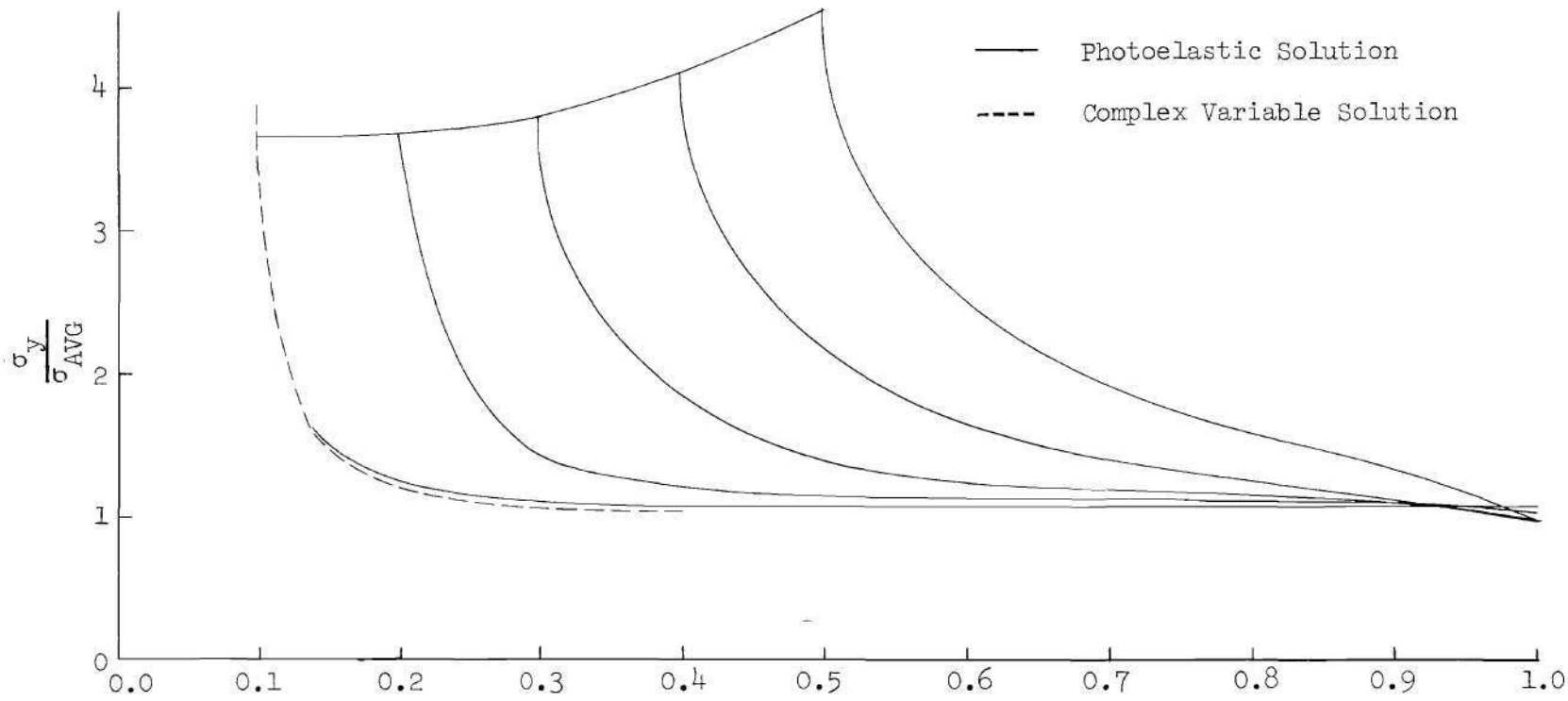

Figure 10(d). σ_y Along x-Axis for $\rho = 0.5$

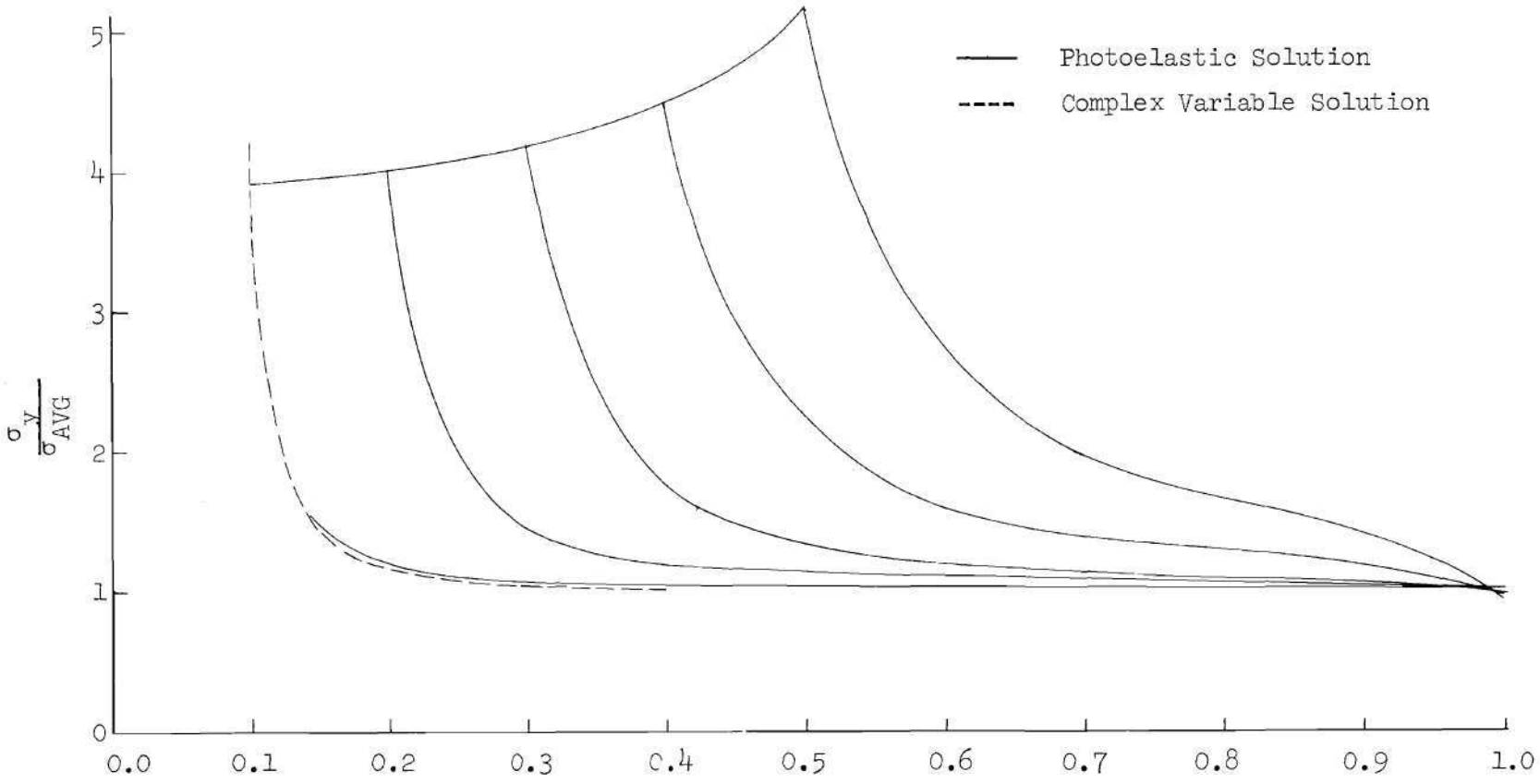

Figure 10(e) σ_y Along x-Axis for $\rho = 0.4$

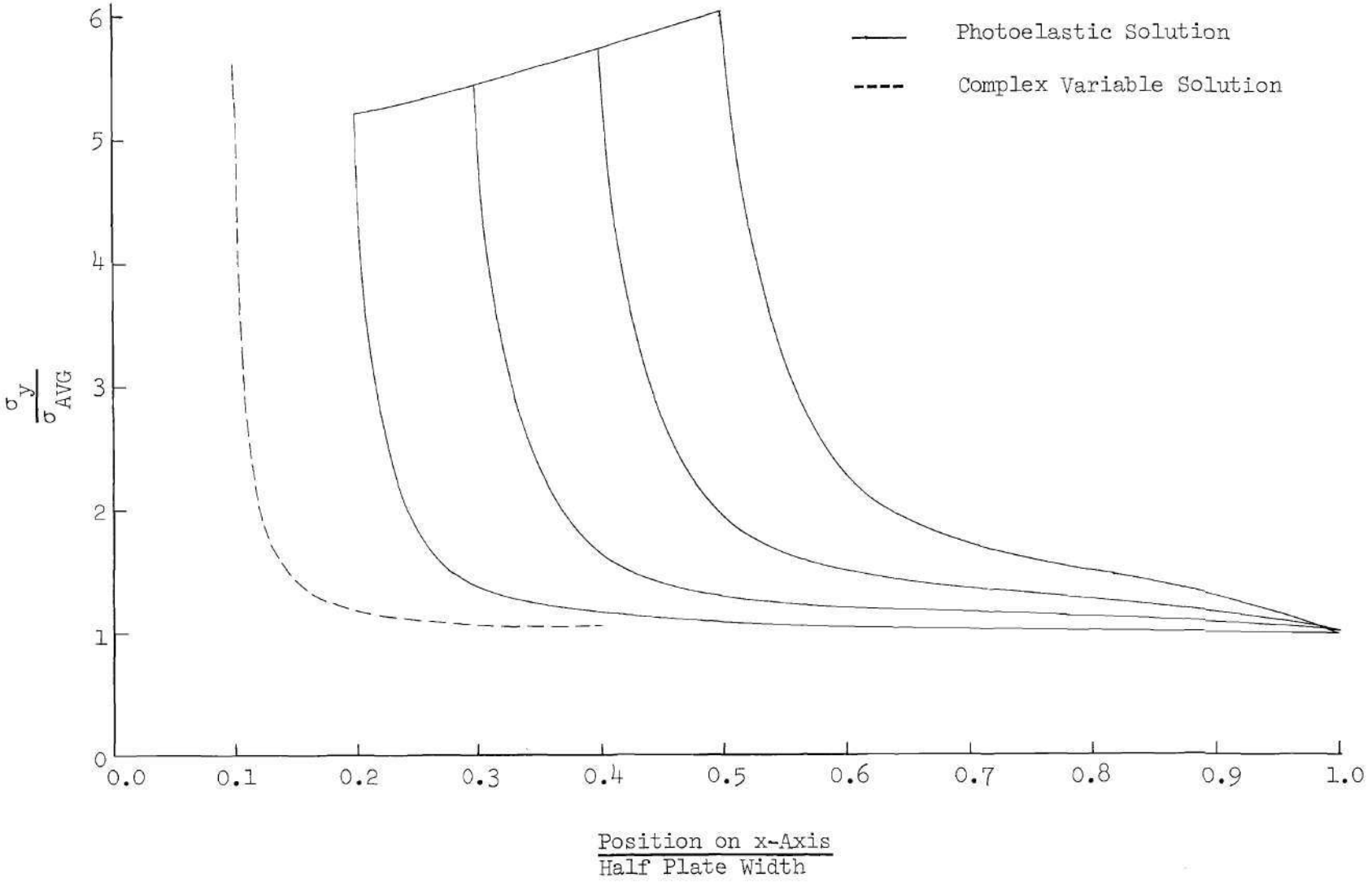

Figure 10(f). σ_y Along x-Axis for $\rho = 0.2$

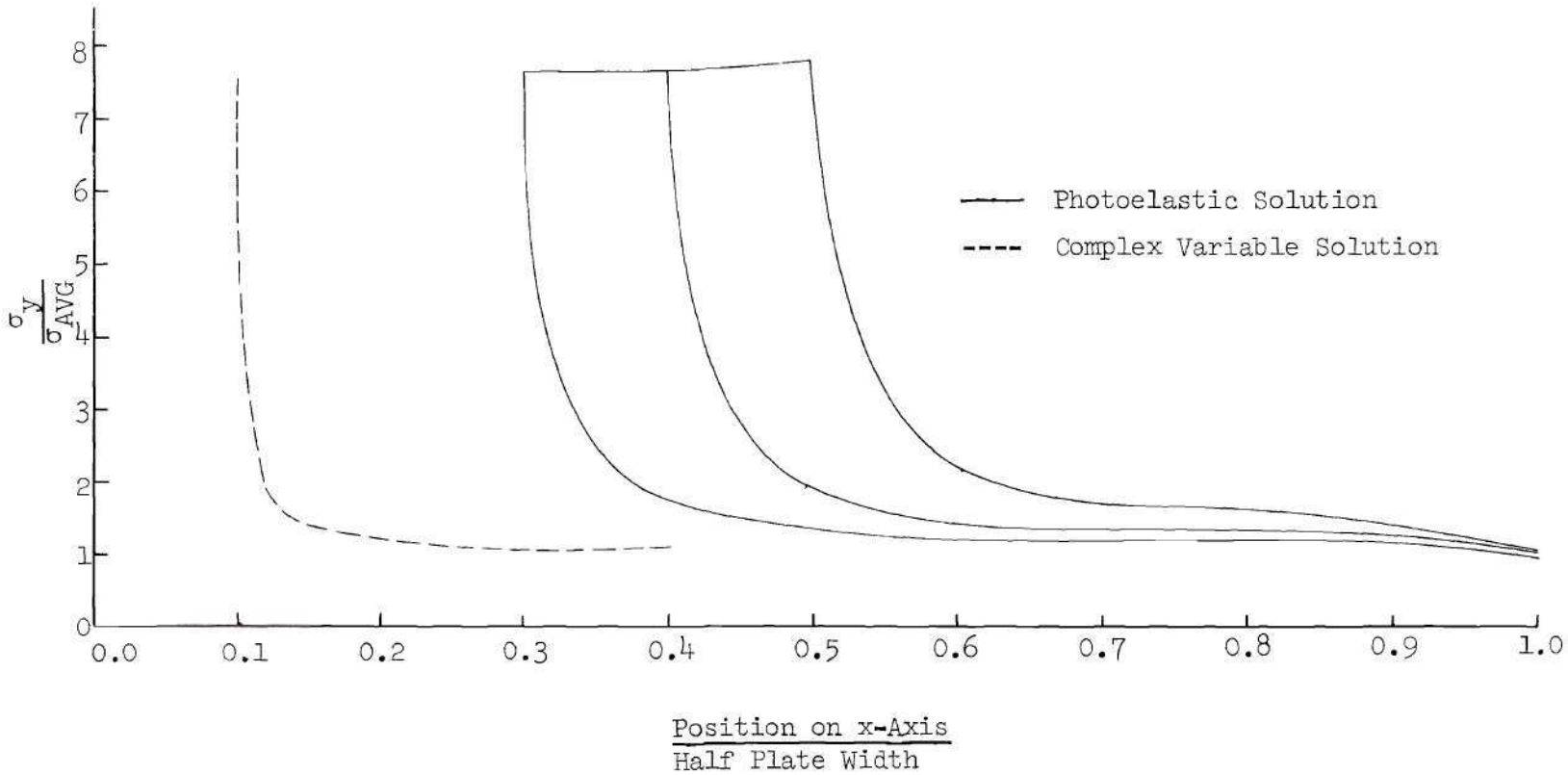

Figure 10(g). σ_y Along x-Axis for $\rho = 0.1$

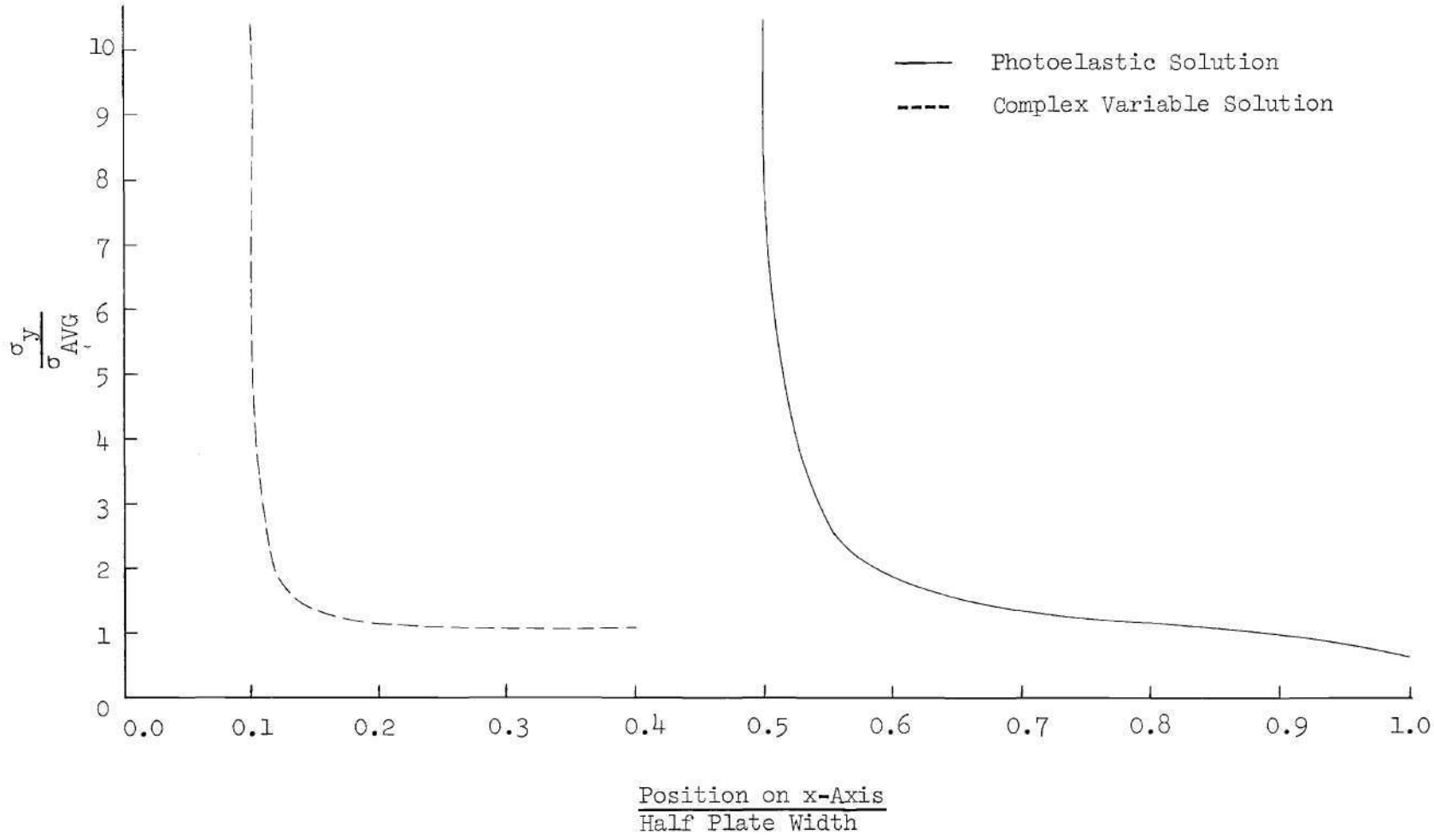

Figure 10(h). σ_y Along x-Axis for $\rho = 0.05$

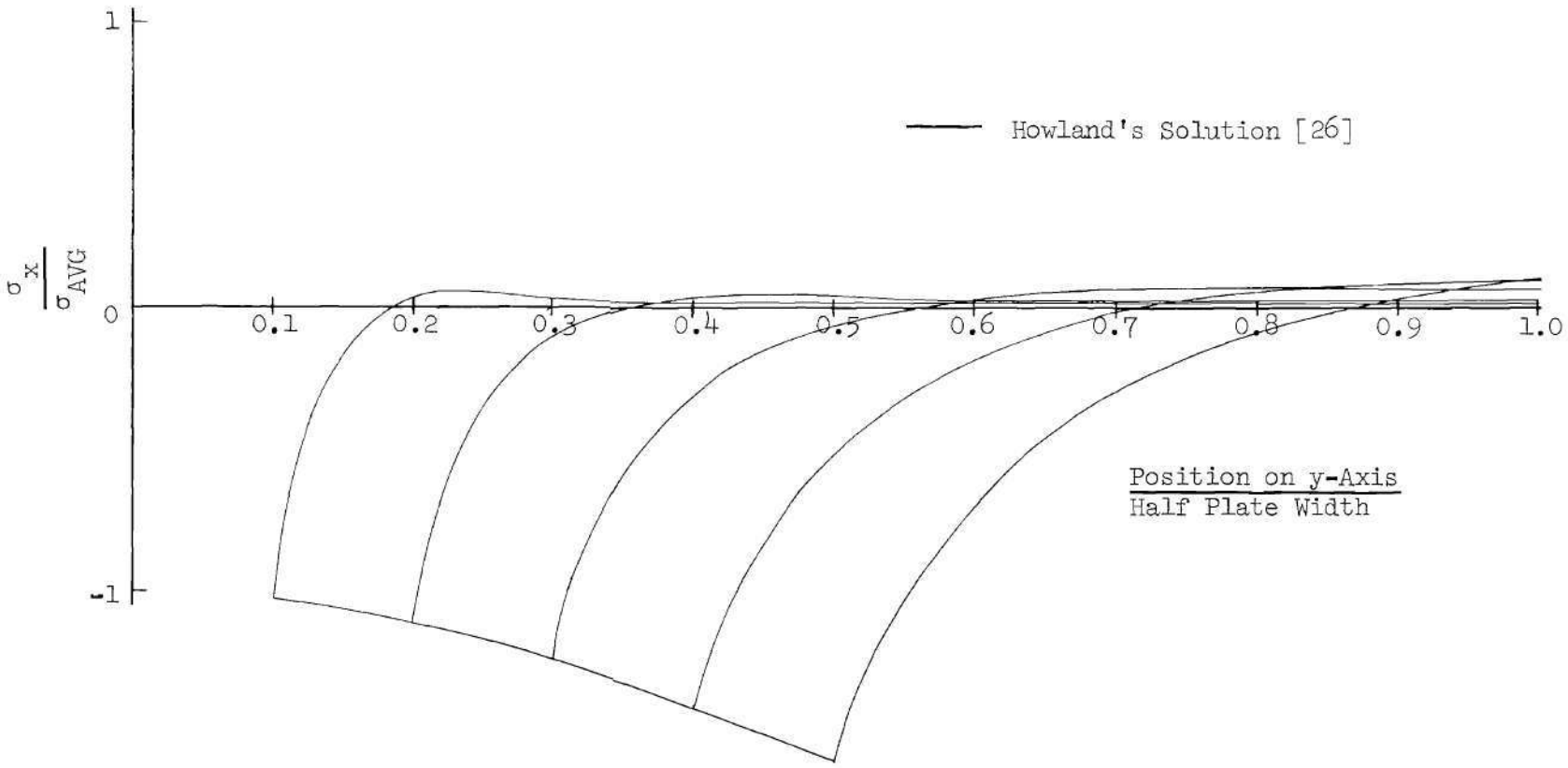

Figure 11(a). σ_x Along y-Axis for $\rho = 1.0$

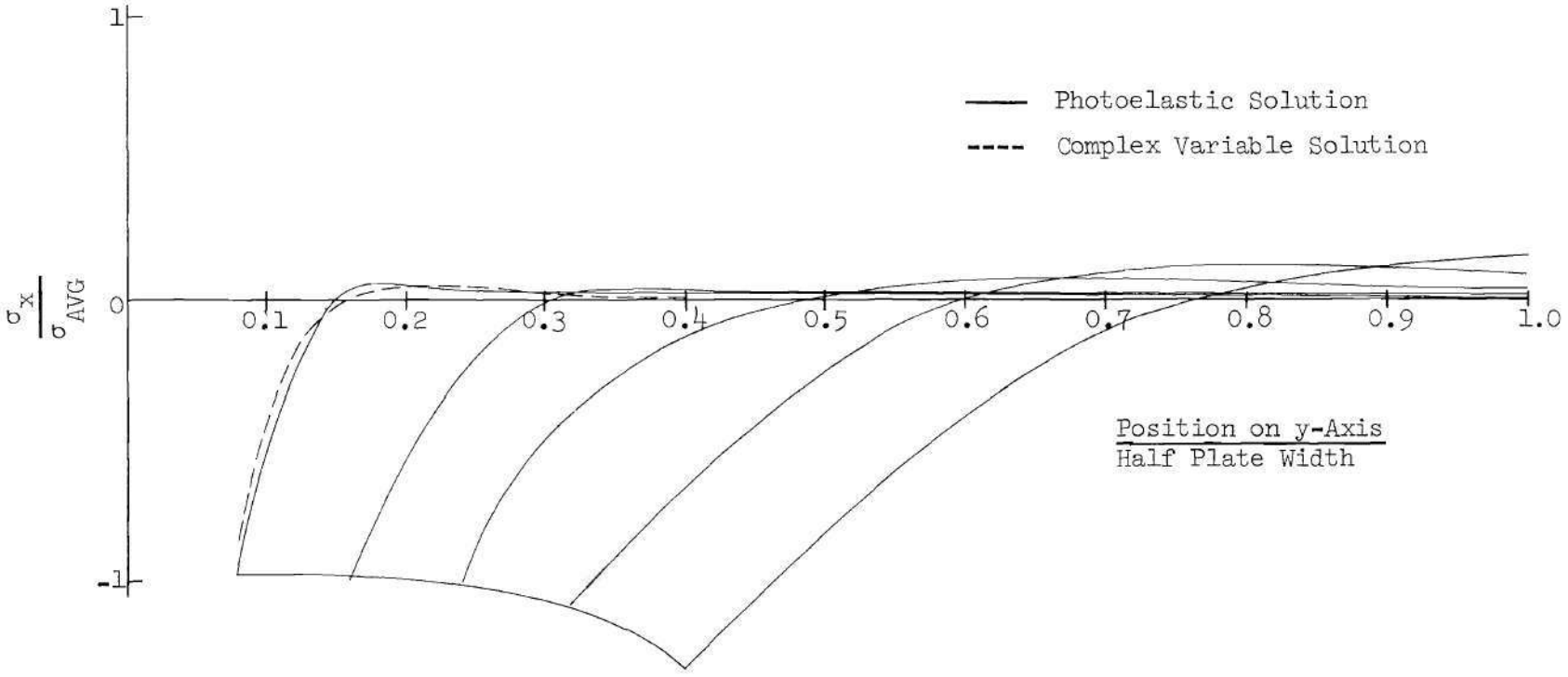

Figure 11(b). σ_x Along y-Axis for $\rho = 0.8$

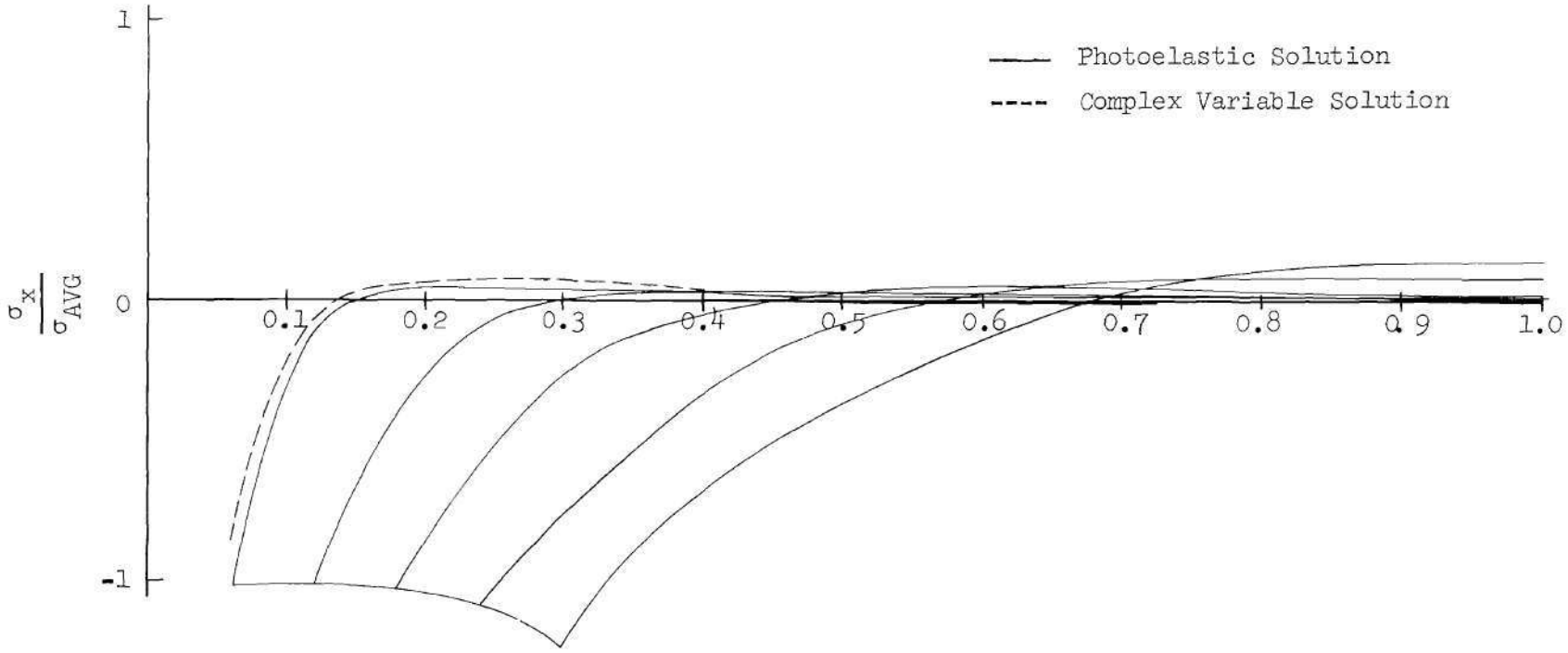

Figure 11(c). σ_x Along y-Axis for $\rho = 0.6$

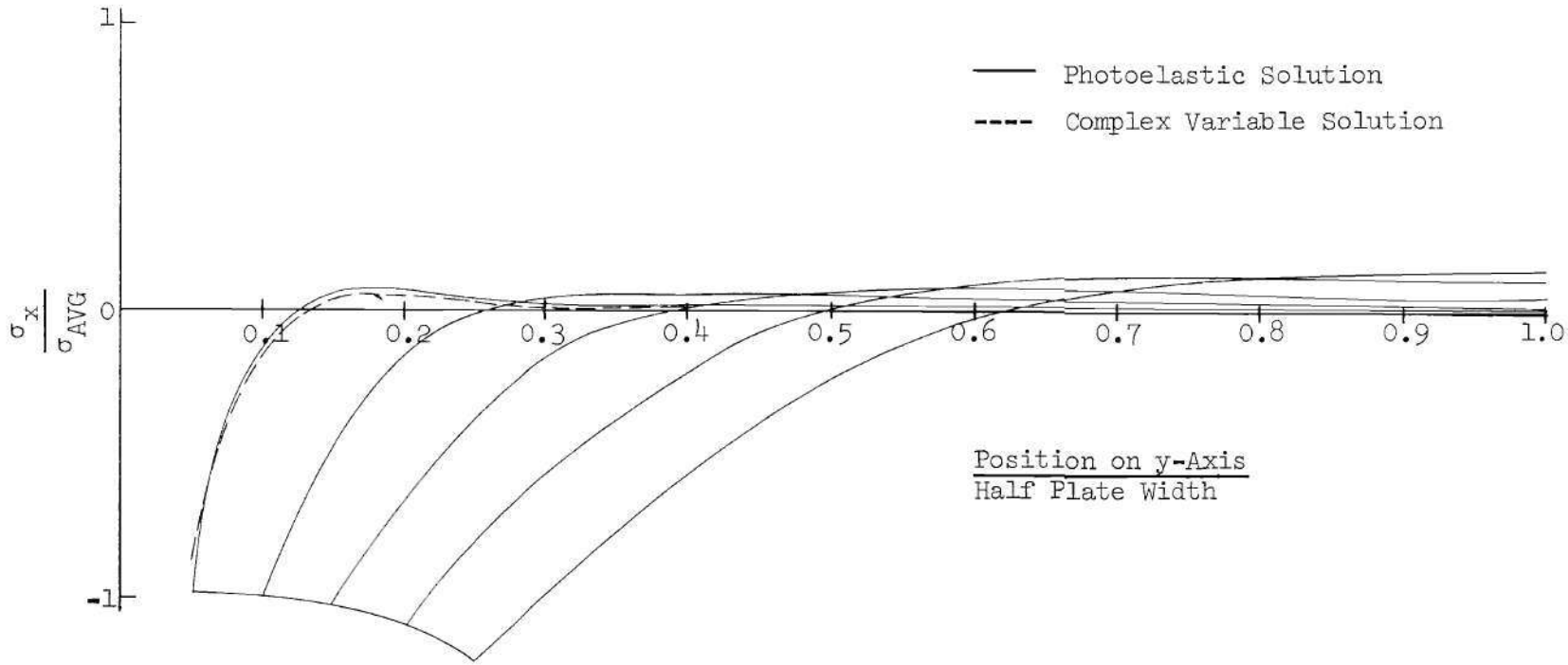

Figure 11(d). σ_y Along y-Axis for $\rho = 0.5$

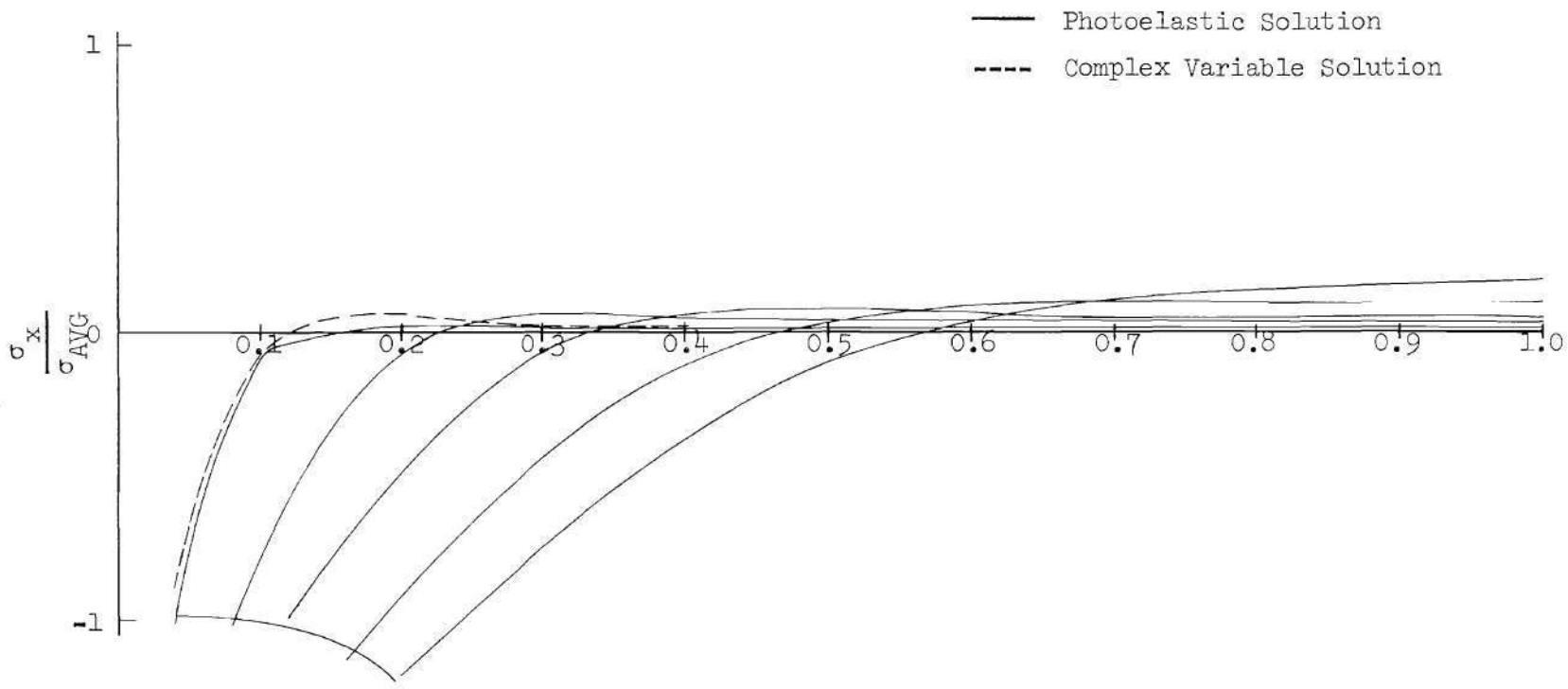

Figure 11(e). σ_x Along y-Axis for $\rho = 0.4$

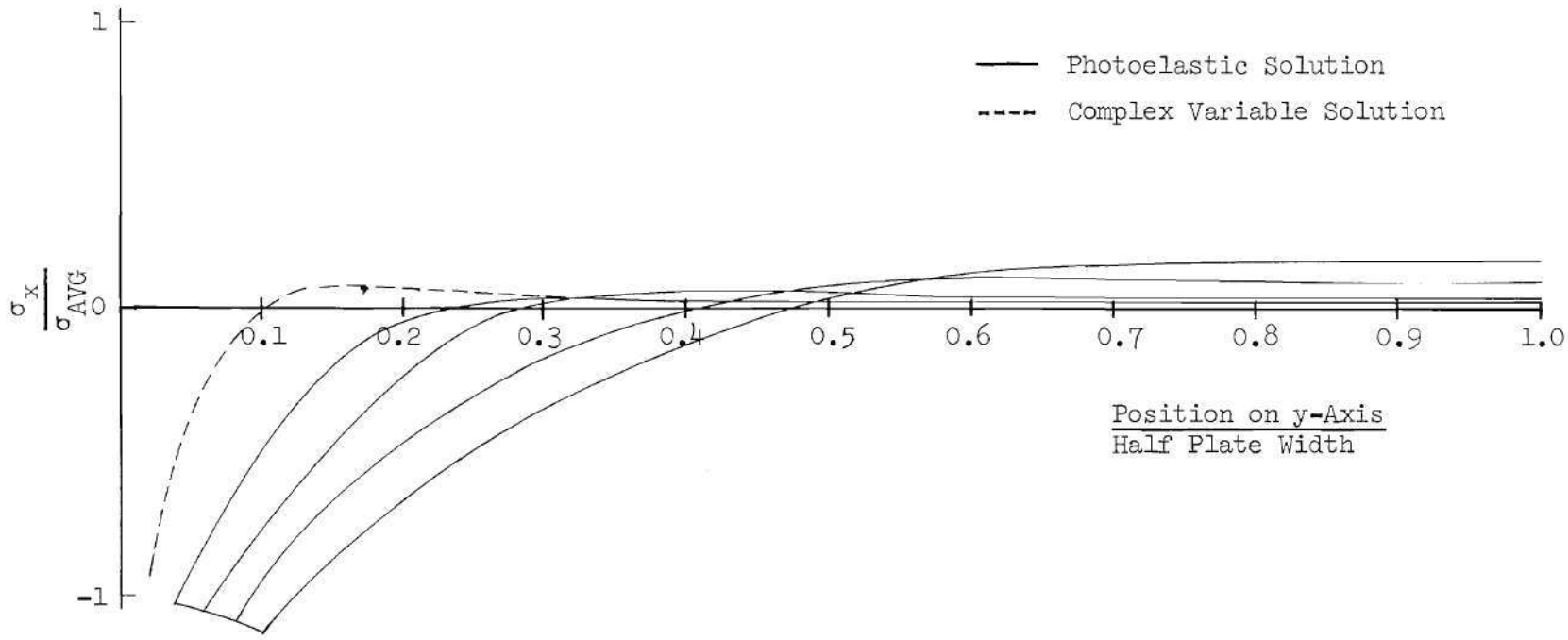

Figure 11(f). σ_x Along y-Axis for $\rho = 0.2$

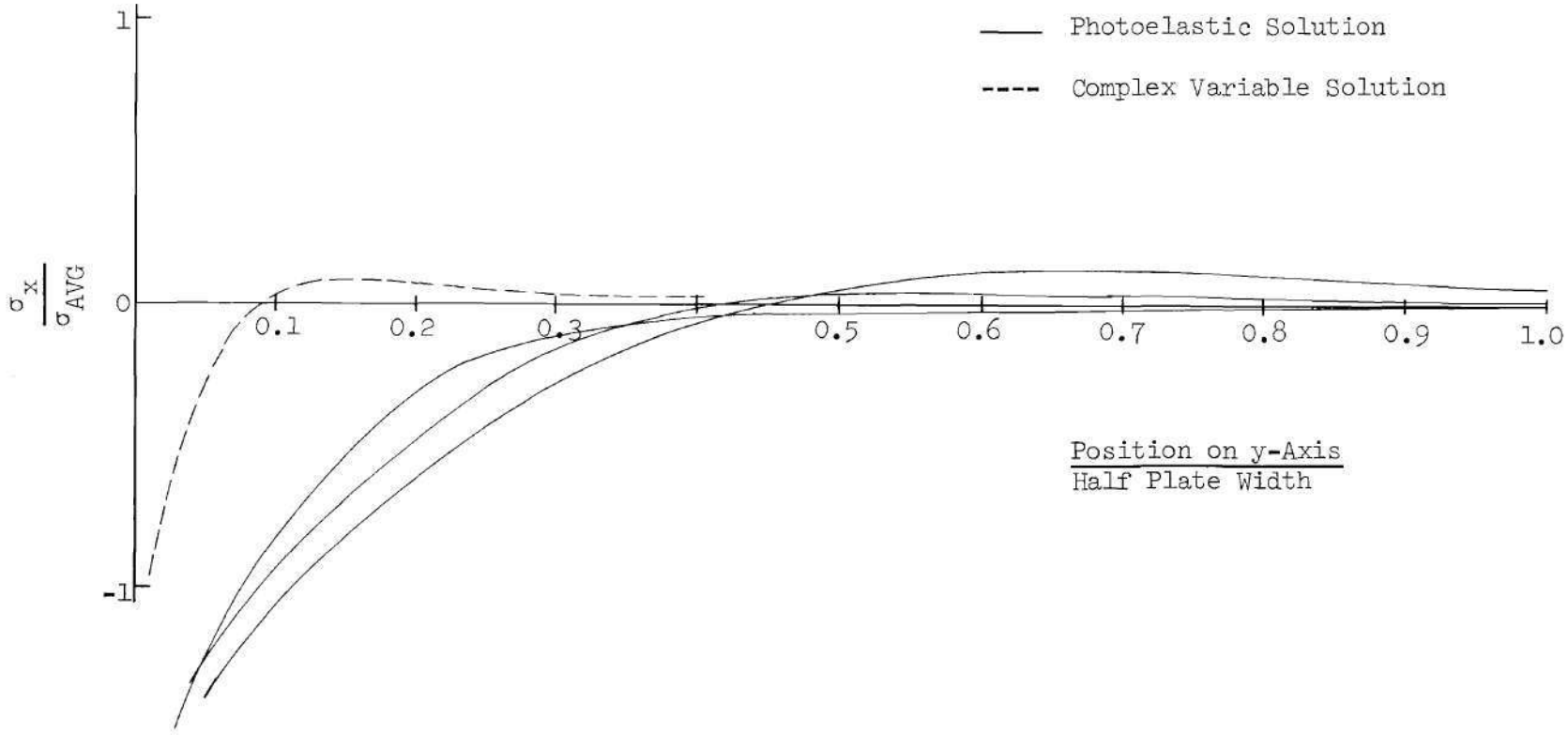

Figure 11(g). σ_x Along y-Axis for $\rho = 0.1$

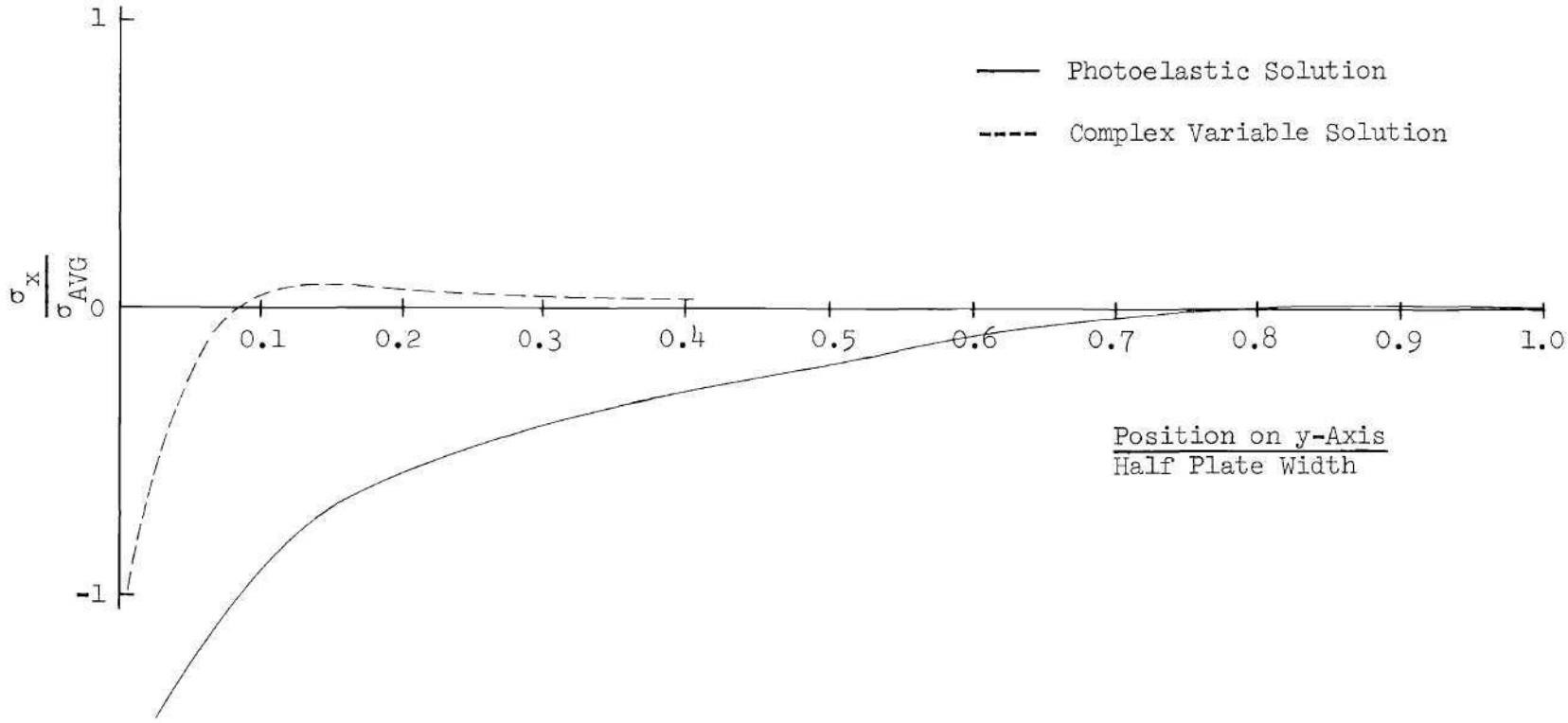

Figure 11(h). σ_x Along y-Axis for $\rho = 0.05$

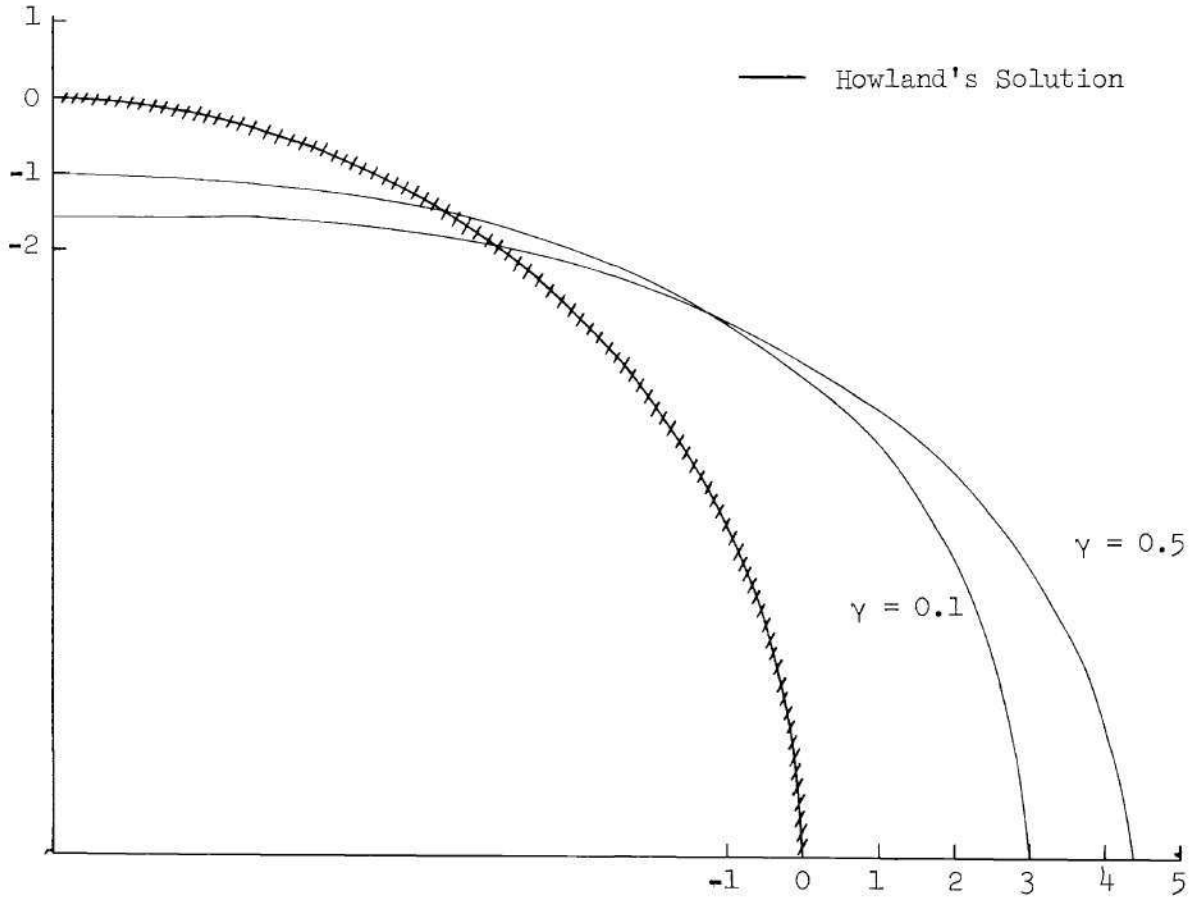

Figure 12(a). Tangential Boundary Stress, σ_t/σ_{AVG}, for $\rho = 1.0$

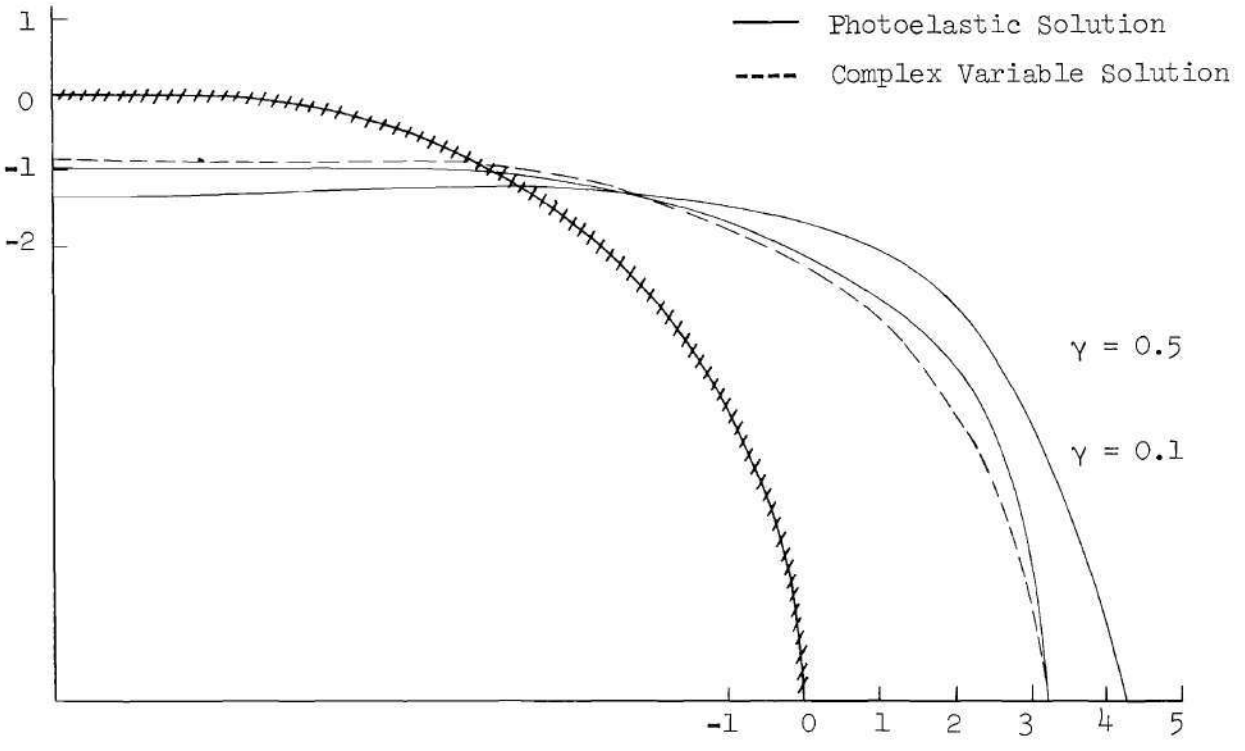

Figure 12(b). Tangential Boundary Stress, σ_t/σ_{AVG}, for $\rho = 0.8$

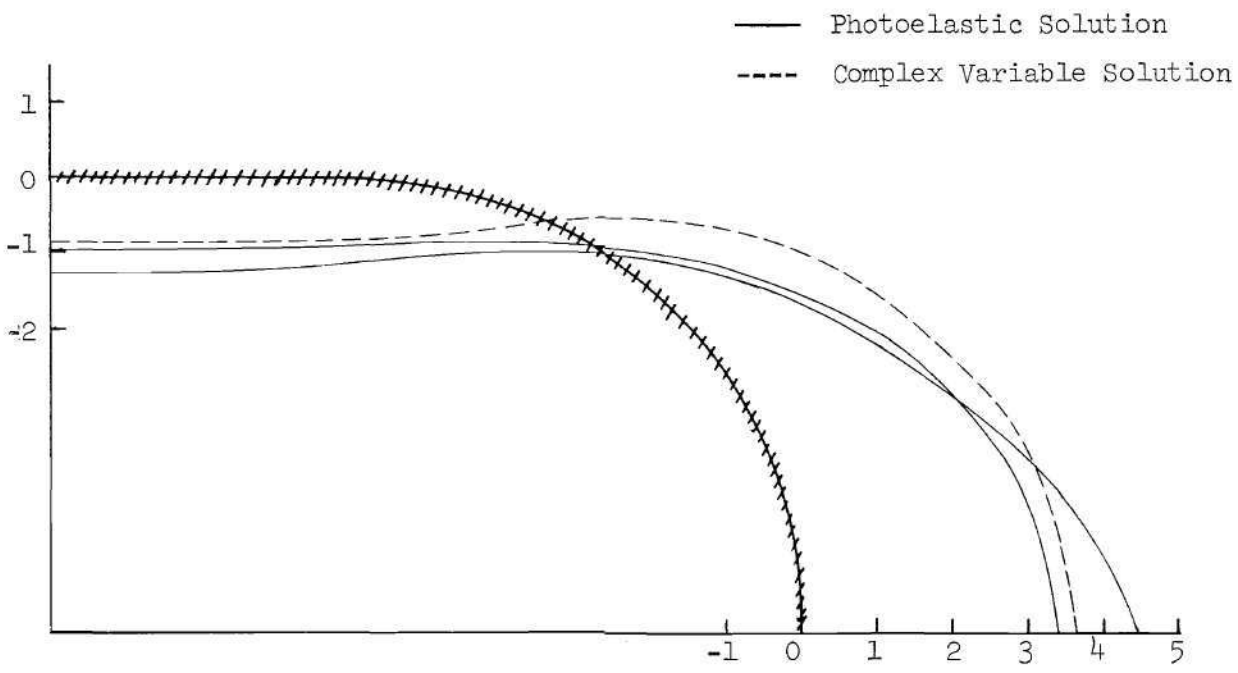

Figure 12(c). Tangential Boundary Stress, σ_t/σ_{AVG}, for $\rho = 0.6$

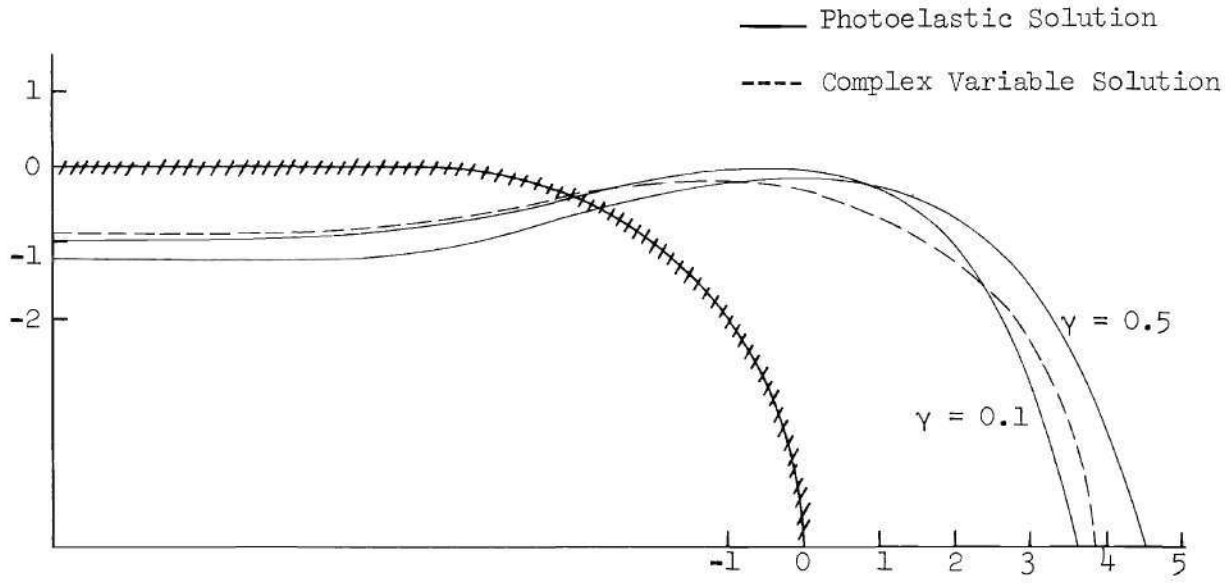

Figure 12(d). Tangential Boundary Stress, σ_t/σ_{AVG}, for $\rho = 0.5$

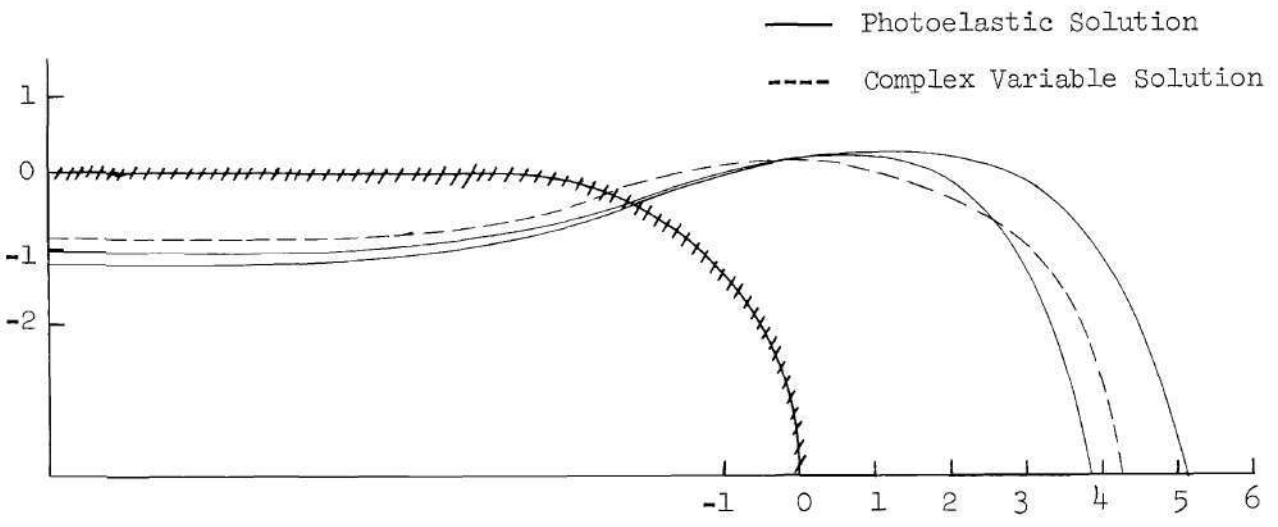

Figure 12(e). Tangential Boundary Stress, σ_t/σ_{AVG}, for $\rho = 0.4$

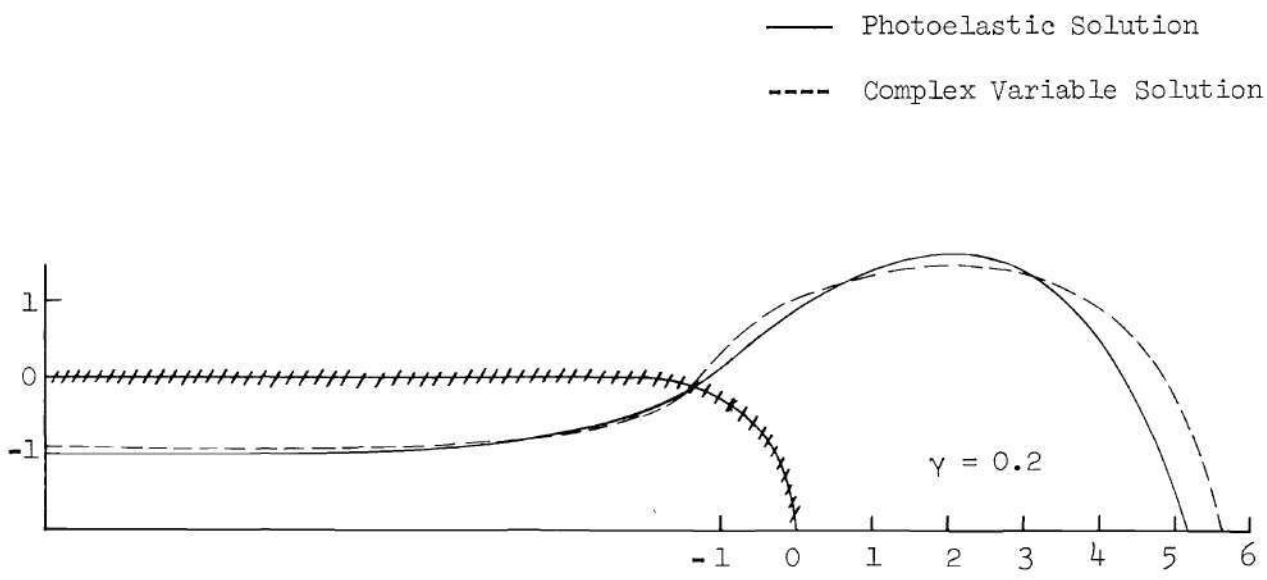

Figure 12(f). Tangential Boundary Stress, σ_t/σ_{AVG}, for $\rho = 0.2$

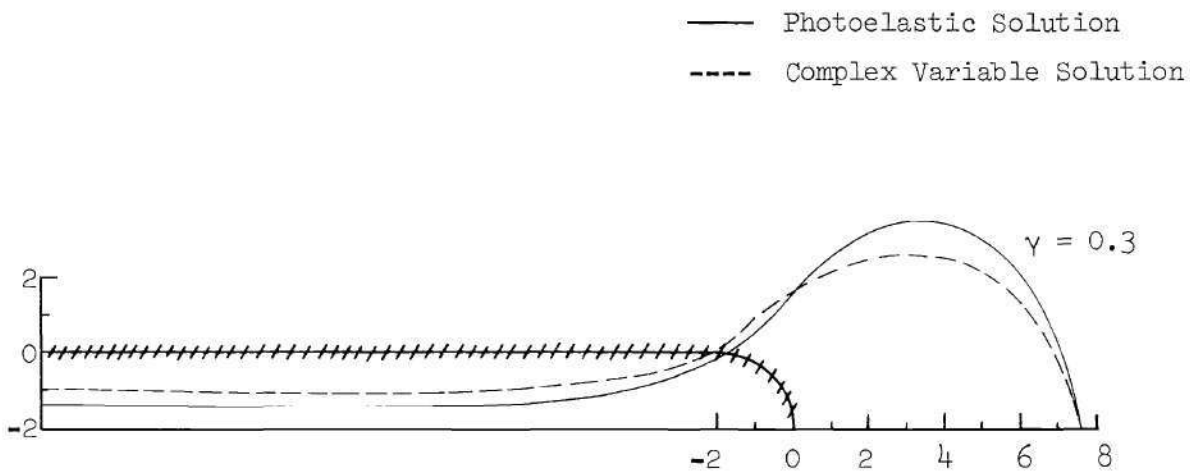

Figure 12(g). Tangential Boundary Stress, σ_t/σ_{AVG}, for $\rho = 0.1$

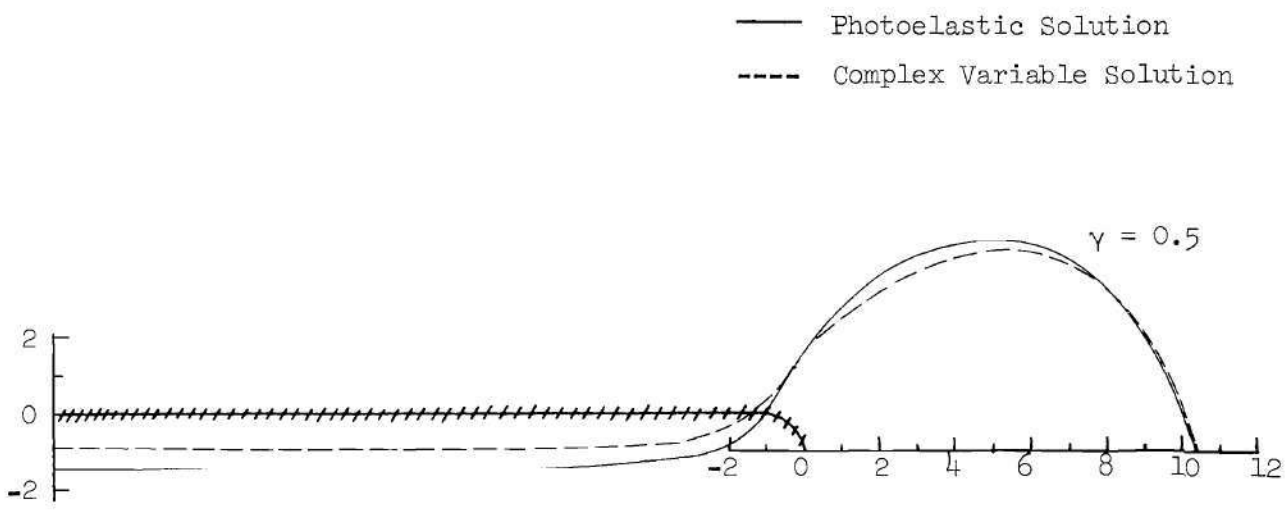

Figure 12(h). Tangential Boundary Stress, σ_t/σ_{AVG}, for $\rho = 0.05$

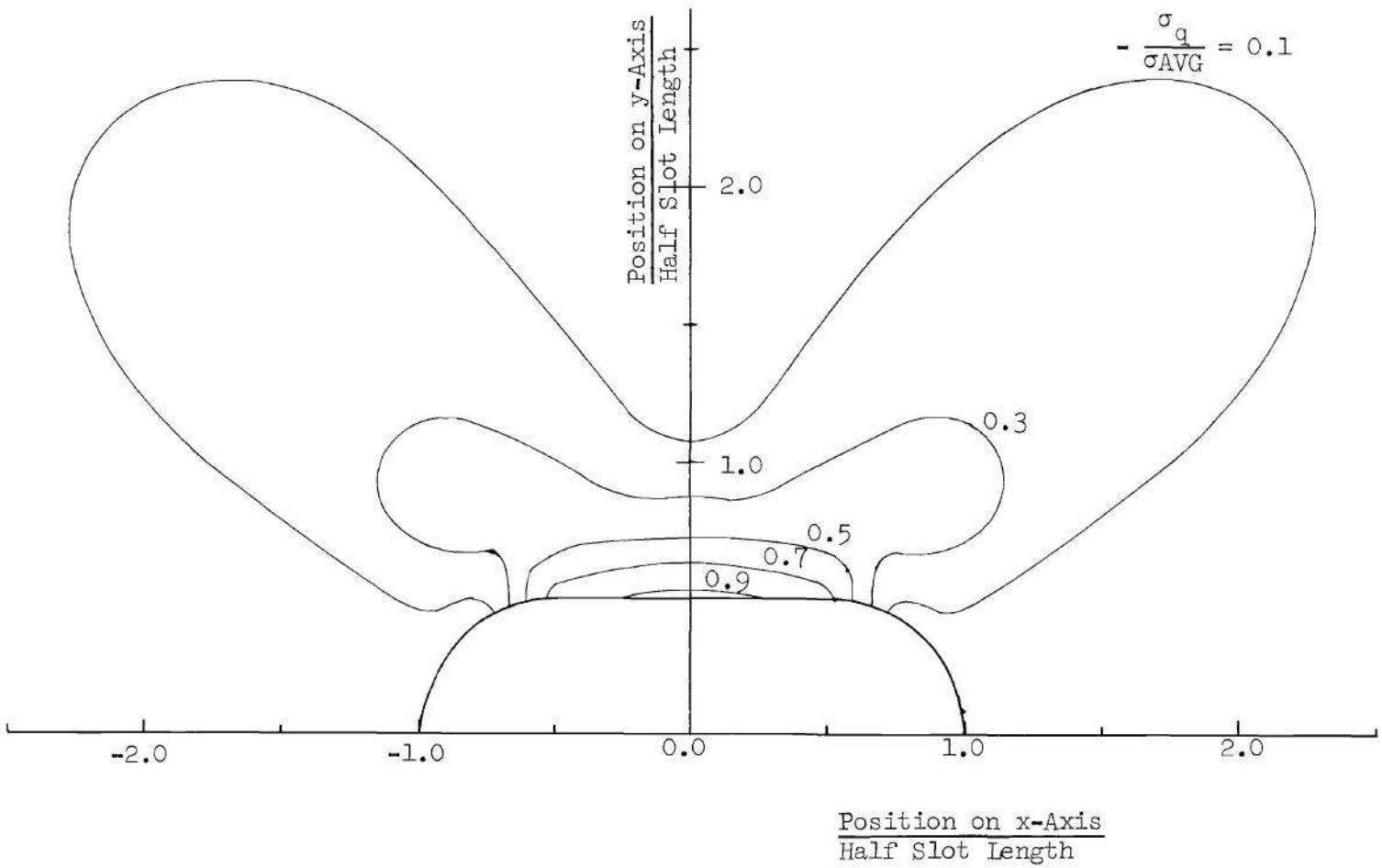

Figure 13. Lines of Constant Value of Compressive Principal Stress for $\rho = 0.5$ and $\gamma = 0.2$

CHAPTER IV

DETERMINATION OF TENSILE STRESS TO CAUSE BUCKLING IN PLATES WITH HOLES

The objective of this chapter is to derive a relation which can be used to predict the tensile stress at which a sheet with a slot will undergo a local buckling type phenomenon. This will be done by analyzing experimental results obtained on specimens whose geometric parameters are varied. The buckling load of the perfect system will be inferred from an examination of the data obtained from the imperfect system.

Depending upon the type of imperfect system being examined, the method of inferring a buckling load for a perfect system may differ. The validity of the inference should always be justified. Often, the justification given is simply of an empirical nature. It is preferable, if possible, to use as a starting point an analysis of a mathematical model of the physical behavior involved.

The problem examined here is similar to a supported plate under edge compression in that the load versus lateral displacement curve is of the form generally recognized as associated with a stable post-buckling configuration. A system of this type may be depicted as in Figure 14. The vertical load axis and $C\text{-}P_1\text{-}C'$ represent equilibrium branches of a perfect system. The vertical branch is stable up to a

bifurcation point, P_1. For loads greater than P_1, branches P_1-C and P_1-C′ are stable and the vertical branch is unstable. The curve O-A-B represents an equilibrium path for a corresponding imperfect system. The dashed curves O-A-D and P_1-D′ will be discussed in a subsequent section.

Dixon and Strannigan [41] have examined the problem of determining the tensile buckling load for thin sheets with central slots. The problem of ultimate interest to them was the cracked sheet. They determined upper and lower limits of the buckling load from observations made on load-displacement curves similar to O-A-B in Figure 14.

In another investigation Bingham [57] determined tensile buckling loads of thin sheets with central, rectangular cut-outs. Bingham attached a photoelastic strip to the sheet and analyzed the resulting fringe pattern. The photoelastic fringe pattern was similar to that developed in a column under end compression. The bending component of the fringe patterns was then analyzed by a Southwell technique to determine the critical loads.

In a series of papers [54, 65, 66] dealing with the behavior of cracked sheets in tensile fields, Clarkson and his associates also determined buckling loads. They were primarily concerned with behavior under dynamic conditions where the excitation of the plate was caused by acoustic pressure fluctuations. They associated the buckling condition with observations of the frequency response of the plate.

The applicability of the Southwell technique to plates with nonuniform prebuckle stress states has been examined by Carlson and

his students [67, 68]. Some of this work checked the feasibility of the Southwell method of analysis for this problem. It was found that the Southwell method could be applied provided certain restrictions were imposed. It may be shown that the condition for applicability of the Southwell method is that middle surface stretching due to bending must be negligible. This may be experimentally determined if the midsurface strains are measured. For the sake of completeness a discussion of the Southwell technique as presented in reference [67] will now be presented.

Southwell Technique

In order to discuss the applicability of the Southwell technique on a mathematical basis, it is essential to begin with the governing differential equations of the problem. These have already been given in Chapter II. The compatibility equation is given by

$$\nabla^4 F = E\left[(w,_{xy})^2 - w,_{xx}\, w,_{yy} - (w_o,_{xy})^2 + w_o,_{xx}\, w_o,_{yy}\right] \qquad (1)$$

where here terms involving the initial deviation from flatness, w_o, have been included. It should be noted that $(w - w_o)$ is the deflection due to the applied load. The transverse equilibrium equation is

$$D\nabla^4(w - w_o) = h(F,_{yy}\, w,_{xx} + F,_{xx}\, w,_{yy} - 2\, F,_{xy}\, w,_{xy}). \qquad (2)$$

Body forces and temoerature effects are not included in the above

equations. The associated boundary conditions and auxiliary conditions necessary for the solution of these equations have been presented in Chapter II and change only slightly when the w_o terms are included.

In a linearized version of this theory the terms on the right hand side of Equation (1) are neglected. Thus, the equations become uncoupled* and it is possible to solve Equation (1) for the stress function. This procedure is valid if the deflection and the initial deviation from flatness are sufficiently small. It may also be noted that

$$(w_{,xy})^2 - w_{,xx}\, w_{,yy}$$

and

$$(w_{o,xy})^2 - w_{o,xx}\, w_{o,yy}$$

represent, respectively, the Gaussian curvatures of the total deflection function and the initial deviation from flatness function. Thus, if these functions represent developable surfaces, Equations (1) and (2) are indeed uncoupled.

The uncoupled forms of Equations (1) and (2) are thus

$$\nabla^4 F = 0 \tag{3}$$

---

* See discussion of perturbation technique in Chapter VI of this dissertation.

and

$$D \nabla^4 W - hF,_{yy} W,_{xx} - hF,_{xx} W,_{yy} + 2hF,_{xy} W,_{xy} \qquad (4)$$

$$= hF,_{yy} w_{o},_{xx} + hF,_{xx} w_{o},_{yy} - 2hF,_{xy} w_{o},_{xy}$$

where, for convenience, the substitution ($W = w - w_o$) has been made. Due to the uncoupling, the in-plane stress distribution is linearly proportional to the external loading and a load intensity factor, λ, can be introduced such that

$$\frac{hF,_{yy}}{D} = \lambda\ p_1\ (x,y) \quad ,$$

$$\frac{hF,_{xx}}{D} = \lambda\ p_2\ (x,y) \quad . \qquad (5)$$

and

$$\frac{2hF,_{xy}}{D} = \lambda\ p_3\ (x,y) \quad .$$

Then Equation (4) may be expressed as

$$\nabla^4 W - \lambda(p_1 W,_{xx} + p_2 W,_{yy} + p_3 W,_{xy}) \qquad (6)$$

$$= \lambda(p_1 w_{o},_{xx} + p_2 w_{o},_{yy} + p_3 w_{o},_{xy}) \quad .$$

If $w_o \equiv 0$ in Equation (6), and the applied loading is capable of producing buckling, then an eigenvalue problem arises. Associated with this problem are eigenfunctions W_1, W_2 . . . and eigenvalues λ_1, λ_2, . . . This eigenvalue problem is in general extremely difficult to solve

for stress distributions such that p_1, p_2, and p_3 are other than constants. This development, however, is not concerned with the actual solutions of problems but rather the properties of these solutions.

The eigenfunctions of this problem are linearly independent [68] thus suggesting that the continuous deviation from flatness function may be well represented by the expression

$$w_o = \sum_{n=1}^{m} a_k W_k \quad , \tag{7}$$

where the admissible w_o are restricted to those having the same boundary conditions as the W_k. Reference [67] describes two possible schemes for computing the a_k. If Equation (7) is a good representation of w_o, then the solution of Equation (6) is the particular solution which can be written as

$$W = \frac{a_1}{\left(\frac{\lambda_1}{\lambda} - 1\right)} W_1 + \sum_{k=2}^{m} \frac{a_k}{\left(\frac{\lambda_2}{\lambda} - 1\right)} W_k \quad . \tag{8}$$

If the eigenvalues of the problem are well separated, then as λ approaches λ_1, the first term on the right of Equation (8) will dominate. Equation (8) can then be rewritten as

$$W = \lambda_1 \left(\frac{W}{\lambda}\right) - a_1 W_1 - \sum_{k=2}^{m} \left(\frac{\lambda_1 - \lambda}{\lambda_2 - \lambda}\right) a_k W_k \quad . \tag{9}$$

The above equation is of the Southwell form if the terms of the summation are neglected. If an experimental investigation is carried out under the restrictions imposed by Equations (3) and (4), then an emerging linearity of a plot of $\left(\frac{W}{\lambda}\right)$ versus W should be observed as λ aproaches λ_1. A judicious choice of the point where measurements are taken can increase the accuracy of the results considerably. For instance, choosing the point so that it is a relative maximum of the W_1 shape and a node of the W_2 shape can markedly increase the sensitivity.

A simple effective way to check the applicability of the Southwell method to plate problems is to plot the midsurface strain as a function of load intensity λ. This, in essence, provides a check on the validity of Equations (5). A departure from linearity of the above type of plot indicates that there is middle surface stretching due to bending and then the terms on the right-hand side of Equation (1) cannot be neglected.

Description of Specimens and Experimental Procedure

The experiments described in this chapter were designed to provide data from which the buckling loads of slotted thin sheet specimens could be determined. The sheet specimens were designed to eliminate the effect of sheet length from the behavior of interest. Each specimen can then be characterized by only two nondimensional parameters. These are the hole length to sheet width ratio, γ, and the hole height to hole length ratio, ρ. The dimensional specifications of each of the specimens tested are given in Table 2. It should be

Table 2. Model Specifications*

	2H	$\widetilde{W}$	Model 1 2R	Model 2 2R	Model 3 2R	Model 4 2R	Model 5 2R	Model 6 2R	Model 7 2R	Model 8 2R
Series K	1.20	12	—	—	—	0.48	0.60	0.72	0.96	1.20
Series L	2.40	12	—	—	0.48	0.96	1.20	1.44	1.92	2.40
Series M	3.60	12	—	0.36	0.72	1.44	1.80	2.16	2.88	3.60
Series N	4.80	12	—	0.48	0.96	1.92	2.40	2.88	3.84	4.80
Series P	6.00	12	0.30	0.60	1.20	2.40	3.00	3.60	4.80	6.00

Series	2R=	$\widetilde{W}$=	Model 1	Model 2	Model 3	Model 4
Q, Cracks	0.0063	12	2H = 2.0	2H = 2.2	2H = 3.0	2H = 4.0

*All dimensions in inches.

noted that the results on specimens with cracks, series Q, have been reported in reference [67] and are referred to in that reference as the prestressed models.

The prestressing referred to is simply a process of transforming the crack buckling problem into an elastic problem. This was done by applying a slight lateral pressure to the sheet during the initial loading cycle. The sheet was thereby restrained from buckling and upon unloading was still flat. Because of the very high stress concentration factor at the crack tip, residual stresses were of course present, but subsequent loading involved only an elastic response as long as the prestress load was not exceeded.

In test series, K, L, M, N and P the slot tip radii range from 0.30 inch to 6.00 inches. The loads applied to the specimens of these series were kept well below the known proportional limit of the material. This was possible since there was an apriori knowledge of the stress concentration factor obtained from the photoelastic results.

The specimens were made from 0.020 inch thick sheet of the aluminum alloy 2024-T3. End plates made of 0.365 inch thick bar stock of the aluminum alloy 2024-T4 were bonded on both faces of the sheet with a room temperature curing epoxy. Two dowel pins were used at each end to assure proper alignment of the end plates on the sheet. A typical specimen is illustrated in Figure 18.

For the crack models, series Q, a crack was simulated by use of a jeweler's saw with a blade width of 0.0063 inch. Access for the

blade was made by drilling a hole in the center of the specimen with a No. 74 carbon steel drill. The slot configurations were machined on a milling machine using a fly cutting process. Each series of slot configurations represents one model with a fixed length of slot. The change of configuration then amounted to increasing the end radius until a circle was produced.

Each specimen was loaded in an Instron testing machine with the load range being determined by the estimated buckling load and the load increments being chosen to provide sufficient data for analysis.

In the section in which the applicability of the Southwell technique was discussed it was indicated that lateral deflection measurements should be obtained. Actually any measurement which is linearly proportional to the deflection is just as suitable or sometimes, as in this particular case, more suitable. Since the bending strain is linearly proportional to the curvature, two strain gages were mounted back-to-back in the standard configuration for measuring bending strain. The gages were centered on the specimen and as close to the slot edge as practical with their strain sensitive direction perpendicular to the line of loading. The gages were connected to a BLH strain indicator through a BLH switching and balancing unit. The switching and balancing unit was connected to yield both the output of the individual gages and the difference in the gage outputs. The output from the individual gages represented the surface strains while the difference of the gage outputs was twice the bending strain. The algebraic average of the two individual gage outputs, on the other hand, represents the middle surface strain. The measurement of the middle

surface strain, as noted earlier, is used to establish the range of validity of the extended Southwell method of analysis.

In addition to strain gages, displacement transducers (LVDT's) were used to measure displacements. Although the data from the LVDT's should have yielded the same results as the strain gages, the agreement was not consistent. In some instances Southwell data from each source produced results which were in agreement, whereas in other cases they did not. For the LVDT system the discrepancy appeared to stem from rigid body motions and sheet straightening which took place during loading. These observations and the fact that the LVDT measurements produced results which were not internally consistent led to a decision to use results based on the strain gage measurements. These proved to provide both a high sensitivity and good consistency.

Test Results

It has already been mentioned that bending strain measurements were analyzed to determine buckling loads. This is a convenient quantity to use since twice the bending strain is equivalent to the algebraic difference of the two surface strains. The surface strains must be obtained to compute the midsurface strain which is the algebraic average of the two surface strains. It has already been noted that the midsurface strain is used to determine the range of applicability of the Southwell analysis. In most instances the bending strain behaved erratically at relatively small loads. This type of erratic behavior is common during the initial application of load. Lundquist [70] observed the presence of this behavior in column experiments and

to eliminate the error associated with incorrect load data, he proposed a modified Southwell plot which overcomes some of this initial erratic behavior.

A Lundquist type relation can be obtained in the same way as the Southwell type relation presented previously in this chapter. The Southwell relation has the form

$$\lambda_1 \left(\frac{W}{\lambda}\right) = W + a_1 W_1 \quad ,$$

where the plotted variables are

$$\left(\frac{W}{\lambda}\right) \quad \text{and} \quad W \quad .$$

In a modified form of the Lundquist type, the basic relation is

$$\left(\lambda_1 - \lambda_0\right)\left[\frac{W - W_0}{\lambda - \lambda_0}\right] = \left(W - W_0\right) + \left(a_1 + W_0\right) W_1 \quad . \tag{10}$$

In relation (10) the plotted variables are $(W - W_0)/(\lambda - \lambda_0)$ and $(W - W_0)$. It should be noted that the zero subscript refers to a point on the load vs. deflection curve where the erratic initial behavior appears to have been overcome.

If twice the bending strain is defined as $\Delta\varepsilon$, then the variables to be plotted are*

$$\frac{\Delta\varepsilon - \Delta\varepsilon_o}{P - P_o} \quad \text{and} \quad (\Delta\varepsilon - \Delta\varepsilon_o) \quad .$$

The inverse of the slopes of these lines may then be identified as the quantity of $(P_1 - P_o)$ where P_1 is the value corresponding to the smallest eigenvalue.

A typical set of curves is shown in Figures 15, 16, and 17. Figure 15 represents the strain differences, $\Delta\varepsilon$, Figure 16 represents the midsurface strain, and Figure 17 is the corresponding Lundquist Plot. Point A in Figure 16 indicates the deviation from linearity which imposes the limit of applicability of the Southwell method. The location of point A has also been indicated in Figures 14 and 15, and is reflected in the Lundquist plot by a decrease in slope beyond point A. This is related to the stiffening characteristic indicated beyond point A in curves O-A-B of Figures 14 and 16. The dashed curves of Figure 14, i.e., curves P_1 - D′ and A-D, correspond to the solution of the perfect and imperfect linear, uncoupled problem.

If point A has not been determined from Figure 16, then an attempt to use the Lundquist plot of the data in Figure 17 would tend to

---

*Note that the conversion from the deflection function to the strain differences in the Lundquist relation can be readily performed by differentiation of W twice with respect to the appropriate independent variable and use of the strain-curvature relations.

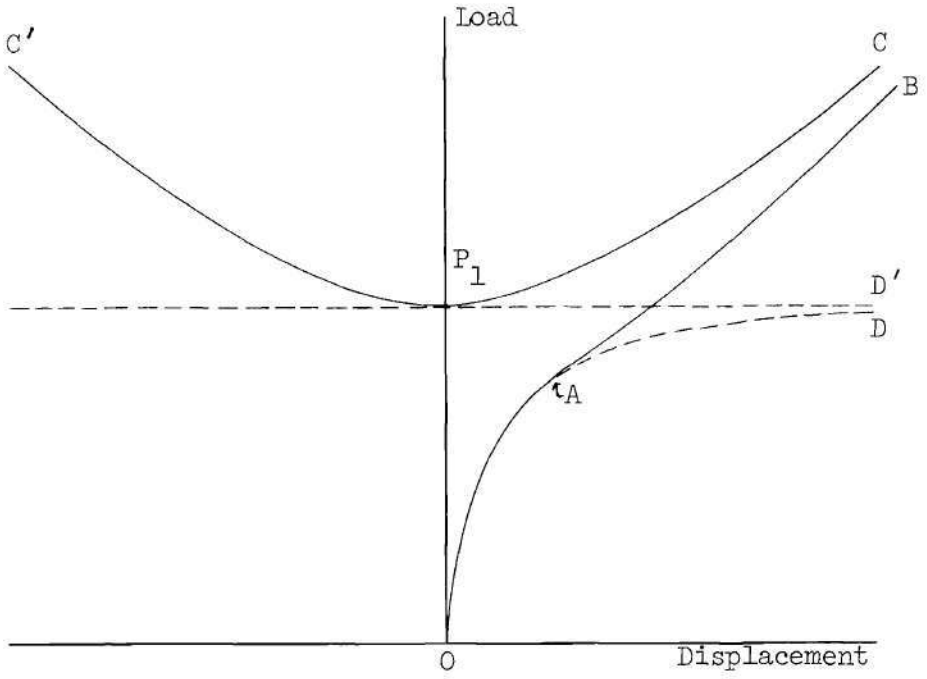

Figure 14. Load vs. Displacement Curves for Typical System

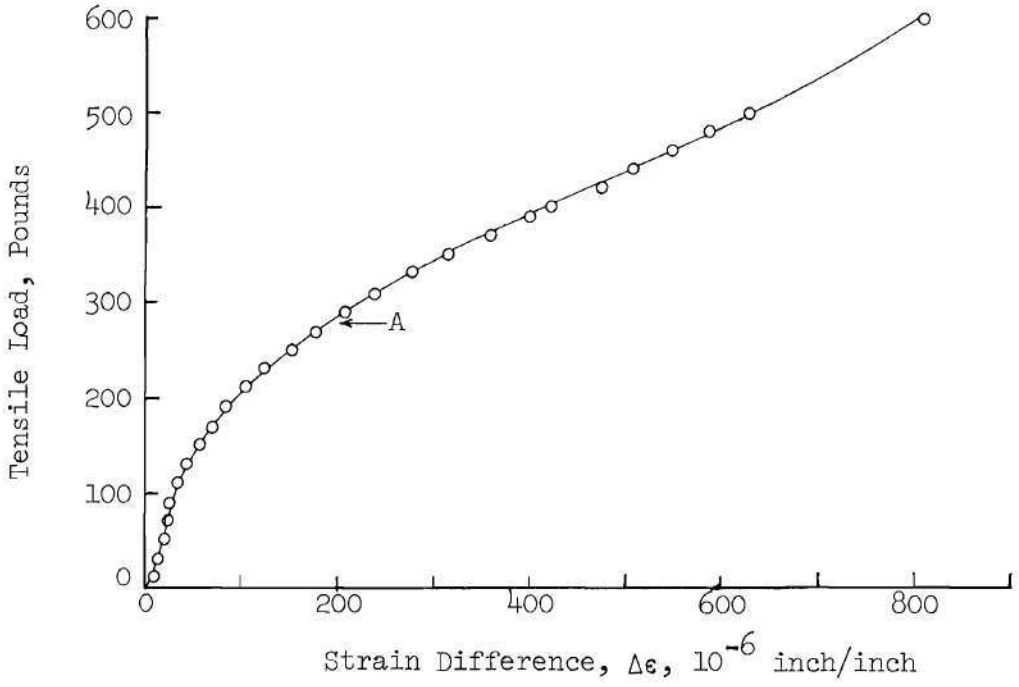

Figure 15. Typical Load vs. Strain Difference Curve

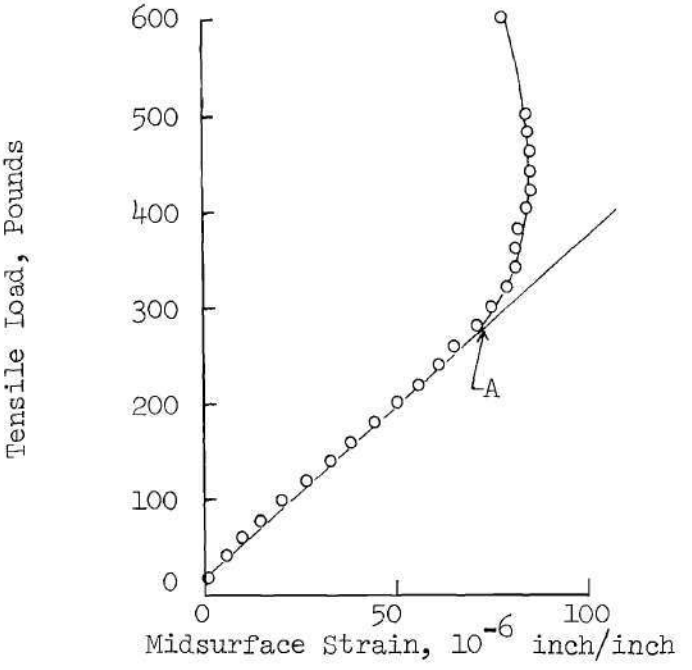

Figure 16. Typical Load vs. Midsurface Strain Curve

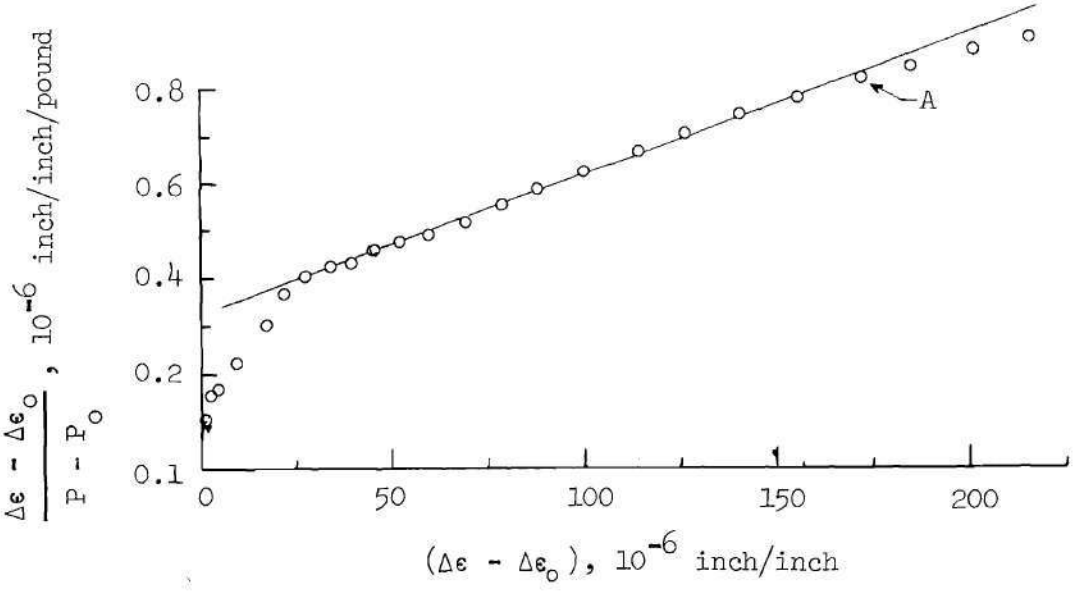

Figure 17. Typical Lundquist Plot

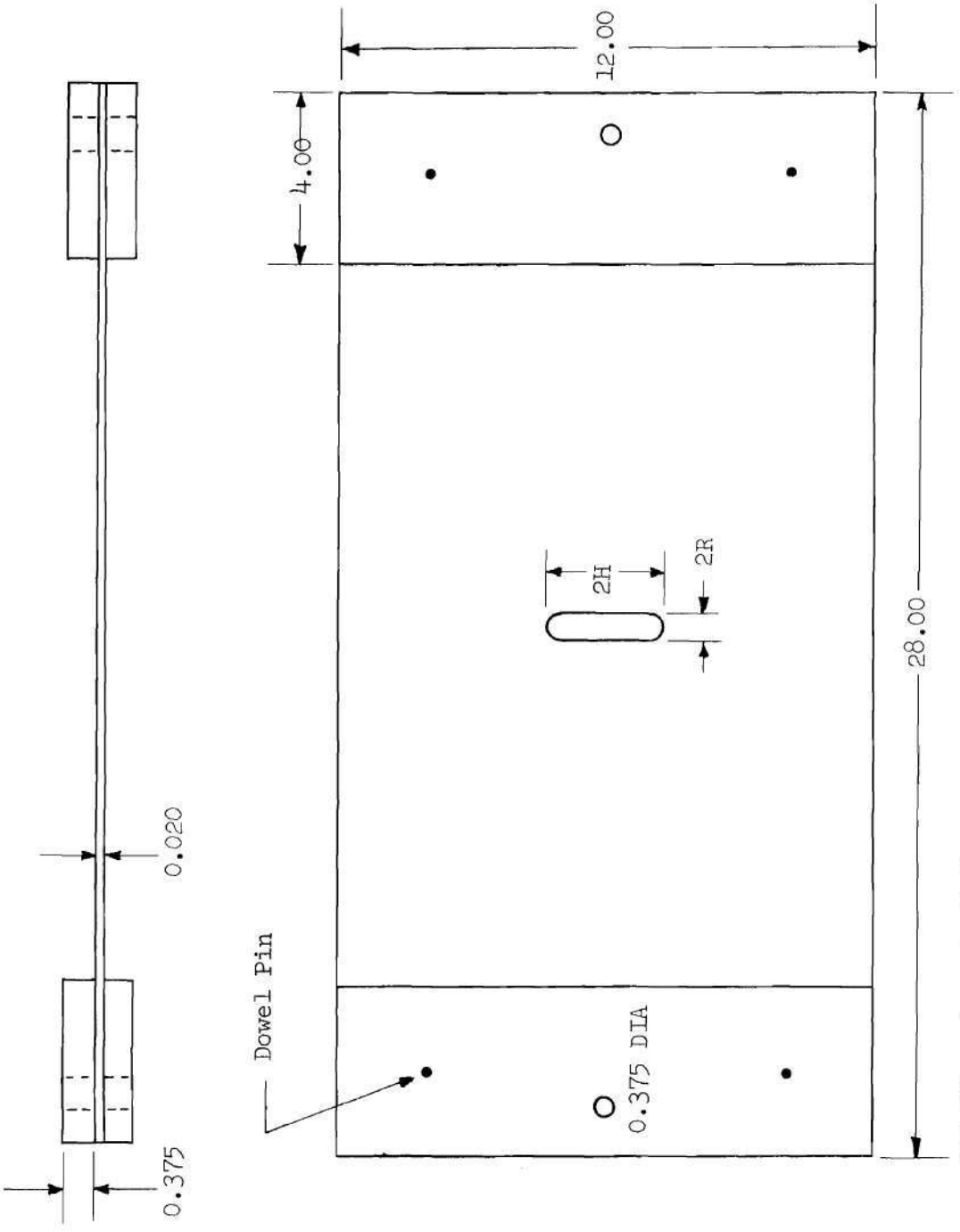

All Dimensions in Inches

Figure 18. Typical Metal Specimen

result in a straight line of smaller slope than that shown. This follows because the analyst would probably try to include data beyond point A. The smaller slope would, however, produce an overestimation of the critical load, so this observation demonstrates the importance of determining the limits of applicability of the Southwell or Lundquist methods.

Table 3 gives values of P_{cr} for each of the models. These values are the average obtained from Lundquist plots using several values of P_o. The slopes of the lines were computed by a least square method. An average of several values was obtained since total variations of as much as 10 percent were observed when different values of P_o were used.

Analysis of Results

The results presented in Table 3 indicate general trends that had been expected. These are:

(1) The critical load decreased as the length of the slot increased

(2) The critical load increased as the end radius increased.

The first trend is the most dominant and has received the most attention in the literature. The only mention of the effect of radius found in the literature is in the work of Bingham [57]. Bingham concluded that increasing the corner radii of rectangular holes in plates under tension caused the buckling load to increase.

In the present discussion the critical stress will be defined as the critical load divided by the total cross sectional area of the

plate (i.e., the area of a cross-section not passing through the slot). The critical stress has been represented as

$$\sigma_{cr} = K\, E \left(\frac{t}{2H}\right)^2 \quad . \tag{11}$$

References [41, 51, 54, 55] have all used relations comparable to Equation (11). In these papers the quantity K is not constant and it is usually given for each model or series of models for which results are reported.

Walker [53] has suggested that an analogy be made between the crack buckling problem and a column on an elastic foundation. If this type of analogy is used, Equation (11) would not be a constant. Guided by this observation, one might propose an equation of the form

$$\sigma_{cr} = C\, E \left(\frac{t}{2H}\right)^2 \left(1 + \widetilde{F}\right) \tag{12}$$

where C is a constant and the quantity F may depend on dimensionless ratios of the geometrical parameters.

Assuming that Equation (12) provides a valid representation, and defining a new non-dimensional critical stress parameter $\bar{\sigma}_{cr}$ gives

$$\bar{\sigma}_{cr} = \frac{\sigma_{cr}}{E\left(\frac{t}{2H}\right)^2} = C(1 + \widetilde{F}) \tag{13}$$

The values of $\bar{\sigma}_{cr}$ for all of the models tested in this program are given in Table 4. It is seen that trends are not as apparent in this

Table 3. Critical Loads, P_{cr}

	Model 1 $\rho = 0.05$	Model 2 $\rho = 0.1$	Model 3 $\rho = 0.2$	Model 4 $\rho = 0.4$	Model 5 $\rho = 0.5$	Model 6 $\rho = 0.6$	Model 7 $\rho = 0.8$	Model 8 $\rho = 1.0$
Series K 2H = 1.2	____	____	____	4400	4500	4560	5130	5420
Series L 2H = 2.4	____	____	720	835	970	1030	1210	1220
Series M 2H = 3.6	____	475	605	640	666	700	730	770
Series N 2H = 4.8	____	455	344	310	338	388	418	434
Series P 2H = 6.0	157	226	240	254	270	284	312	340

Series Q, Cracks	2H = 2.0 P_{cr} = 1000	2H = 2.2 P_{cr} = 850	2H = 3.0 P_{cr} = 410	2H = 4.0 P_{cr} = 270

* P_{cr} is given in pounds
2H is given in inches
$\rho = 2R/2H$

Table 4. Nondimensional Critical Stresses, $\bar{\sigma}_{cr} = \dfrac{\sigma_{cr}}{E\left(\frac{t}{2H}\right)^2}$ *

	Model 1 $\rho = 0.05$	Model 2 $\rho = 0.1$	Model 3 $\rho = 0.2$	Model 4 $\rho = 0.4$	Model 5 $\rho = 0.5$	Model 6 $\rho = 0.6$	Model 7 $\rho = 0.8$	Model 8 $\rho = 1.0$
Series K $2H = 1.2$	___	___	___	6.29	6.43	6.52	7.16	7.73
Series L $2H = 2.4$	___	___	4.12	5.07	5.54	5.89	6.92	6.97
Series M $2H = 3.6$	___	6.10	7.78	8.20	8.53	8.98	9.38	9.90
Series N $2H = 4.8$	___	10.40	7.87	7.10	7.73	8.86	9.55	9.90
Series P $2H = 6.0$	5.61	8.08	8.58	9.07	9.66	9.98	11.15	12.15

Series Q, Cracks	$2H = 2.0$ $\bar{\sigma}_{cr} = 3.97$	$2H = 2.2$ $\bar{\sigma}_{cr} = 4.08$	$2H = 3.0$ $\bar{\sigma}_{cr} = 3.66$	$2H = 4.0$ $\bar{\sigma}_{cr} = 4.28$

* 2H is given in inches

$\rho = \dfrac{2R}{2H}$

form of tabulation as they are in the tabulation of the critical loads. It is evident, however, that except for models N2 and N3, there is a gradual rise in the value of $\bar{\sigma}_{cr}$ as ρ increases for a given slot length. In addition there is in general an increase in $\bar{\sigma}_{cr}$ as ρ is held constant and slot length is increased.

The increase in $\bar{\sigma}_{cr}$ with increasing ρ was expected and is the same trend as noted with the critical loads. The increase of $\bar{\sigma}_{cr}$ with increasing slot length, however, was not expected. If the dependence of $\bar{\sigma}_{cr}$ on the ratio (t/2H) had been correctly assumed, then any change in $\bar{\sigma}_{cr}$ as slot length increased might naturally be attributed to a width effect, i.e., on the ratio γ. It would certainly be possible to say under these conditions, then that an increase in γ would result in an increase in $\bar{\sigma}_{cr}$ based on results in Table 4. This is equivalent to a stabilizing effect. Dixon and Strannigan [41] have presented results for this problem which seem to indicate a dependence on plate width. The results of Danis [56] are presented in a similar fashion and appear to show a dependence on plate width.

In Chapter III of this dissertation a thorough investigation of the stress distribution around slots in plates was presented. Some characteristics of the region of compression were noted from these stress distributions. In particular it was noted that for a fixed hole geometry there was an increase in the magnitude of the maximum compressive stress as the value of γ increased. Also, there was a very slight but noticeable increase in the overall size of the region of large compressive stresses. The region of large compressive stresses is considered as that area in which one of the normalized principal

stresses, σ_q, has a value

$$\sigma_q \leq -0.3 \quad .$$

Thus it can be concluded from the trends noted in the stress distributions that both the magnitude of the compressive stress and the size of the compressive region increases as γ increases. Both of these trends would intuitively be expected to have a destabilizing effect on the buckling behavior. On the basis of these features of the stress distributions, then, it is inconsistent to conclude that increasing γ has a stabilizing effect. It appears then that the implicit assumption that σ_{cr} depends on the ratio (t/2H) in the form expressed in Equation (11) is not acceptable.

An examination of the data in Table 4 for fixed ρ reveals that as the length of the slot increases, which means the value of (t/2H) decreases, the ratio $\bar{\sigma}_{cr}$ increases. An inverse relation is thus observed between the two variables $\bar{\sigma}_{cr}$ and (t/2H). For convenience let the dimensionless ratio (t/2H) be defined as

$$\beta = \frac{t}{2H} \quad .$$

Tentatively, let it be assumed that the relation between $\bar{\sigma}_{cr}$ and $(1/\beta)$ is linear for constant values of ρ. This admittedly is a simplifying assumption but the scatter of the points and the amount of data available at each value of ρ does not justify a more complicated assumption.

On the basis of the preceding discussion an empirical relation of the form

$$\bar{\sigma}_{cr} = a + b\left(\frac{1}{\beta}\right)$$

was selected. Values of a and b for each value of $\rho \geq 0.4$ were calculated by a least squares method. This procedure was adopted because five data points were available for these values of ρ while less than five data points were available for values of $\rho < 0.4$. The computer values of a and b are presented in Table 5. From an examination of the results it is apparent that both a and b are functions of ρ. The functional dependence of b on ρ could be obtained by curve fitting. It may be noted, however, that the values of $b/\rho^{\frac{1}{2}} = 0.0204 \pm 0.0009$. For convenience a value of $b/\rho^{\frac{1}{2}} = 0.02$ has been selected for use in the development of an emperical relation.

The functional dependence of a on ρ is assumed to be linear and a straight line has been fitted to the points by a least squares method. The result of this computation gives

$$a = 4.18 + 1.69\,\rho \quad .$$

The relation for $\bar{\sigma}_{cr}$ can finally be expressed as

$$\bar{\sigma}_{cr} = \frac{\sigma_{cr}}{E\beta^2} = \left(4.18 + 1.69\,\rho + 0.02\,\frac{\rho^{\frac{1}{2}}}{\beta}\right) \quad . \qquad (14)$$

Table 5. Least Squares Coefficients

For $\sigma_{cr} = a + b\left(\frac{1}{\beta}\right)$

ρ	a	b x 10^2	$b/\rho^{\frac{1}{2}}$ x 10^2
1.0	5.80	1.96	1.96
0.8	5.69	1.75	1.96
0.6	5.08	1.65	2.13
0.5	5.00	1.44	2.03
0.4	4.89	1.255	1.98

Equation (14) exhibits the dependence of the quantity K in Equation (11) on the geometric parameters ρ and β.

The equation for the actual critical stress may be written in the form

$$\sigma_{cr} = E \left(\frac{t}{2H}\right)^2 \left[4.18 + 1.69 \left(\frac{2R}{2H}\right) + 0.02 \left(\frac{2R}{2H}\right)^{\frac{1}{2}} \left(\frac{2H}{t}\right)\right] \quad . \qquad (15)$$

Figure 19 shows Equation (15) in graphical form for constant values of β. The curves represent Equation (15) while the circles are the experimental points for the same values of β. The agreement is very good for most of the points.

An empirical relation has now been deduced which can be used to predict the tensile stress at which a local buckling behavior will be encountered around slots in thin sheets. It has been shown that this relation gives results which agree well with the experimental results conducted as part of this study. The question of whether the relation will be valid for other thickness plates and for other models in general remains to be examined. The results of several papers will now be examined and the empirical relation, Equation (15), will be applied to each of the model configurations presented in these papers.

The work of Bingham [57] has been mentioned several times. One of the model configurations which he examined had the following specifications:

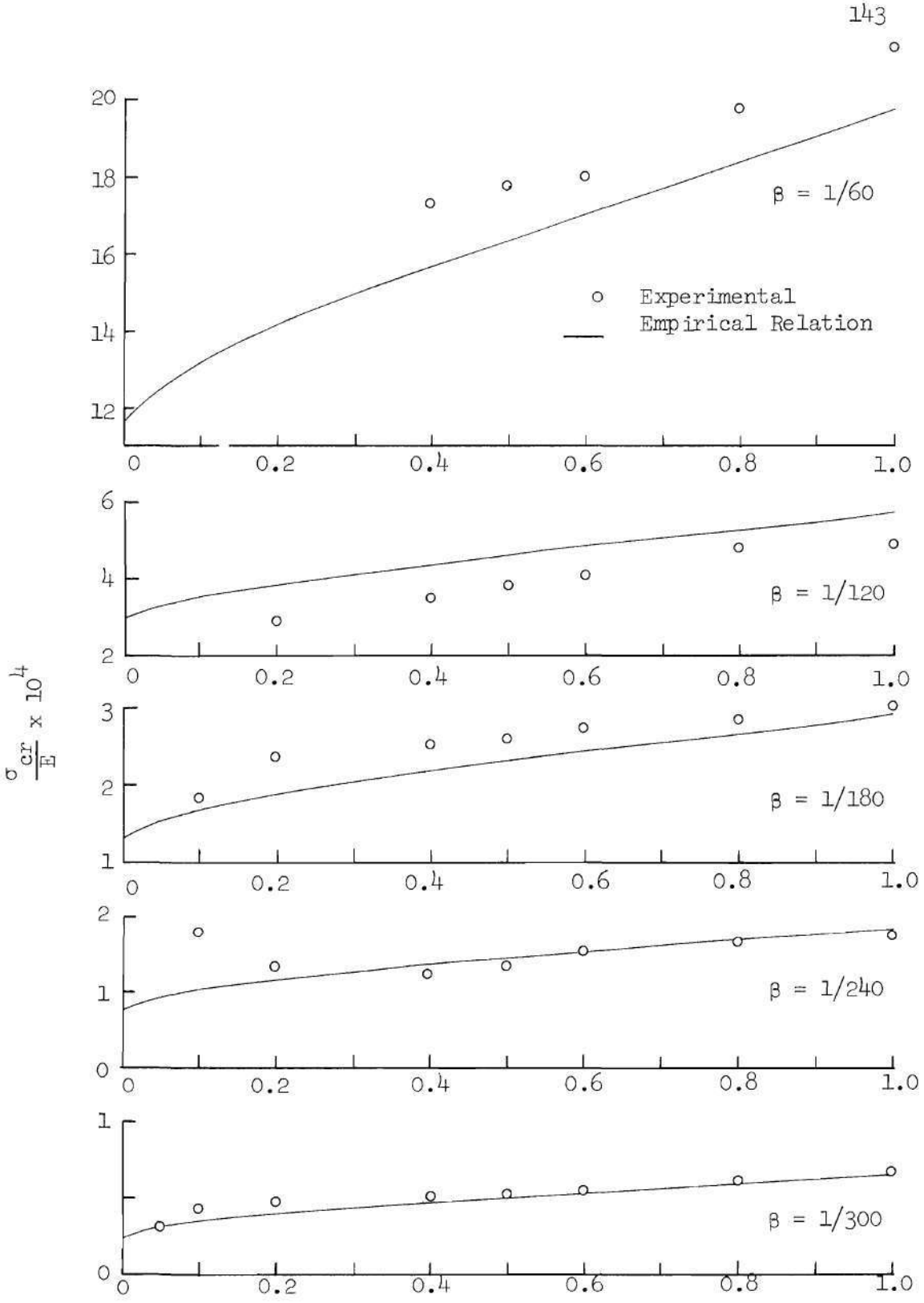

Figure 19. Critical Stress vs. $\rho = \frac{2R}{2H}$

$$2H = 3.0 \text{ inches} \quad ,$$

$$2R = 1.5 \text{ inches} \quad ,$$

$$t = 0.062 \text{ inches} \quad ,$$

$$\widetilde{W} = 6.0 \text{ inches} \quad ,$$

and

$$E = 10.5 \times 10^{6} \text{ psi} \quad .$$

For the above specifications the following parameter values apply:

$$\rho = \frac{2R}{2H} = \frac{1.5}{3.0} = 0.05 \quad ,$$

and

$$\beta = \frac{t}{2H} = \frac{0.062}{3.0} = 0.0207 \quad .$$

Substituting these values into Equation (15) yields

$$\sigma_{cr} = 2.69 \times 10^{4} \text{ psi.}$$

Bingham's experimental result was

$$\sigma_{cr} = 2.60 \times 10^{4} \text{ psi.}$$

The correlation with Bingham's result is seen to be excellent.

Another paper mentioned was that of Pellett, Costello, and Brock [51]. In this paper the critical stress in an infinitely wide plate with a circular hole is determined. The result for the lowest calculated buckling mode can be expressed as

$$\sigma_{cr} = 6.88\ E \left(\frac{t}{2R}\right)^2 .$$

Equation (15) for $\rho = 1.0$ yields

$$\sigma_{cr} = E \left(\frac{t}{2R}\right)^2 \left[5.87 + 0.02 \left(\frac{2R}{t}\right)\right] \quad .$$

A comparison of σ_{cr} values computed by use of these relations reveals that for values of (2R/t) less than 50, the stress predicted by the theoretical solution is larger. For values of (2R/t) greater than 50 the stress predicted by the empirical relation is greater. The range of (2R/t) values for the tests conducted for this dissertation was 60 to 300. Figure 20 shows stresses calculated by the empirical relation, Equation (15), and the theoretical solution of Pellett, Costello, and Brock.

The last paper which will be examined is that of Dixon and Strannigan [41]. They have presented their results graphically and these have been reproduced in Figures 21 and 22. Note that the two lines given as Dixon and Strannigan's results in each of these figures represent upper and lower estimates of the buckling loads. It has already been mentioned that care must be taken when examining these results not to confuse a slot length effect with a plate width effect. Again it is seen that correlation between the emperical results of Equation (15) and Dixon and Strannigan's experimental results is excellent in Figure 21.

The correlation exhibited in Figure 22 between the empirical relation, Equation (15), and Dixon and Strannigan's thicker models

(t = 0.79 inch) is not as good as the correlation of the other results so far examined. This reveals, by illustration, one of the restrictions of the technique used in the study presented herein. It is important to realize that the Southwell technique, as developed earlier in this chapter, is applicable only to elastic systems or systems in which any plastic zone developed is small. For specimens of the same slot length and slot height, the buckling stress increases rapidly with increasing thickness. For this reason plastic zones in thicker specimens will be larger and the degree to which the buckling process becomes elastic-plastic increases. Since the only difference in the specimens of Figures 21 and 22 is thickness, the emergence of the elastic-plastic effect is clear and indicates that the empirical relation can not be used to extrapolate into either the very short slot length or the thick specimen ranges. Naturally, this restriction is more important for cracks than for openings with smaller stress concentrations.

It is still possible, however, to use the technique of Dixon and Strannigan to obtain upper and lower limits of the buckling load because its response reflects the inelastic behavior. Note that just as in the case of the buckling of "short" columns, the buckling load of the elastic-plastic system is less than that of a corresponding elastic system. The buckling stresses for Dixon and Strannigan's 0.079 inch thick models were of such a magnitude that there was undoubtedly a considerable plastic zone at the ends of the slots. This accounts for the results predicted by Equation (15) being so much

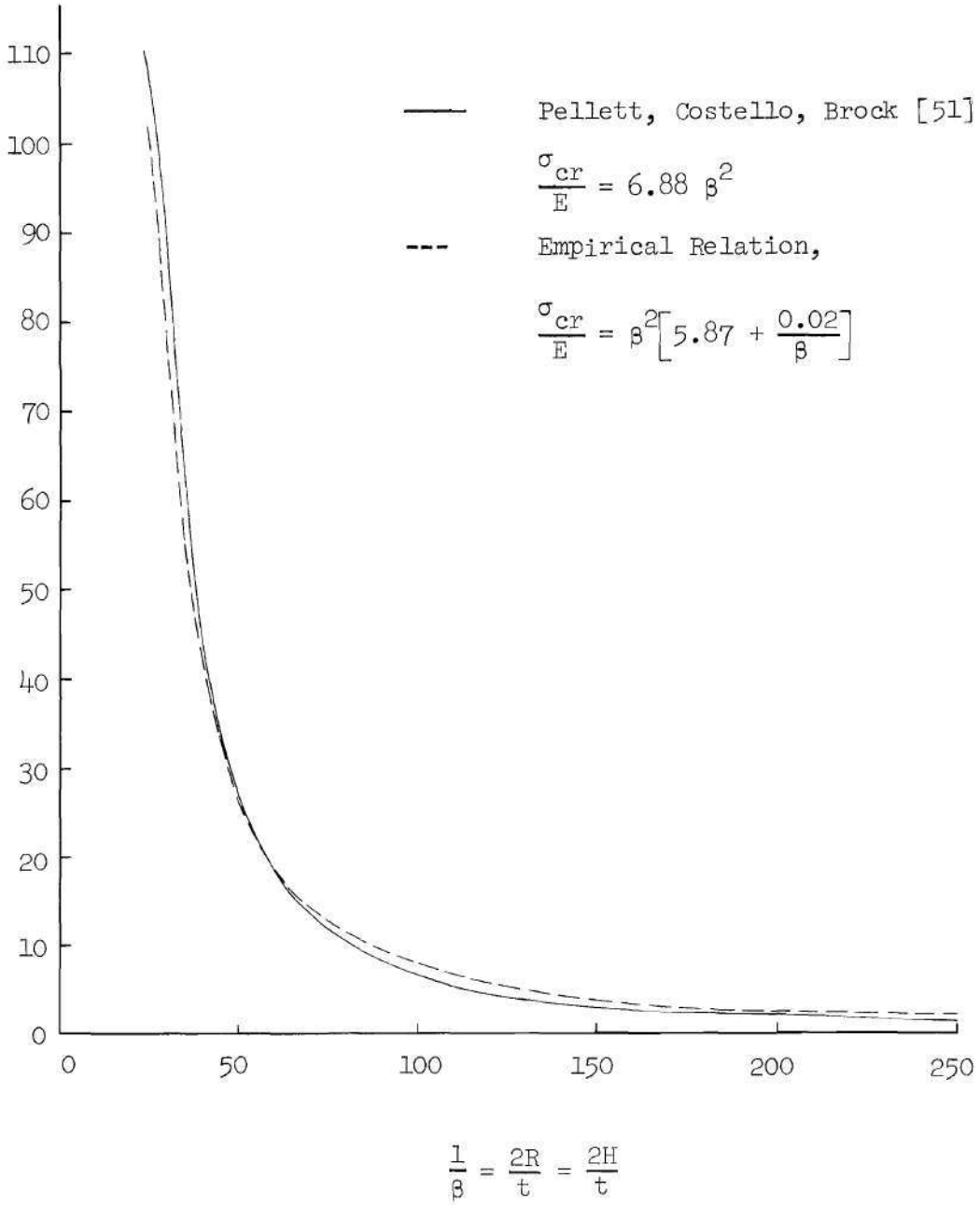

Figure 20. Critical Stress vs. $(1/\beta)$ for Circular Holes; i.e. $\rho = 1.0$

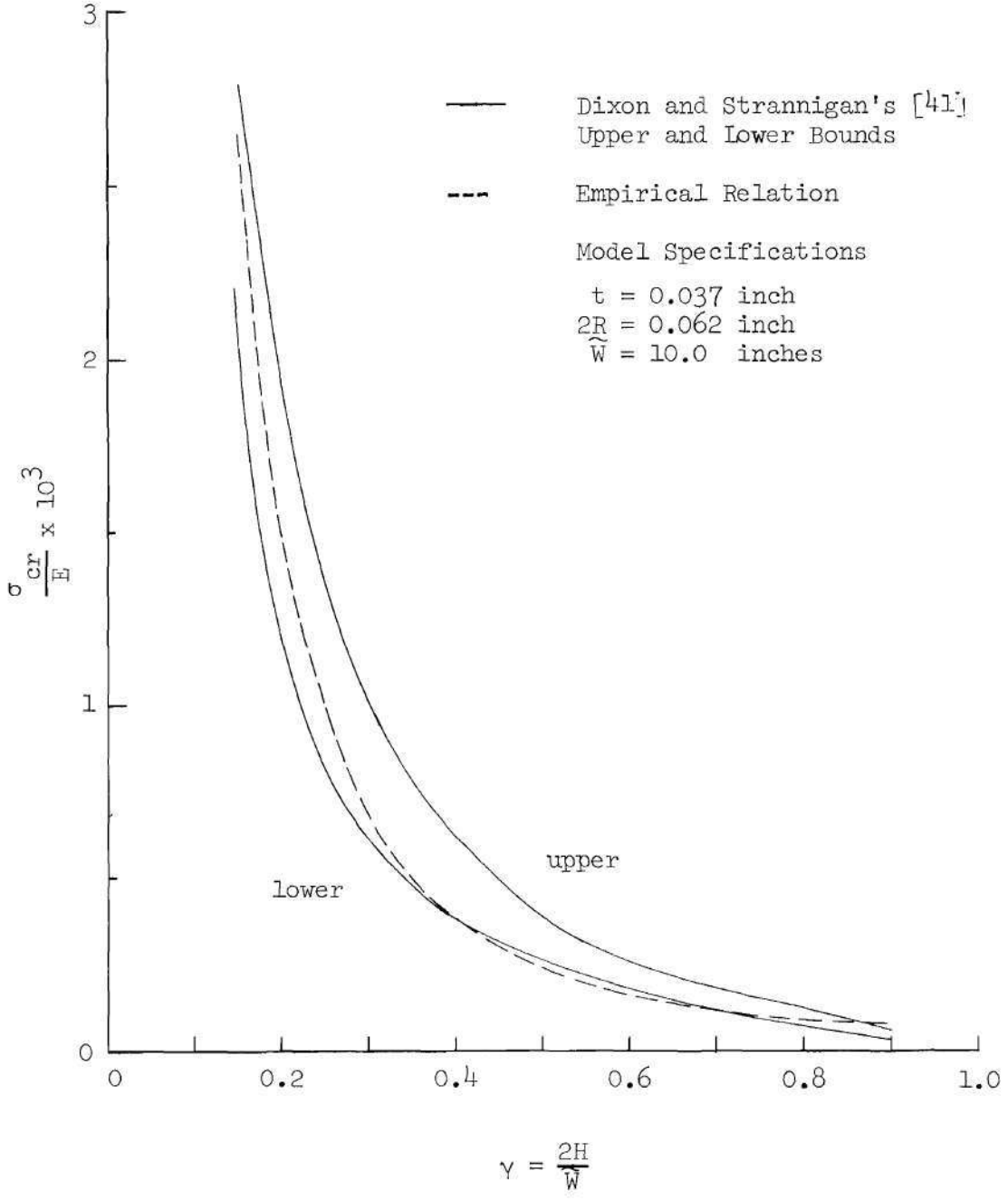

Figure 21. Critical Stress vs. Slot Length to Plate Width Ratio

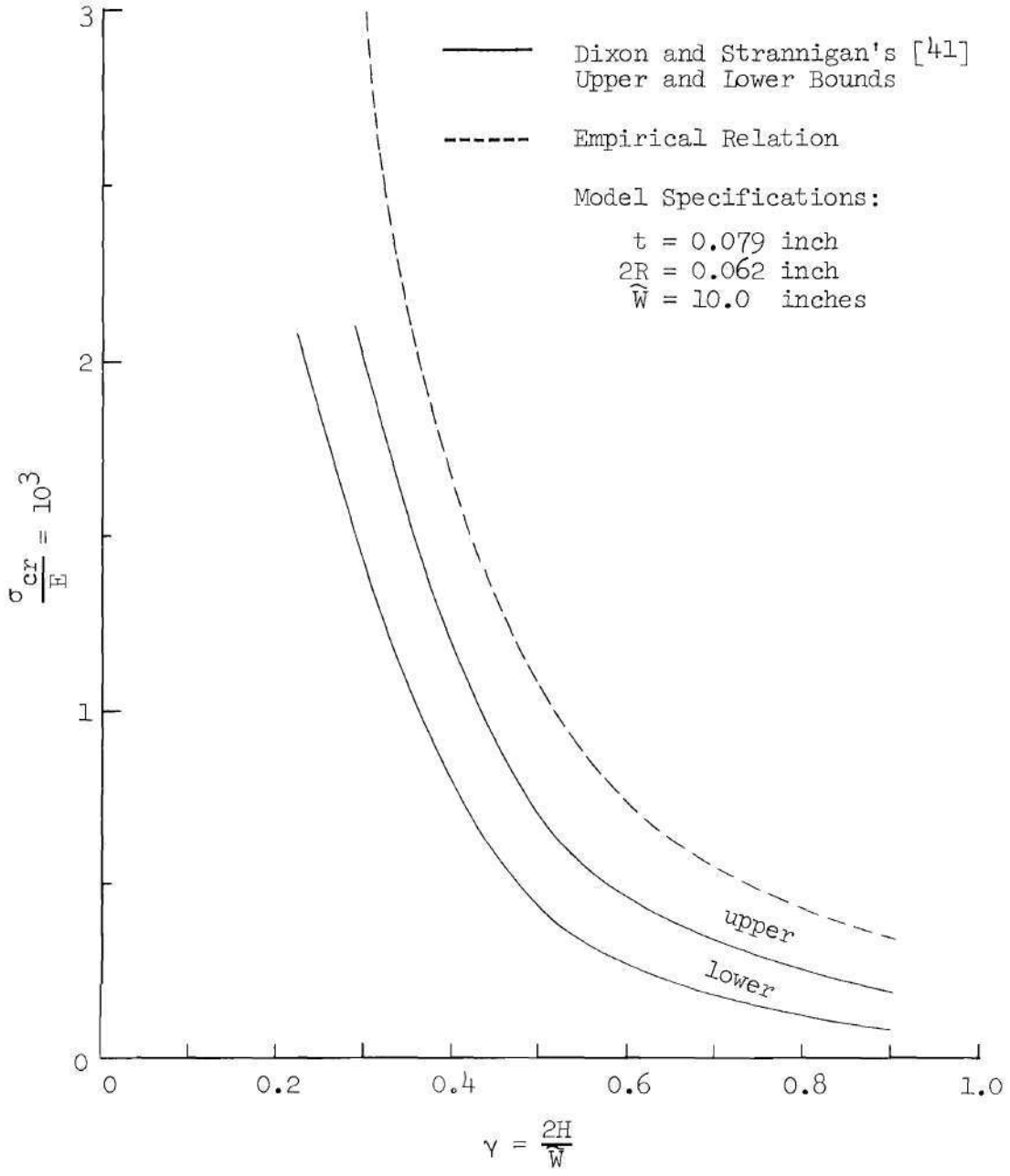

Figure 22. Critical Stress vs.
Slot Length to Plate Width Ratio

greater than the experimental results of Dixon and Strannigan.

The question of what effect a finite plate width has on the buckling stress has not yet been resolved and some discussion should be included at this point. In a preliminary study of slot buckling performed as a Special Problem in the School of Aerospace Engineering at the Georgia Institute of Technology [70], the effect of finite plate width was studied. The model contained a centrally located slot and the buckling stress was measured as the plate width was decreased. These tests covered a range of $\gamma = 2H/\widetilde{W}$ of 0.2 to 0.3. No significant changes occurred in the buckling stress and it appeared that the tests shed no light on the width effect problem.

Petyt [72] has also examined the effect of finite plate width on the buckling stress of tensioned plates containing cracks. This was both an experimental and analytical study. The buckling stress was determined for plates containing a five inch long, centrally located crack with plate widths of 10, 20, and 40 inches. In the experimental results the buckling stress for the 10 and 20 inch wide specimens was the same while the buckling stress in the 40 inch wide specimen was greater by a factor of three. In the analytical finite element solution, however, there was a continuous increase in the buckling stress with increasing plate width. The computed buckling stress in the 40 inch wide plate was approximately three times that of the 10 inch wide plate. On the surface this seems to suggest a definite plate width effect which would be, in effect, consistent with the observed changes in the stress distributions.

The validity of this conclusion is questionable, however, for several reasons. The experimental and finite element models used by Petyt had changing plate widths but the length of the models was fixed at 13.5 inches. For the 10 inch wide plates this was probably sufficient to be able to assume that the effect of plate length could be neglected. In the 40 inch wide plate it is doubtful, however, that plate length effects can be ignored.

This observation is supported by some of Petyt's results. In his discussion of the finite element method he calculates the stresses along the plate centerlines for a cracked, 10 inch wide and 13.5 inch long plate. In this case the stresses which he computed are in excellent agreement with the theoretical stresses distribution for an infinite plate. However, as Petyt increases the plate width, while keeping the length constant, drastic changes occur in the distribution and the magnitude of the compressive stresses. Petyt associates these changes with the increase in the buckling stress. It is not, however, consistent to conclude that as plate width becomes larger (i.e., tends toward infinity) the change in the stress distribution becomes less like that in an infinite plate and that this change may be attributed to a width effect. The plate width to plate length ratio should also be examined in order to be consistent. Thus, although Petyt's results may very well be correct for the problem which he solved they are not comparable with the problem of interest herein.

On the basis of the preceding discussion and also on the basis of the results of this dissertation, it may be concluded that at least for $\gamma < 0.5$ the plate width probably has very little effect on the

tensile buckling stress of thin plates containing holes. The predominant parameter in the range examined is the thickness to hole length ratio, β. The shape of the hole is also of major interest and is a parameter which influences the buckling stress. The examination of the data presented indicates that Equation (15) accounts properly for both the thickness to hole length ratio effect and the shape effect within the range of γ specified.

CHAPTER V

CONCLUSIONS

The principal objectives of the research program described in the last section of Chapter I have been achieved. The major topics examined are given in the following list:

(1) The general governing equations for the class of problems of interest (i.e., multiply connected plates experiencing moderately large deflections) were developed and analyzed.

(2) The stress distribution in infinite sheets with specified hole geometries was determined by the use of complex variable stress functions. The stress distribution in finite sheets with the same hole geometries was determined by the use of two dimensional photoelasticity.

(3) A parametric investigation was conducted to determine the tensile buckling loads in sheets as a function of the geometric parameters.

A summary of the results obtained and the conclusions which were reached during this investigation are presented in the discussion which follows.

In Chapter II of this dissertation the moderately large deflection plate equations of Karman were extended to include applications involving multiply connected plates. The difference between the simply and multiply connected versions of the above equations is the existence of a set of auxiliary conditions which must be satisfied on each of the interior boundaries. These auxiliary conditions arise as a

consequence of the requirement that the stress function be such as to insure a compatible state of deformation.

A nondimensionalization of the governing equations reveals that, although multiply connected plates can be modeled by materials with different values of Young's modulus, the values of Poisson's ratio must be equal. This restriction, incidentally, also applies in the modeling of simply connected plates undergoing moderately large deflections.

An examination of the Karman equations made it possible to identify the features of plate stability behavior which can be expected to affect the validity and usefulness of an application of an extended Southwell method to the problems of interest in this dissertation; i.e., buckling of slotted sheets in a tensile field. The important features are the degree to which the bent surface approaches a developable surface, the magnitude of the deflection, and the eigenvalue separation for the corresponding perfect plate problem. It was shown that if appropriate conditions are satisfied, the nonlinear coupled governing equations can be replaced by a set of linear uncoupled equations, and a Southwell type deflection-load relationship can be derived.

The conditions involved are related to the extent to which stiffening due to middle surface stretching influences the relation between the external load and the internal stress response in a given problem; i.e., is the response linear or nonlinear? The presence of this effect can, fortunately, be evaluated experimentally, and by this means, the applicability of the extension of the Southwell method can

be checked and controlled. The experimental results obtained indicate that if experiments are correctly designed and carefully conducted, and if the range of applicability is properly monitored, buckling loads can be determined.

The investigation of the stress distribution in slotted plates under tensile loadings revealed two important trends. The first of these was that the magnitude of the maximum compressive stress increased as the slot length to plate width ratio, γ , increased. The second trend observed was that for a given hole size and geometry, the size of the region of high compressive stress increased as γ increased. These two trends would both be expected to have a destabilizing effect on the behavior of the sheet. The resulting response should be a decrease in the tensile buckling loads as γ increases. An evaluation of the buckling data generated, however, suggests that the buckling stress is not sensitive to this effect for the values of slot length to plate width ratios less than 0.5. In fact a comparison of trends exhibited in the stress distributions with the trends exhibited in the buckling data indicates that for the range of parameters investigated, the ratio γ has little or no effect on the value of the buckling stress.

This observation proved to be quite important because it made it possible to derive a relatively simple empirical relation from the buckling stress data. The emperical relation developed for the critical tensile stress applied to the sheet is

$$\sigma_{cr} = E \left(\frac{t}{2H}\right)^2 \left[4.18 + 1.69 \left(\frac{2R}{2H}\right) + 0.02 \left(\frac{2R}{2H}\right)^{\frac{1}{2}} \left(\frac{2H}{t}\right)\right]$$

Good correlations were observed when this relation was applied to data presented both for experiments described in this dissertation and for experiments on other model configurations reported by other investigators. The range of applicability of this equation extends from very narrow slots, which approach cracks, to circular holes.

The empirical relation that has been developed is based upon an elastic analysis presented in Chapter IV. In cases in which large plastic zones are present in the vicinity of the slot ends, the derived relation does not, therefore, give accurate results. This will usually be the case for very short slots or for longer slots in thicker sheets. Naturally, the magnitude of the elastic limit enters into these considerations. In any event, however, the applicability of the formula for a particular problem can be checked by multiplying the critical stress calculated from the formula by the stress concentration factor for the slot (note that the stress concentration factor should be based on the total plate cross sectional area). If this value is less than the elastic limit of the material the empirical relation should be applicable. For cases in which the computed value exceeds the elastic limit, the degree to which the formula can be expected to be useful depends on the size of the plastic zone developed at the tip of the slot.

CHAPTER VI

RECOMMENDATIONS FOR FUTURE STUDIES

In this dissertation the tensile buckling behavior in thin sheets containing centrally located slots has been carefully examined. In the course of the investigation several intriguing points concerning this local buckling phenomenon came to light.

One class of problems which would be interesting to consider is the coupled problem formulated in Chapter II; i.e., the multiply connected sheet undergoing moderately large transverse deflection. The solution of problems of this class would reveal the effect that in-plane stretching due to bending has on stress concentration factors. Knowledge of these factors has obvious application in design. In addition, these solutions would, of course, also provide a knowledge of load versus deflection or extension behavior over the entire range of loading.

Along the same lines, it would also be interesting to solve the related large deflection problem for the case in which the bending stiffness vanishes; i.e., the case when the plate is assumed to be a membrane. A solution of the membrane problem for the limiting case of a crack would provide a check on the theoretical work of Cherepanov [49].

Among the shapes other than slots which are of particular interest is the elliptical hole. It has been mentioned previously that the magnitude of the maximum compressive stress in plates containing elliptical holes is greatly affected by the plate width. Under these

circumstances it is probable that the conclusions that were reached with regards to finite plate width in Chapter IV may, at least in some cases, no longer be applicable.

Solutions to Large Deflection Equations

Theoretical Solutions

The set of equations which describes the behavior of multiply connected plates has been presented in Chapter II. The solution of this set of equations is a formidable task. For the problem of interest here, the terms which contain body force and temperature in these equations would not be present. The terms that would remain are those that involve F and w and their derivatives.

One possible way of solving the nonlinear coupled plate problem is to proceed in a manner similar to Stein [73]. The assumption is made that the quantities F and w can be expanded in the forms

$$F = \sum_{n=0,2}^{\infty} F_{(n)} \, \varepsilon^n \quad ,$$

and

$$w = \sum_{n=1,3} w_{(n)} \, \varepsilon^n \quad .$$

If these equations are substituted into the relations given in Chapter II, a set of linear uncoupled relations can be obtained by grouping terms of like powers of ε. This type of solution is effective if the linear set of equations can be solved. Naturally, consideration of

the convergence of the sums is necessary.

Another possible approach to a solution of the coupled nonlinear relations would be a successive approximation procedure. In this procedure the plate is initially assumed to remain flat and the plane stress problem is solved. The solution for the stress function is then used in the coupled equilibrium equation to obtain w. The stress function is then improved by including the calculated w function in the compatibility relations. The process is then repeated until a desired criterion of convergence is reached. This type of procedure is readily adaptable to approximate methods.

No effort has been made by this author to evaluate the merits of the two procedures outlined above for this problem. It is noted, however, that the starting point of both methods is the same; i.e., a determination of the uncoupled stress distribution. This part of the problem has been solved in Chapter III of this dissertation.

Experimental Solutions

A complete solution to the problem of interest in this dissertation is difficult to obtain by experimental methods. In the region of primary interest, i.e., in the vicinity of the hole, the plate can experience large lateral deflections. Coupled with these deflections there will be in-plane stretching which results in a stress distribution that is different from that of the undeflected plate.

In a paper by Rogers, Zielsdorff, and Carlson [74] a method was presented for the solution of large deflection plate problems. Basically, the method uses photoelastic techniques to solve for the mid-

surface stress distribution and displacement measurements to solve for the deflection function. Curvatures are obtained by differentiation of the deflection function. The bending moments are found from the usual moment curvature relations and thus, from the definitions of the bending moments, the bending stresses can be found.

In reference [74] a clamped circular plate subjected to uniform lateral pressure was considered. The symmetry of such a problem considerably simplified the task of obtaining a solution. Comparisons of the proposed method with theoretical solutions for the same problem were made. The results obtained indicated that the proposed method was both more simple to apply and less restricted in terms of deflection magnitude than methods of solution which have previously been proposed for the given problem.

It was noted in this reference, however, that the application of the proposed technique has restrictions in so far as the photoelastic portion is concerned. The two-dimensional photoelastic techniques normally used and the optical theory upon which these techniques are based depend on the assumption that the principal stress directions are constant through the plate thickness. Often this is not the case when lateral bending is present. As a result there will be a retardation of the light vector due to the optical rotation. The resulting fringe pattern is thus not a true indication of the midsurfaces stress distribution.

Even with the above complication, the method proposed can be used to solve many practical problems such as the uniformly loaded circular plate. In many other problems where the entire midsurface

stress distribution cannot be found, there exist lines of symmetry along which the principal stress direction is constant through the plate thickness. In these cases it is possible to obtain very useful and accurate results along these lines. Often, these lines are within regions which are of primary interest.

For the problem of concern in this dissertation the method described above would be applicable along the axes of the plate. A model was made with the intention of performing such an analysis. The desired results, however, could not be obtained. The reason for this was that the slot which was examined had a hole height to hole length ratio, ρ , of 0.10. Also, the model was made of a highly sensitive photoelastic material and had a reflective back surface. The reflective surface doubles the optical thickness of the plate and thus doubles the fringe order at a point. These three factors (i.e., the slot geometry, the optical sensitivity of the material, and the use of reflection techniques) all had the overall effect of increasing the fringe order. It was, therefore, impossible to obtain accurate readings near the ends of the slot due to the density of the fringes in these areas.

It is recommended, therefore, that if further investigations are conducted along these lines, care should be taken to avoid the above difficulties. Changes in procedure based on the above observations would be simple to make.

Effects of Large Deflections

As the load applied to the plate is increased it has been noted that, initially, the stress distribution in the plate remains constant. That is, the stresses at all points in the plate are linearly proportional to the applied load. If the plate remains flat, this condition would continue until the onset of inelastic behavior. Actually, however, an imperfect plate will begin to deflect laterally in the vicinity of the hole well within the elastic range.

In Chapter IV of this dissertation the importance of the limit of applicability of a linear analysis was discussed. It was shown then that the midsurface stress at the location of the strain gages exhibited a distinct and significant deviation from linearity. Of course, there is also stretching due to bending at other locations in the plate.

It would be especially significant to establish the effect of stretching on the stress concentration factor. Dixon and Strannigan [41] have established that the stress concentration factor increases as the plate deflects and stretching becomes significant. It is felt that further studies are needed in order to establish quantitatively the effect of stretching due to bending on the stress concentration factor. This noted increase very likely accounts, for example, for the reduction in static strength that has been reported in the literature [41,53] when buckling is permitted to take place.

Another effect of large deflections in tensioned sheets with holes is that the dynamic response characteristics of the sheet change. Clarkson [54] has exploited this phenomenon in order to define a tensile

load which he identifies with buckling. He noted that as the tensile load is increased the dominant natural frequency first increases and then decreases. During this initial range, the dominant mode shape was that associated with the vibration of the entire plate. At some load which Clarkson defines as the buckling load, the portion of the plate in the vicinity of the crack changes its mode of response. From this point further increases in load are observed to result in an increase in the dominant natural frequency of the plate.

Much more work needs to be done in the area of the dynamic response of tensioned sheets with holes. There are other associated problems, also, which have yet to be solved. One of the most important for the aircraft industry is the effect that local buckling around holes may have on fatigue life characteristics.

In summary then, it is apparent that though this dissertation has provided for an improved understanding of the buckling behavior in tensioned sheets with holes, the results presented have really only indicated more clearly the need for continuing work.

APPENDIX A

STRAIN DATA

Table A1. Midsurface Strain, Series K, 10^{-6} inch/inch

Load, Pounds	Model K4	Model K5	Model K6	Model K7	Model K8
0	0	0	0	0	0
100	10	16	13	15	15
200	26	37	33	35	28
300	45	60	56	55	45
400	62	84	76	76	63
500	83	106	99	98	83
600	100	130	121	121	101
700	119	153	142	141	119
800	138	176	164	163	140
900	157	201	184	183	158
1000	175	224	205	205	179
1100	196	246	225	225	198
1200	213	271	246	247	217
1300	233	294	269	270	236
1400	252	318	292	292	254
1500	271	341	313	314	274
1600	291	365	333	335	294
1700	309	389	356	358	312
1800	328	411	376	381	332
1900	347	434	398	401	350
2000	365	458	420	422	370
2100	383	482	438	442	389
2200	401	505	458	464	409
2300	420	528	481	486	428
2400	441	551	501	507	448
2500	458	575	523	529	466
2600	474	---	545	550	476
2700	494	---	564	569	504
2800	511	---	585	590	524
2900	530	---	605	611	541
3000	547	682	626	632	562

Table A2. Midsurface Strain, Series L, 10^{-6} inch/inch

Load, Pounds	Model L3	Model L4	Model L5	Model L6	Model L7	Model L8
0	0	0	0	0	0	0
60	15	16	20	22	24	19
100	23	29	34	38	39	37
120	30	35	41	45	45	44
140	35	40	48	52	52	54
160	39	45	55	59	60	62
180	45	53	62	66	67	70
200	50	58	67	73	73	77
220	56	63	73	80	79	85
240	62	68	80	87	85	93
260	68	75	85	93	92	100
280	71	80	91	100	97	109
300	76	85	97	105	104	114
320	83	92	102	112	109	121
340	86	100	109	118	113	128
360	90	105	114	124	119	135
380	97	112	120	130	124	140
400	100	118	126	137	129	148
420	108	123	133	143	134	152
460	118	136	144	154	146	164
500	127	147	155	166	153	177
540	136	157	167	177	164	190
580	143	168	177	188	174	201
620	153	181	187	200	181	213
660	157	192	197	211	190	224
700	165	202	208	221	199	234
740	170	214	216	232	206	245
780	175	222	227	241	214	257
820	180	233	232	250	220	268
860	186	243	241	258	226	278
900	186	252	249	268	234	285

Table A3. Midsurface Strain, Series M, 10^{-6} inch/inch

Load, Pounds	Model M2	Model M3	Model M4	Model M5	Model M6	Model M7	Model M8
0	0	0	0	0	0	0	0
60	15	21	13	14	13	15	- 2
100	24	36	25	24	24	25	3
120	28	43	31	30	31	31	10
140	34	49	36	36	36	37	14
160	38	55	42	42	43	43	20
180	43	61	48	49	47	49	24
200	47	66	54	55	53	54	30
220	50	73	60	60	58	220	33
240	55	77	64	65	65	66	39
260	60	84	70	71	69	71	43
280	63	88	75	76	75	77	48
300	67	92	80	81	80	82	53
320	69	97	84	86	85	87	58
340	73	100	89	90	88	91	62
360	76	103	93	94	93	96	68
380	79	106	97	98	96	101	72
400	80	108	100	100	102	105	77
420	84	111	104	104	104	109	81
440	85	114	106	106	108	113	86
460	86	114	109	110	111	117	89
480	90	116	112	113	113	119	93
500	90	118	114	115	114	123	96
600	95	120	119	124	126	134	112
700	99	118	125	129	131	141	124
800	99	116	125	130	135	143	132
900	99	---	126	132	138	145	140

Table A4. Midsurface Strain, N, 10^{-6} inch/inch

Load, Pounds	Model N2	Model N3	Model N4	Model N5	Model N6	Model N7	Model N8
0	0	0	0	0	0	0	0
20	7	1	3	3	- 5	1	-12
40	17	8	7	7	- 3	6	- 7
60	25	14	14	12	3	10	- 3
80	34	22	20	17	8	15	3
100	42	27	27	23	14	21	10
110	46	30	31	26	16	24	14
120	49	34	35	29	19	27	16
130	54	37	40	32	22	30	19
140	56	39	42	36	25	33	23
150	60	42	40	28	35	35	28
160	62	42	50	42	31	38	32
170	66	45	54	45	35	42	36
180	68	46	58	48	39	45	40
190	70	49	63	52	42	48	46
200	72	50	66	54	44	51	50
220	76	54	71	59	50	56	59
240	79	55	76	63	58	61	67
260	81	59	82	68	62	65	75
280	83	59	86	71	67	71	83
300	83	62	87	72	71	75	92
320	---	---	88	75	74	79	101
340	---	---	86	75	78	81	110
360	---	---	86	77	80	81	116
380	---	---	85	73	82	82	123
400	---	---	82	76	84	84	130
420	---	---	80	75	86	85	135
440	---	---	78	74	86	85	139
460	---	---	76	74	85	85	140
480	---	---	73	72	85	84	146
500	---	---	71	72	84	84	500

Table A5. Midsurface Strain, Series P, 10^{-6} inch/inch

Load, Pounds	Model P1	Model P2	Model P3	Model P4	Model P5	Model P6	Model P7	Model P8
0	0	0	0	0	0	0	0	0
10	7	3	2	3	5	3	5	8
20	16	7	7	6	8	6	9	10
30	22	9	10	8	10	9	13	12
40	30	12	15	10	13	11	16	16
50	33	17	17	11	16	14	20	20
60	38	20	20	14	18	17	23	23
70	41	22	25	15	20	19	28	24
80	45	25	29	17	23	21	30	27
90	48	30	32	20	26	23	34	30
100	49	34	35	23	29	26	38	32
110	49	37	38	25	32	29	42	34
120	50	40	41	29	35	32	45	35
130	51	41	45	32	37	35	49	37
140	50	45	48	35	40	39	53	37
150	50	47	50	38	42	42	56	37
160	50	50	51	38	45	45	60	42
170	49	52	55	40	47	47	64	43
180	48	54	57	42	50	50	68	45
190	47	55	58	44	52	53	70	45
200	47	57	59	44	55	56	73	48
220	--	--	62	45	60	62	79	51
240	--	--	62	45	63	66	85	51
260	--	--	63	45	67	72	87	53
280	--	--	63	43	67	78	90	56
300	--	--	64	41	66	84	91	57
400	--	--	--	--	60	82	93	47

Table A6. Strain Difference, $\Delta\varepsilon$, Series K, 10^{-6} inch/inch

Loads, Pounds	Model K4	Model K5	Model K6	Model K7	Model K8
0	0	0	0	0	0
100	17	52	68	67	42
200	35	70	88	96	62
300	48	82	100	113	72
400	59	93	110	129	80
500	69	103	120	141	87
600	79	112	130	153	85
700	88	122	140	165	102
800	99	133	149	178	111
900	109	143	160	190	117
1000	116	154	169	203	127
1100	130	167	178	217	136
1200	141	179	188	229	142
1300	154	192	200	245	152
1400	168	208	213	258	162
1500	181	221	226	273	174
1600	199	238	240	291	188
1700	214	255	255	309	200
1800	232	272	272	328	211
1900	252	294	290	348	226
2000	271	318	309	369	241
2100	294	343	327	389	255
2200	319	369	349	413	271
2300	344	398	376	440	290
2400	378	430	403	467	309
2500	409	467	434	494	327
2600	440	---	469	528	346
2700	480	---	501	558	368
2800	522	---	542	598	390
2900	570	---	582	638	420
3000	620	698	633	682	447

Table A7. Strain Difference, $\Delta\varepsilon$, Series L, 10^{-6} inch/inch

Loads Pounds	Model L3	Model L4	Model L5	Model L6	Model L7	Model L8
0	0	0	0	0	0	0
60	10	8	21	22	48	25
100	15	12	24	31	70	33
120	19	15	29	37	79	37
140	23	16	34	41	89	40
160	27	17	37	44	98	44
180	32	18	41	47	109	48
200	37	20	45	50	120	52
220	42	22	49	54	131	53
240	48	25	54	58	142	57
260	54	28	59	63	154	58
280	61	32	64	68	167	59
300	68	36	70	74	174	60
320	76	41	76	79	193	62
340	85	46	82	85	207	64
360	95	51	88	91	222	68
380	107	58	96	98	239	72
400	120	66	106	106	253	79
420	135	67	113	112	267	83
460	160	82	130	128	298	90
500	186	101	148	148	322	100
540	218	122	170	168	356	110
580	253	144	191	191	392	123
620	290	169	221	217	421	138
700	375	230	278	274	498	172
740	421	265	312	310	537	191
780	474	304	360	347	572	210
820	526	348	400	387	623	238
860	582	397	449	430	660	268
900	638	448	500	476	708	303

Table A8. Strain Difference, $\Delta\varepsilon$, Series M, 10^{-6} inch/inch

Loads, Pounds	Model M2	Model M3	Model M4	Model M5	Model M6	Model M7	Model M8
0	0	0	0	0	0	0	0
60	---	22	20	21	48	32	1
100	22	42	31	35	66	52	2
120	28	52	38	42	78	62	6
140	40	66	48	53	89	72	10
160	50	80	58	63	102	83	17
180	64	96	71	78	115	95	24
200	78	112	81	91	131	108	34
220	95	132	98	105	147	122	45
240	110	150	111	120	166	137	56
260	133	174	132	140	183	151	66
280	153	198	149	158	203	168	80
300	170	226	171	180	224	187	94
320	183	258	191	200	245	205	110
340	210	282	211	224	266	222	124
360	230	304	233	248	290	242	141
380	263	340	261	273	312	264	161
400	285	367	283	297	339	290	177
420	310	400	315	328	365	310	192
440	334	429	338	353	393	335	212
460	368	463	368	385	418	358	231
480	395	490	395	409	450	387	252
500	420	526	427	441	482	411	272
600	550	684	565	585	630	556	383
700	680	838	712	732	771	707	502
800	805	982	850	874	926	855	638
900	925	---	992	1015	1070	1010	760

Table A9. Strain Difference, $\Delta\varepsilon$, Series N, 10^{-6} inch/inch

Load, Pounds	Model N2	Model N3	Model N4	Model N5	Model N6	Model N7	Model N8
0	0	0	0	0	0	0	0
20	25	2	7	4	0	12	-31
40	47	8	9	7	4	18	-33
60	68	17	8	9	7	21	-34
80	92	30	11	11	12	25	-35
100	119	48	12	21	17	29	-35
110	134	56	15	27	20	33	-34
120	148	68	18	33	23	39	-33
130	166	79	21	39	28	46	-31
140	182	92	23	47	36	52	-30
150	201	105	30	54	40	58	-26
160	220	122	34	61	48	63	-21
170	240	138	39	70	54	70	-17
180	256	159	44	80	63	76	-15
190	278	179	52	92	70	83	-11
200	295	200	60	102	79	91	- 8
220	336	239	82	133	97	112	- 1
240	379	284	110	168	119	134	10
260	428	328	153	202	148	163	25
280	472	372	205	238	180	196	44
300	522	411	260	282	212	225	69
320	---	---	322	322	246	258	95
340	---	---	373	358	286	300	123
360	---	---	431	402	322	340	153
380	---	---	478	438	362	379	193
400	---	---	528	480	398	423	235
420	---	---	571	518	439	468	288
440	---	---	611	555	470	508	336
460	---	---	648	589	510	550	396
480	---	---	687	622	549	590	448
500	---	---	719	655	586	630	500

Table A10. Strain Difference, $\Delta\varepsilon$, Series P, 10^{-6} inch/inch

Load, Pounds	Model P1	Model P2	Model P3	Model P4	Model P5	Model P6	Model P7	Model P8
0	0	0	0	0	0	0	0	0
10	3	8	3	8	6	10	20	7
20	20	12	10	12	11	11	22	28
30	39	15	12	15	15	12	26	38
40	60	19	19	19	18	12	30	50
50	86	22	21	21	19	13	32	60
60	118	26	28	26	22	13	35	70
70	157	32	31	29	25	14	40	78
80	202	37	39	32	29	14	45	87
90	239	43	48	38	31	15	52	92
100	271	50	55	43	35	16	59	101
110	306	59	65	49	38	17	67	108
120	337	71	75	56	42	19	75	118
130	367	83	88	63	46	20	84	120
140	391	99	101	70	52	21	91	124
150	421	115	117	83	59	22	102	129
160	446	133	137	96	68	24	112	140
170	475	152	157	108	78	26	126	152
180	497	178	180	123	91	28	138	166
190	522	199	201	143	103	31	157	182
200	542	225	228	161	120	37	175	198
220	---	---	276	206	157	52	213	248
240	---	---	325	258	192	68	250	309
260	---	---	380	303	243	94	290	422
280	---	---	426	354	300	140	332	531
300	---	---	472	402	360	225	385	629
400	---	---	---	---	600	600	580	978

REFERENCES

1. Greenspan, M., "Axial Rigidity of Perforated Structural Members," Journal of Research, Vol. 31, p. 305, 1943; Stang, A. &. Greenspan, M., Vol. 28, p. 669; Vol. 28, p. 687; Vol. 29, p. 270; Vol. 30, p. 15; Vol. 30, p. 177; Vol. 30, p. 411.

2. McFarland, R. A., Human Factors in Air Transport Design, McGraw-Hill Book Co., Inc., New York, N. Y., 1946, p. 488.

3. McFarland, R. A., Human Factors in Air Transportation, McGraw-Hill Book Co., Inc., New York, N. Y. 1953, p. 707.

4. Marshall, C. S. R., "Human Factors in Supersonic Transport Aircraft," in Human Problems of Supersonic and Hypersonic Flight, A. B. Barbour & Sir Harold E. Whittingham eds., Pergamon Press, London 1962, p. 99.

5. Masefield, P. G., "Some Problems of the Supersonic Vehicle," in Human Problems of Supersonic and Hypersonic Flight, A. B. Barbour & Sir Harold E. Whittingham eds., Pergamon Press, London, 1962, p. 302.

6. Hoff, N. J., "A Short History of the Development of Airplane Structures," American Scientist, Vol. 34, Nos. 2 and 3, p. 212, April 1946.

7. Hoff, N. J., "Thin Shells in Aerospace Structures," Astronautics and Aeronautics, Vol. 5, No. 2, p. 26, February 1967.

8. Van der Neut, A., "Post Buckling Behavior of Structures," NATO Advisory Group for Aeronautical Research and Development, rep. 60, August 1956.

9. Pollard, H. J., "Some Developments in Aircraft Construction," Jour. of the Royal Aeronautical Society, Vol. 38, No. 283, p. 651, July 1934.

10. Shanley, F. R., Weight-Strength Analysis of Aircraft Structures, Dover Publications, Inc., New York, N. Y., 1960, p. 188.

11. Younger, J. E., Structural Design of Metal Airplanes, McGraw-Hill Book Co., Inc., New York, N. Y., 1935, p. 239.

12. Sechler, E. E. and Dunn, L. G., Airplane Structural Analysis and Design, John Wiley & Sons, Inc., New York, N. Y., 1942, p. 374.

13. Hansen, G., "Stress Distribution Near a Rectangular Cut-Out in a Reinforced Circular Cylinder due to Direct Shear Loading and Torque, Part 1 - Test Results," The Coll. of Aero., Cranfield, Rep. No. 51, 1952

14. Hoff, N. J. and Boley, B. A., Stresses in, and General Instability of, Monocoque Cylinders with Cut-outs. I - Experimental Investigation of Cylinders with a Symmetric Cut-out Subjected to Pure Bending," NACA TN 1013, 1946.

15. Hoff, N. J., Boley, B. A., and Klein, B., "Stresses in, and General Instability of, Monocoque Cylinders with Cut-outs. II - Calculation of the Stresses in a Cylinder with a Symmetric Cut-out." NACA TN 1014, 1946.

16. Hoff, N. J., Boley, B. A., and Klein, B., "Stresses in, and General Instability of, Monocoque Cylinders with Cut-outs. III - Calculation of the Buckling Load of Cylinders with a Symmetric Cut-out subjected to Pure Bending," NACA TN 1263, 1947.

17. Hoff, N. J., Boley, B. A., and Viggiano, L. A., "Stresses in, and General Instability of, Monocoque Cylinders with Cut-outs. IV - Pure Bending Tests of Cylinders with Side Cut-outs". NACA TN 1264, 1947.

18. Hoff, N. J. and Klein, B., "Stresses in, and General Instability of, Monocoque Cylinders with Cut-outs. V - Calculation of the Stresses in Cylinders with Side Cut-out." NACA TN 1435, 1948.

19. Hoff, N. J., Klein, B., and Boley, B. A., "Stresses in, and General Instability of, Monocoque Cylinders with Cut-outs. VI - Calculation of the Buckling Load of Cylinders with Side Cut-out subjected to Pure Bending." NACA TN 1436, 1948.

20. Hoff, N. J., Boley, B. A. and Mele, J. J., "Stresses in, and General Instability of, Monocoque Cylinders with Cut-outs. VII - Experimental Investigation of Cylinders having Either Long Bottom Cut-outs or Series of Side Cut-outs." NACA TN 1962, 1949.

21. Hoff, N. J., Boley, B. A. and Mandel, M. W., "Stresses in and General Instability of, Monocoque Cylinders with Cut-outs. VIII - Calculations of the Buckling Load Cylinders with Long Symmetric Cut-out subjected to Pure Bending." NACA TN 1963, 1949.

22. Brogan, F. and Almroth, B., "Buckling of Cylinders with Cut-outs," AIAA Paper No. 69-92, 1969.

23. Kuhn, P., Stresses in Aircraft and Shell Structures, McGraw-Hill Book Co., Inc., New York, N. Y., 1956.

24. Brown, L. W., "An Experimental Investigation into Some of the Problems Associated with Stress Diffusion in the Vicinity of Chordwise-Cut-outs in the Wing, and a Comparison with Existing Theories," The Coll. of Aero., Cranfield, rep. 83, 1954.

25. Kirsch, G., "Die Theorie der Elasteität und die Bedürfnisse der Festigheitslehre," Zeit, V.D.I., Vol. 42, No. 29, 1898, p. 797.

26. Howland, R.C.J., "On the Stresses in the Neighborhood of a Circular Hole in a Strip Under Tension," Phil. Trans. Roy. Soc., London, A229, p. 49, 1929.

27. Neuber H., Theory of Notch Stresses: Principles for Exact Stress Calculation, DTMB Translation 74, No. 1945.

28. Neuber, H., and Hahn, H. G., "Stress Concentration in Scientific Research and Engineering," Applied Mechanics Review, Vol. 19, No. 3, p. 187, March 1966.

29. Kolosov, G. V., "On an Application of Complex Function Theory to a Plane Problem of the Mathematical Theory of Elasticity" (in Russian), Yuriev, 1909.

30. Muskhelishvili, N. I., Some Basic Problems of the Mathematical Theory of Elasticity, (Translation by J. R. M. Radok) P. Noordhoff, Ltd., Groningen, Holland, 1953.

31. Radok, J. R. M., "Complex Variable and Direct Variational Methods," Proc. Intern. Symp. of IUTAM, Tiflis, USSR, Vol. 1, p. 76, 1963.

32. Morley, L.S.D., "A Variational Method of Solution for Problems in Plane Elasticity," Journal of the Institute of Mathematics and its Applications, Vol. 1, p. 76, 1965.

33. Chen Lin-Si, Problems of Continuum Mechanics, P. Noordhoff, Ltd., Groningen, Holland, 1961, p. 69.

34. Low, E. F. and Chen, W. F., "Stress Concentration Around Shaped Holes," Journal of Eng. Mech. Div., Proc. ASCE, Vol. 93, EM 3, p. 33.

35. Savin, G. N., "Stress Concentration Around Holes," (Translation by E. Gros), Pergamon Press, Inc., New York, N. Y., 1961.

36. Heller, S. R., Jr., Brock, J. S., and Bart, R., "The Stresses Around a Rectangular Opening with Rounded Corners in a Uniformly Loaded Plate," Proceedings, U. S. National Congress of Applied Mechanics, Vol. 3, 1958, p. 357.

37. Frocht, M. M. and Leven, M. M., "Factors of Stress Concentration for Slotted Bars in Tension and Bending," Journal of Appl. Mech. Vol. 18, p. 107, March 1951.

38. Durelli, A. J., Parks, V. J. and Uribe, S., "Optimization of a Slot End Configuration in a Finite Plate Subjected to Uniformly Distributed Load," Journal of Appl. Mech., Vol. 35, p. 403, June 1968.

39. Durelli, A. J., Parks, V. J. and Feng, H. C., "Stresses Around an Elliptical Hole in an Infinite Plate Subjected to Axial Loadings," Journal of Appl. Mech., Vol. 33, p. 192, 1966.

40. Dixon, J. R., "Stress Distribution Around a Central Crack in a Plate Loaded in Tension: Effect of Finite Width of Plate," Jour. of Roy. Aero. Soc., London, Vol. 64, p. 414, 1960.

41. Dixon, J. R. and Strannigan, J. S., "Stress Distribution and Buckling in Thin Sheets with Central Slits," 2nd International Conference on Fracture, Brighton, U. K., April 13-18, 1969.

42. Mansfield. E. H., "Neutral Holes in Plane Sheets; Reinforced Holes which are Elastically Equivalent to the Uncut Sheet," A.R.C. R.& M. No. 815, Sept. 1950.

43. Mansfield, E. H., "On the Design of a Row of Windows in a Pressurized Cylindrical Fuselage," A.R.C. R. & M. No. 3360, May 1963.

44. Wittrick, W. H., "Stresses Around Reinforced Elliptical Holes with Application to Pressure Cabin Windows," Aeronautical Quarterly, Vol. 10, p. 373, Nov. 1953.

45. Davies, G. A. D., "Plate-Reinforced Holes," Aeronautical Quarterly, Vol. 18, p. 43, February 1967.

46. Houghton, D. S. and Rothwell, A., "The Stresses Around Some Unreinforced Cut-Outs under Various Loading Conditions," The College of Aero., Cranfield, Rep. 146, 1961.

47. Houghton, D. S. and Rothwell, A., "The Effect of Curvature on the Stress Concentrations Around Holes in Shells," The College of Aero., Cranfield, Rep. 156, May 1962.

48. Peterson, R. E., "The Role of Stress Distribution in Fatigue," Experimental Mechanics, Vol. 1, No. 2, p. 105.

49. Cherepanov, G. P., "On the Buckling Under Tension of a Membrane Containing Holes," Applied Mathematics and Mechanics, (Translation of PMM), Vol. 27, No. 2, 1963, p. 405.

50. Cherepanov, G. P., "On the Solution of Certain Problems with an Unknown Boundary in the Theory of Elasticity and Plasticity," Appl. Math. and Mech. (Translation PMM), Vol. 28, No. 1, 1964, p. 162.

51. Pellett, D. A., Costello, R. G. and Brock, J. E., "Buckling of a Tension Panel Containing a Circular Hole," AIAA Journal, Vol. 6, No. 10, p. 2012, October 1968.

52. Forman, R. G., "Experimental Program to Determine Effect of Crack Buckling and Specimen Dimensions on Fracture Toughness of Thin Sheet Materials, AFFDL-TR-65-146, 1965.

53. Walker, E. K., "A Study of the Influence of Geometry on the Strength of Fatigue Cracked Panels," AFFDL-TR-66-92, 1966.

54. Clarkson, B. L., "The Propagation of Fatigue Cracks in a Tensioned Plate Subjected to Acoustic Loads," In Trapp, W. J., and Forney, O. (Eds.), Acoustical Fatigue in Aerospace Structures, Syracuse Univ.

55. Welbourne, E. R., "An Analysis of Fatigue Crack Propagation in Sheet Material," In Current Aeronautic Fatigue Problems, Schijve, J. Heath-Smith, J. R., & Welbourne, E. R. (Eds.), Pergamon Press, London, 1965, p. 268.

56. Danis, J. F., "Buckling Near a Hole Centered in a Tension Field," Thesis Naval Postgraduate School, Monterey, Calif., 1957.

57. Bingham, W. L., "A Contribution to Photoelastic Structural Stability Analysis," Ph. D. Thesis, The Pennsylvania State University, 1961.

58. Mindlin, R. D. and Salradori, M. G., "Analogies," Chapter 16 of Handbook of Experimental Stress Analysis, M. Hetenyi, ed., John Wiley & Sons, Inc., New York, N. Y., 1950.

59. Goodier, J. N. and Thomson, W. T., "Applicability of Similarity Principles to Structural Models," NACA TN 933, July 1944.

60. Brock, J. S., "The Relation Between Stress Concentration and Boundary Displacement for Simple Openings," Journal of Appl. Mech., Vol. 27, p. 356, June 1960.

61. Sobey, A. J., "The Estimation of Stresses Around Unreinforced Holes in Infinite Elastic Sheets," A.R.C. R & M No. 3354, Oct. 1962.

62. Milne-Thomson, L. M., Plane Elastic Systems, Sprinser, Berlin, 1960.

63. Whittaker, E. T. Sir and Robinson, G., The Calculus of Observations; An Introduction to Numerical Analysis, Dover Publications, New York, N. Y. 1967.

64. Frocht, M. M., Photoelasticity, John Wiley and Sons, Inc., New York, N. Y., Vol. I, 1941, Vol. II, 1948.

65. Clarkson, B. L. and Pietrusewicz, S. A., "The Propagation of Fatigue Cracks by Random Pressures in a Turbulent Boundary Layer," U. of Southampton, Institute of Sound and Vibration Research Memorandum No. 104, February 1964.

66. Pietrusewicz, S. A., "Further Notes on the Behavior of Plates Under Constant Stress Subjected to High Intensity Noise," Bath University of Technology, School of Engineering Report No. 150, May 1969.

67. Carlson, R. L., Zielsdorff, G. F. and Harrison, J. C., "Buckling in Thin Cracked Sheets," in Proceedings of the Air Force Conference on Fatigue and Fracture of Aircraft Structures and Materials, AFFDL TR 70-144.

68. Carlson, R. L. and Datta, P. K., "On the Analysis of Plate Stability Experiments," Presented at the Joint Meeting of the IV Pan American Symposium of Structures, October 1970.

69. Mikhlin, S. G., Approximate Methods for Solution of Differential and Integral Equations, American Elsevier, New York, N. Y., 1967, p. 195.

70. Lundquist, E. E., "Generalized Analysis of Experimental Observations in Problems of Elastic Stability," NACA TN-658, 1938.

71. Zielsdorff, G. F., "Continuation of a Parametric Study of the Stability Around a Cut-Out in a Thin Sheet Subject to a Tensile Load," Special Problem in School of Aerospace Engineering, Georgia Institute of Technology, Atlanta, Ga., 1968.

72. Petyt, M., "The Vibration Characteristics of a Tensioned Plate Containing a Fatigue Crack," Journal of Sound and Vibration, Vol. 8, No. 3, p. 377, 1968.

73. Stein, M., "Loads and Deformations of Buckled Rectangular Plates," NASA TR R-40, 1959.

74. Rogers, C. C., Zielsdorff, G. F. and Carlson, R. L., "On the Photoelastic Analysis of a Nonlinear Plate Problem," submitted to the Journal of Strain Analysis for publication.

VITA

George F. Zielsdorff was born on August 6, 1943 in Somerville, New Jersey. He attended grammar school in Manville, New Jersey and graduated from Manville High School in 1961.

Mr. Zielsdorff attended the Georgia Institute of Technology from September 1961 through March 1964. During this time he also worked with ARO, Inc. of Tullahoma, Tennessee.

In May of 1964 he enlisted in the United States Air Force. He attended an Air Force school and was graduated with honors as a Nuclear Weapons Specialist. Mr. Zielsdorff was assigned to Larson, AFB, Washington in the Strategic Air Command. In December of 1965 he was named Maintenance Man of the Month for the 16th Strategic Aerospace Division.

Mr. Zielsdorff accepted an appointment in the Air Force's Airman Education and Commissioning Program in 1966 and returned to Georgia Tech to complete his undergraduate program. He completed requirements for the degree B. S. in A. E. in December 1967 and afterward attended the Air Force's Officer Training School where he was a distinguished graduate.

Mr. Zielsdorff returned to Georgia Tech for graduate work under the sponsorship of the Civilian Institutions Division of the Air Force Institute of Technology. He was awarded an M. S. in A. E. in June of 1970.

He presently holds the rank of Captain in the regular component of the U. S. Air Force.

He is married to the former Barbara Gail Tumpack of Titusville, Florida. They have two children and presently reside in Dayton, Ohio.